RATIONAL DESIGN OF HIGH PERFORMANCE CONJUGATED POLYMERS FOR ORGANIC SOLAR CELLS

Huaxing Zhou

A dissertation submitted to the faculty of the University of North Carolina at Chapel Hill in partial fulfillment of the requirements for the degree of Doctor of Philosophy in the Department of Chemistry.

Chapel Hill
2011

Approved by:

Valerie Ashby

Maurice Brookhart

Jeff Johnson

Thomas Meyer

Wei You

ABSTRACT

HUAXING ZHOU: Rational Design of High Performance Conjugated Polymers for Organic Solar Cells
(Under the direction of Wei You)

The research on the polymer based solar cells (PSCs) has attracted increasing amount of attention in recent years and great progresses have been made in the field of bulk heterojunction (BHJ) polymer solar cells since its inception in 1995. The power conversion efficiency (PCE) has increased from 1% in the 1990s to over 9% just recently. These great advances are mainly fueled by the development of conjugated polymers used as the electron-donating materials in BHJ solar cells.

My research was focused on the rational design of those conjugated polymers. And first we investigated the positioning effect of alkyl side chains on the properties of conjugated polymers and found the best attaching position where high molecular weight and good solubility of conjugated polymers can be achieved without introducing large steric hindrance. Then, we proposed and demonstrated a "weak donor-strong acceptor" designing strategy to construct donor-acceptor type polymers with controlled energy levels.

With those strategy to increase molecular weight, solubility and to control energy levels, we designed and synthesized several "weak donor" based conjugated polymers with solubilizing chains. Those polymers exhibited low HOMO levels, good solubility and large molecular weight, thus high open circuit voltage (V_{oc}) over 0.8V and high PCE over 5% were obtained.

Since most of the conjugated polymers developed so far have high-lying LUMO levels than desired LUMO, we developed some “strong acceptor” units to decrease the LUMO level of conjugated polymers. Combined with the methods we developed, conjugated polymers with high molecular weight, good solubility and near ideal energy levels were synthesized and they exhibit excellent PCE over 6%.

In addition, by introducing fluorine atoms into conjugated backbone, we successfully created polymers with both low-lying HOMO and LUMO levels. Although band gap of this polymer is not ideal, large short circuit current (J_{sc}), open circuit voltage (V_{oc}) and fill factor (FF) can still be obtained. Amazing PCE over 7% was demonstrated, which is among the best performances for polymer solar cells.

To my wife Yueyang Yu,
To my parents.

Acknowledgements

First, I would like to express my deepest gratitude to Dr. Wei You, for his excellent guidance, caring, patience and providing me with an excellent atmosphere for doing my research.

I also would like to thank my committee members, Prof. Ashby, Prof. Brookhart, Prof. Meyer, Prof. Johnson and Prof. Samulski, for their support and assistance. Many people have been involved with my research and I would like to thank Dr. Samuel Price for the inspiring and helpful discussions, Dr. Shengqiang Xiao for teaching me the basics to be a good Chemist, Liqiang Yang and Andrew Stuart for fabricating and testing thousands of solar cell devices, Dr. Shubin Liu for carrying out the DFT calculations, and Sarah Stoneking, Kelly Knight, Nabil Kleinhenz and Mike Aubrey for helping me with monomer syntheses.

Many thanks go to my labmates in Kenan C541, Rycel Uy, Jason Dyke, Wentao Li, Rui Jin and James Blair. I also would like to thank all present members of the You group.

Finally, special thanks to my family. This work could not have been completed without the support from my wife Yueyang and my parents. You are my every reason to pick myself up after all the frustrating and down times. And you make all my efforts and achievements meaningful.

TABLE OF CONTENTS

LIST OF TABLES

Table

LIST OF FIGURES

Figure

CHAPTER 1

INTRODUCTION

1.1. Background

In order to sustain the economic growth of the World, there has always been insatiable need for energy, 85% of which is currently provided by burning fossil fuels (such as coal, oil and natural gas). While these natural resources provide cheap and easily accessible energy sources, the large scale consumption of these non-renewable sources presents two serious problems to mankind. The first problem is the limited reserve of these natural resources. Moreover, the tremendous amount of released green house gases (e.g. CO_2) from the combustion of fossil fuels leads to even more severe problems. In realizing these challenges, the scientific community has been looking for new energy sources, which should be environmentally benign and renewable. Currently as a small part of the renewable energy portfolio, harvesting energy directly from the Sun via photovoltaic (PV) technologies is increasingly being recognized as one of the most promising long-term solutions – or maybe the ultimate solution – to a sustainable future. The past six decades witnessed a rapid development of the PV technologies, dominated by silicon-based inorganic semiconductors. These inorganic solar cells have been extensively studied and successfully used for pragmatic terrestrial applications.[1] Though these cells are relatively efficient (12 ~ 15% in the PV modules), the high cost of both materials and manufacturing has hindered the widespread utilization of this technology.[1]

On the other hand, polymer solar cells (PSC) have attracted an increasing amount of attention in the research community due to the potential advantages of PSC over inorganic-based solar cells, including low cost, light weight and fast/cheap roll-to-roll production.[2-8]

1.2. Device Structure of Polymer Solar Cells

In a typical solar cell, an active layer is sandwiched between a transparent anode (typically tin doped indium oxide, ITO) and a metal cathode (**Figure 1-1**). Additionally, a thin layer of poly(3,4-ethylenedioxythiophene) poly(styrenesulfonate) **(**PEDOT:PSS) is generally applied in between the ITO and the active layer to improve the electrical contact between the ITO and the active layer and to adjust energy levels.[9] Some other interfacial layers are also applied in polymer solar cells. [10-19]

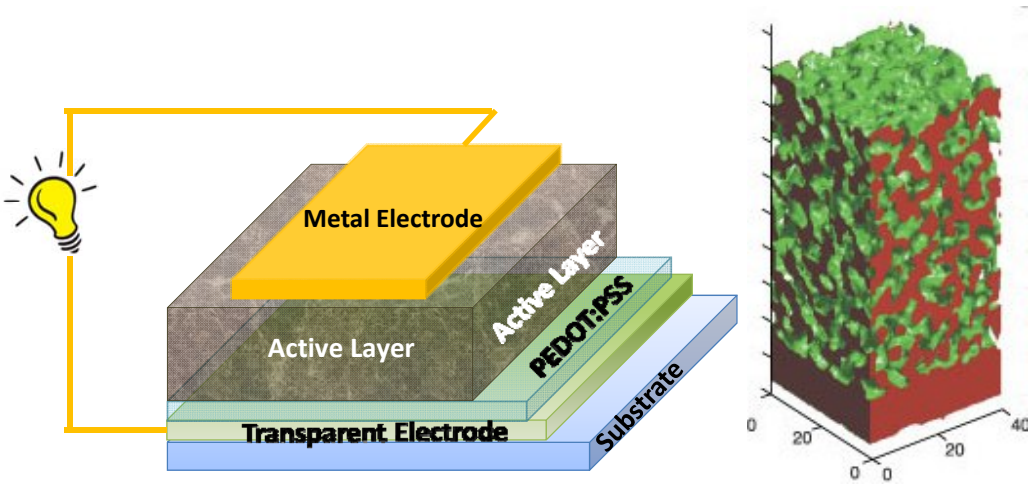

Figure 1-1. Schematic illustration of the structure of a typical bulk heterojunction polymer solar cell device (left) and BHJ configuration of active layer (right)[20] (Reprinted with permission. Copyright 2003 Nature Publishing Group.)

The active layer may have different configurations depending on how the p-type semiconductor (i.e., electron-donors, such as conjugated polymers) and n-type semiconductor (i.e., electron acceptors, such as fullerene derivatives) are blended. In the most successful bulk heterojunction (BHJ) configuration, electron-donors and electron acceptors are blended to form an interpenetrating network (**Figure 1-1**).[4] The interpenetrated network of BHJ offers two advantages: (a) it minimizes the travelling distance of excitons (electron-hole pair generated upon light absorption) to the donor/acceptor (D/A) interface, and concurrently maximizes the D/A interfacial area, thereby ensuring the exciton dissociation at the D/A interface to generate maximum free charge carriers; and (b) it offers charge transport pathways to facilitate the charge collection at electrodes, completing the conversion of the photon energy to electrical energy (i.e., photovoltaic effect).

1.3. Important Parameters of Polymer Solar Cells

The single most important performance parameter of a solar cell is the power conversion efficiency (PCE or η), which is related with the open circuit voltage (V_{oc}), short circuit current (J_{sc}) and fill factor (*FF*) through equation (**1**). All of those parameters can be extracted from the J-V curves under the 1 sun condition (100 mW/cm^2, simulated AM1.5 solar illumination). (**Figure 1-2**) The PCE is calculated by the following equation:

$$\mathrm{PCE} = \frac{\mathrm{V_{oc}} \times J_{\mathrm{sc}} \times \mathrm{FF}}{\mathrm{P_{in}}} \quad (1)$$

And FF is defined as:

$$\mathrm{FF} = \frac{\mathrm{V_{mpp}} \times J_{\mathrm{mpp}}}{\mathrm{V_{oc}} \times J_{\mathrm{sc}}} \quad (2)$$

Where V_{mpp} and J_{mpp} are the voltage and current at the maximum power point in the J-V curve, respectively.

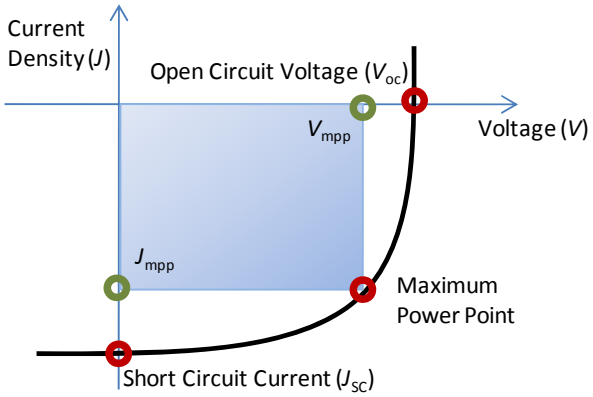

Figure 1-2. A preventative current density-voltage (*J*-V) curve and key parameters of device measurement

1.4. General History of Polymer Solar Cells

The first organic solar cell was made by Kallmann et al. based on a single crystal of anthracene in 1959.[21] It has a super low power efficiency of 2×10^{-4}. This low efficiency is partly due to organic materials with high dielectric constant, which lead to strongly bound electron-hole pairs. Photogenerated excitons are hence poorly separated spontaneously into free charges. In 1986 Tang did a seminal work by using thin-film double-layer photovoltaic cells of copper phtalocyanine (CuPc) and a perylene tetracarboxylic (PT) derivative, which leads to 0.95% efficiency and a fill factor of 65%.[22] Excitons can easily be dissociated into electrons and holes at the interface of CuPc and the PT layer due to their differences in energy levels. The success of this electron donor/acceptor concept largely stimulated the research in the organic photovoltaic field. In 1992, the ultra-fast electron transfer from polymer (MDMO-PPV) to C60 was discovered[23], and a near unity

dissociation efficiency was reported. In 1995, a series of soluble C60 was synthesized[24], which enables the solution process of C60. In the same year, Heeger et al. demonstrated a 1% efficiency of polymer solar cell based on bulk heterojunction (BHJ) active layer with a conjugated polymer PPV and [6,6]-phenyl-C61-butyric acid methyl ester ($PC_{61}BM$) as donor and acceptor respectively[4].**(Figure 1-3)** The BHJ structure and soluble fullerene derivatives were then widely applied in PSC field. From 1995 to 2005, majority of the research was focused on PPV and poly(3-hexylthiophene)(P3HT) based solar cells, (**Figure 1-3**) and the power conversion efficiency had a significant increase up to 5%[25,26]. However, due to some intrinsic problems of those conjugated polymer materials, such as large band gaps, limited chemical modification possibilities, the development of PSC was trapped in a bottleneck. To solve those problems, in recent years low band gaps polymers received heated research attention and huge success. In just five years, the state-of-art PCE of low band gap polymer based solar cell devices has increased from less than 1% to over 9%.[27-34]

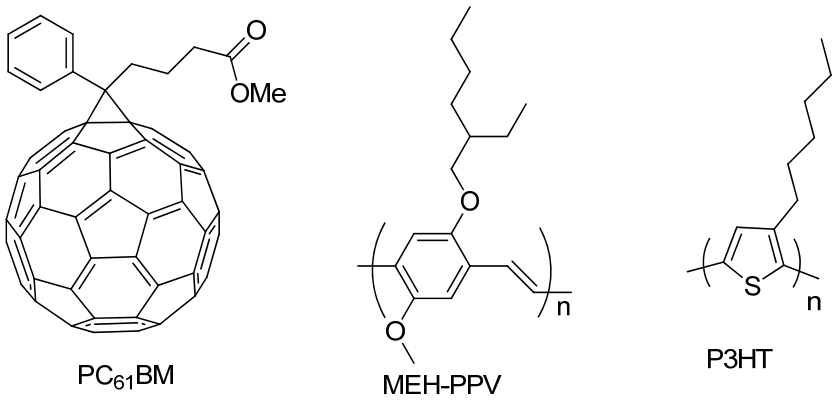

Figure 1-3. Chemical structure of $PC_{61}BM$, MEH-PPV and P3HT

Although some other high performance fullerene derivatives have also been developed over the years,[34-40] the relatively cheap and commercially available $PC_{61}BM$ is still widely applied as the standard acceptor material. In recent years, $PC_{71}BM$, a C_{70} analogue of $PC_{61}BM$ were used in some research groups to increase PCE, because of its better light absorption in visible region.[37]

In this dissertation, I will focus on the rational design of conjugated polymers under the assumption that $PC_{61}BM$/$PC_{71}BM$ is used as the electron acceptor.

1.5. A Brief History of the Development of Conjugated Polymers for Polymer Solar Cells

The rather short history of BHJ solar cells can be roughly divided into three phases from the perspective of the conjugated backbones of donor polymers. Phase one centered on poly(phenylene vinylene)s (PPV), such as poly[2-methoxy-5-(2'-ethylhexyloxy)-p-phenylene vinylene] (MEH-PPV) and (poly[2-methoxy-5-(3,7-dimethyloctyloxy)]-1,4-phenylenevinylen (MDMO-PPV). Power conversion efficiency as high as 3.3% were achieved in PPV based BHJ solar cells with $PC_{61}BM$ as the acceptor material, mainly through the application of chlorinated solvents to tune active layer morphologies.[41,42] A high open circuit voltages (V_{oc}) up to 0.82 V was obtained as a result of the relatively low highest-occupied molecular orbital (HOMO) energy level of – 5.4 eV of MDMO-PPV; however, the large band gap of MDMO-PPV limits the short circuit current density (J_{sc}) to 5-6 mA/cm^2. Therefore, in phase two, a smaller band gap polymer, regio-regular poly(3-hexylthiophene) (rr-P3HT) was thoroughly investigated.[25] P3HT based BHJ devices provide a noticeably higher current density (over 10 mA/cm^2), attributed to its

lower band gap (1.9 eV) as well as to its increased π-stacking and crystallinity which yields a higher hole mobility.[16,43,44] Upon optimization of the active layer morphology via thermal[44] or solvent annealing,[45] an impressive PCE of 5% was achieved.[25,26] Unfortunately, the high HOMO (– 5.1 eV) energy level of P3HT has restricted the V_{oc} to ~ 0.6 V in its related BHJ solar cells with $PC_{61}BM$ as the acceptor, which consequently limits the overall efficiency.

Presently in phase three, numerous polymer backbones have been reported. High V_{oc} over 1V, [46-48] high J_{sc} over 17.3 mA/cm^2 [6] and *FF* over 70%[49,50] have been demonstrated in different polymers based BHJ solar cells. If all these impressive values could be combined in one polymer solar cell, it would give a PCE as high as 12%. However, due to the interplay of polymer properties such as energy levels and band gap and their correlation with V_{oc} and J_{sc}, highest V_{oc} and highest J_{sc} cannot be concurrently obtained.[51] In order to achieve highest possible PCE, one needs to carefully balance the V_{oc} and J_{sc} via judicious control over physical properties of a conjugated polymer (i.e., looking for "ideal polymers").

1.6. Required Properties for Ideal Polymers

To design ideal polymers as the donor in polymer-based BHJ solar cells with high PCE($PCE = V_{oc} \times J_{sc} \times FF / P_{in}$), the following issues needs to be carefully addressed.

(a) Open circuit voltage (V_{oc}). V_{oc} is tightly correlated with the energy difference between the HOMO of the donor polymer and the LUMO of the acceptor (e.g., $PC_{61}BM$).[52] In theory, polymers with low-lying HOMO levels would exhibit higher V_{oc}. However, generally a minimum energy difference of ~ 0.3 eV between the LUMO energy

levels of the donor polymer and the acceptor is required to facilitate efficient exciton splitting and charge dissociation, therefore the HOMO level of the donor polymer cannot be too low, otherwise the band gap of the donor polymer would be too large to effectively absorb the light.[52] The origin of V_{oc} is still under intense debate, and recent data indicate that V_{oc} is decided by a couple of other factors besides just the HOMO level of a polymer.[53,54] Furthermore, bulkiness of side chains, interchain distances and morphology of active layer have also been demonstrated to have a noticeable effect on V_{oc}.[51]

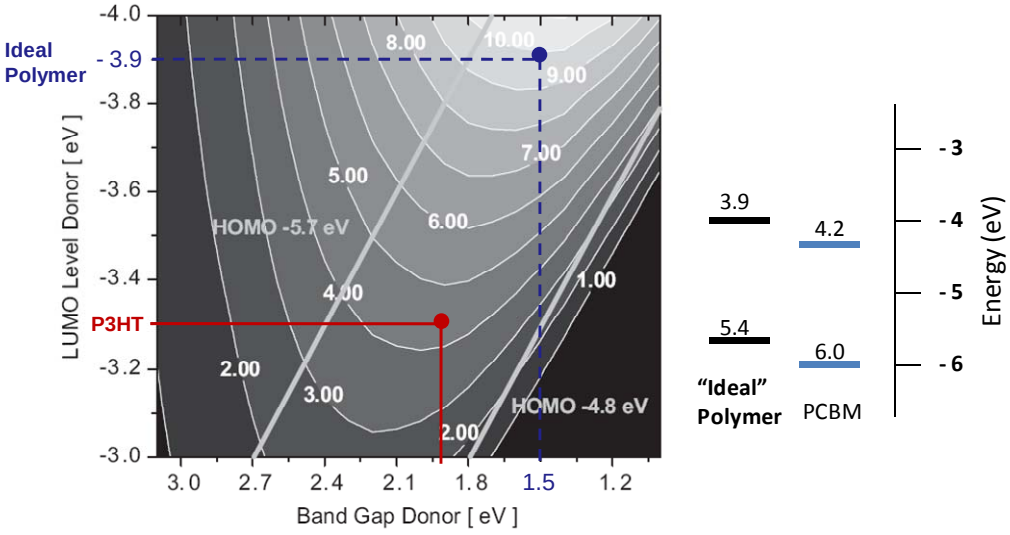

Figure 1-4. Calculated energy-conversion efficiency of P3HT and "ideal" polymer, assuming FF and IPCE at 65%.[52] (Reprinted with permission. Copyright 2006 Wiley-VCH VerlagGmbH&Co. KgaA.)

(b) Short circuit current (J_{sc}). The theoretical upper limit for J_{sc} of any excitonic solar cell is decided by the number of excitons created during solar illumination. Ideally, the absorption of the active layer should be compatible with the solar spectrum to

maximize the exciton generation. Since $PC_{61}BM$ has a poor absorption in the visible and near IR region where most of the solar flux is located, the donor polymer has to serve as the main light absorber. Roughly 70% of the sunlight energy is distributed in the wavelength region from 380 to 900 nm,[55] hence an ideal polymer should have a broad and strong absorption in this range, which requires the polymer band gap to be 1.4 - 1.5 eV. A narrower band gap polymer could absorb more light, which would increase the J_{sc}; however, lowering the band gap would require an increase of the HOMO level of the donor polymer (since the LUMO level cannot be lower than – 3.9 eV with $PC_{61}BM$ as the acceptor for efficient exciton splitting and charge dissociation)[28] and would reduce the V_{oc}.

If one assumes a fill factor of 0.65, an external quantum efficiency of 65%, and an optimal morphology, one can approximate the overall PCE from the optical band gap and the LUMO/HOMO of the donor polymer in a polymer:$PC_{61}BM$ BHJ solar cell (**Figure 1-4**).[52] It is clearly seen that a PCE of 10% can be achieved by an "ideal" polymer with an optimal band gap of 1.5 eV and a HOMO level around – 5.4 eV.

Though the experimentally determined V_{oc} can be very close to the predicted value based on the measured HOMO level of the polymer, the actual J_{sc} extracted from a polymer solar cell is usually a lot lower than the theoretical J_{sc} due to a number of loss mechanisms (e.g., monomolecular or bimolecular recombination) during the charge generation, transport and extraction.[29,55] Thus a few other desirable features need to be included to mitigate these losses, such as high molecular weight, high charge mobility, and optimized active layer morphology, all of which will help improve the actual J_{sc}.

(c) Fill factor (*FF*). From a semiconductor photovoltaic device point of view, a high *FF* requires a small series resistance (R_s) and a large shunt resistance (R_{sh}),[56] both of which are significantly impacted by the morphology of the polymer/fullerene blend and the mobility of both polymer and fullerene. Thus the morphology of the active layer should be optimized to promote charge separation and favorable transport of photogenerated charges, in order to maximize the *FF* and the attainable J_{sc}.

(d) Finally, besides high PCE, solution processability (offered by side chains) and long term stability of polymer solar cells (related with both materials and encapsulation) is of equal importance for future application and commercialization.

In short, the properties desired for a high performance polymer are (1) good solubility, (2) high molecular weight, (3) HOMO level around – 5.4eV, (4) LUMO level around – 3.9 eV and (5) high hole mobility, (6) optimal morphology, and (7) long term stability.

1.7. Structural Features of Conjugated Polymers: A Bird Eye's View

A typical conjugated polymer used as the electron donor in polymer solar cells is illustrated in **Figure 1-5.** Generally, a conjugated polymer can be arbitrarily divided into three constituting components: *the conjugated backbone, the side chains* and *the substituents*. The conjugated backbone is the most important component because it dictates most of the PSC-related physical properties of the conjugated polymer, such as energy levels, band gap and molecular interactions. Hundreds of different backbones have been reported so far;[32-34] however, the design of polymer backbones has been quite empirical. As a result, the discovery of high performance polymers is rather

serendipitous. Therefore, the rational design of conjugated backbone (i.e., the repeating units) is of utmost importance in the further development of polymer solar cells.

On the other hand, side chains play a crucial role in improving the molecular weight, solubility and processability of conjugated polymers. Furthermore, these side chains can adjust intermolecular interactions and allow better mixing with $PC_{61}BM$ to form the desired morphology. However, these insulating side chains also dilute the chromophore density and disturb π-stacking of polymer backbones, which could thwart the light absorption and charge transport. In addition, improper attachment of side chains may introduce steric hindrance and twist of the conjugated backbone, which could lead to a large band gap, low mobility and poor photovoltaic properties. Finally, there are increasing evidences showing that the shape and length of side chains have noticeable impact on the photovoltaic properties of conjugated polymers.

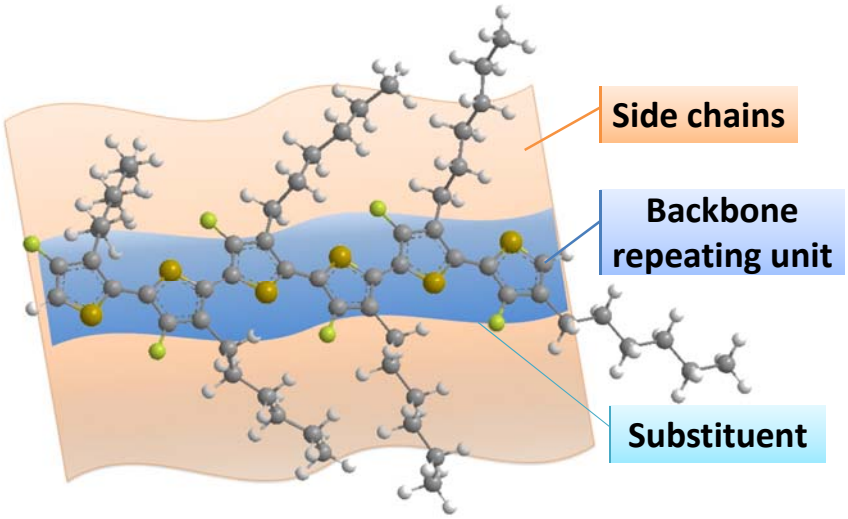

Figure 1-5. Illustration of a typical conjugated polymer for the application in organic solar cells

Lastly, substituents (such as F and CN) are generally used as a fine-tuning method to tweak the physical properties of conjugated polymers, particularly the electronic properties (energy levels, band gap, mobility, etc.). Since photovoltaic properties of conjugated polymers are very sensitive towards their electronic properties, sometimes substituents can have important influence on the photovoltaic performance of related conjugated polymers.

1.8. Different Types of Conjugated Polymer Backbones

All reported conjugated backbones for PSC can be loosely classified into four different categories based on the constitution of the repeating unit, namely (a) homopolymer, (b) donor-acceptor polymer, (c) quinoid polymer and (d) other types of polymers as shown in **Figure 1-6**.

The repeating unit of the homopolymer usually consists of a single aromatic unit or fused aromatics. The physical properties of these polymers are largely determined by the intrinsic properties of the constituting single or fused aromatics, with appreciable contribution from steric hindrance between these repeating units. Thus most of the homopolymers have large band gaps (>1.9 eV), which limit the light absorption of these materials. In addition, very often the aforementioned steric hindrance forces the adjacent repeating units off the desired co-planarity of these units, negatively impacting the band gap and the crystallinity of the polymer, thereby diminishing photovoltaic properties of related BHJ devices. [26,57,58] The best polymer of this type is the regio-regular P3HT with PCE over 5% after thorough optimizations.[25,26,44]

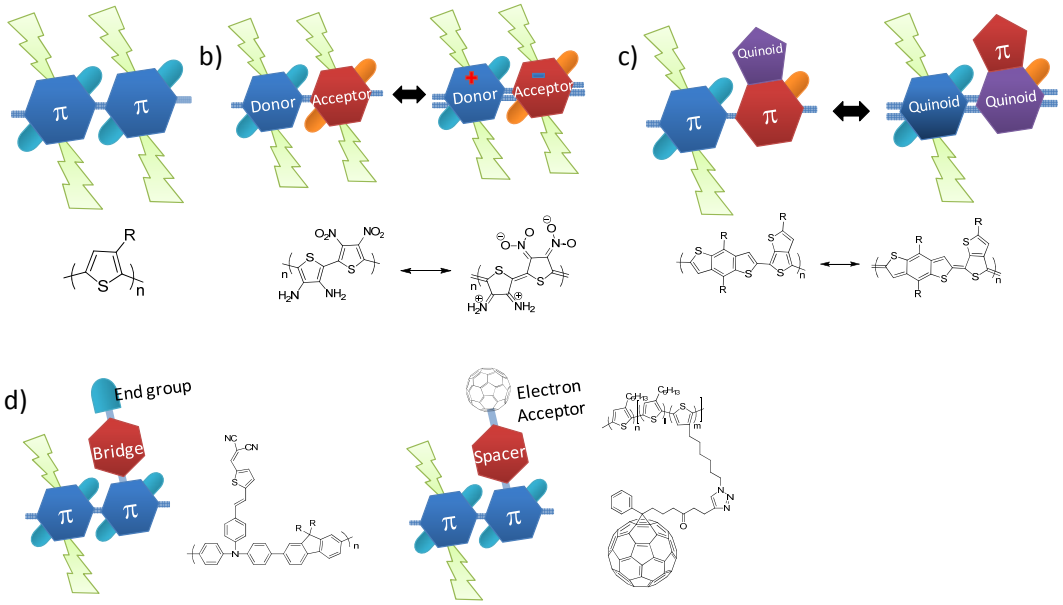

Figure 1-6. Different types of conjugated polymer structures with examples: a) homopolymer; b) donor-acceptor polymer; c) quinoid polymer; d) examples of other types of polymers

On the other hand, it is fairly easy to construct low band gap polymers with tunable energy levels via the donor-acceptor (D-A) approach. The repeating unit of D-A polymers comprises of an electron-rich "donor" moiety and an electron-deficient "acceptor" moiety. The internal charge transfer between the "donor" and the "acceptor" moieties leads to the observed low band gap.[59] This strategy was first proposed in 1993,[60,61] and best illustrated by Tour et al. by using a copolymer of 3,4-aminothiophene and 3,4-nitrothiophene to reach a band gap of 1.0 eV, as shown in **Figure 1-6b**.[62] The internal charge transfer (ICT) intrinsic with the D-A structure leads to more desirable double bond characteristic between repeating units. Therefore, the conjugated backbone

adopts a more planar configuration to facilitate the π-electrons delocalization along the conjugated backbone, leading to a smaller band gap. Most of the conjugated polymers for PSC reported so far are based on this D-A concept, with several of them showing over 7% efficiency in their BHJ cells.[50,63-66]

"Quinoid" polymers employ a different approach to effectively lower the band gap as well. Typically two aromatic units are fused in a particular geometry to take advantage of the larger value of resonance energy of the first aromatic unit (e.g., benzene, 1.56 eV) over the second unit (e.g., thiophene, 1.26 eV), so that the second aromatic unit (e.g., thiophene) tends to de-aromatize to adopt a quinoid structure. Since the quinoid resonance form is lower in energy than the aromatic form, stabilizing the quinoid form will effectively reduce the band gap of related conjugated polymers. **Figure 1-7** shows a few successful examples, including poly(benzo[*c*]thiophene) (E_g = 1.1 eV),[67] poly(thieno[3,4-*b*]pyrazine (E_g = 0.95 eV),[68] and poly(thieno[3,4-*b*]thiophene) (E_g = 0.8-0.9 eV).[69,70] The major drawback of these fused systems lies in their relatively high-lying HOMO energy levels, which explains that low band gap copolymers synthesized by alternating these pre-quinoid monomers with other aromatic rings such as thiophenes and fluorenes showed low V_{oc} in BHJ solar cells.[71-76] Further engineering the substituents on these conjugated backbones can lower the HOMO levels,[76-79] thereby leading to impressive efficiency numbers (over 7%).[77,80]

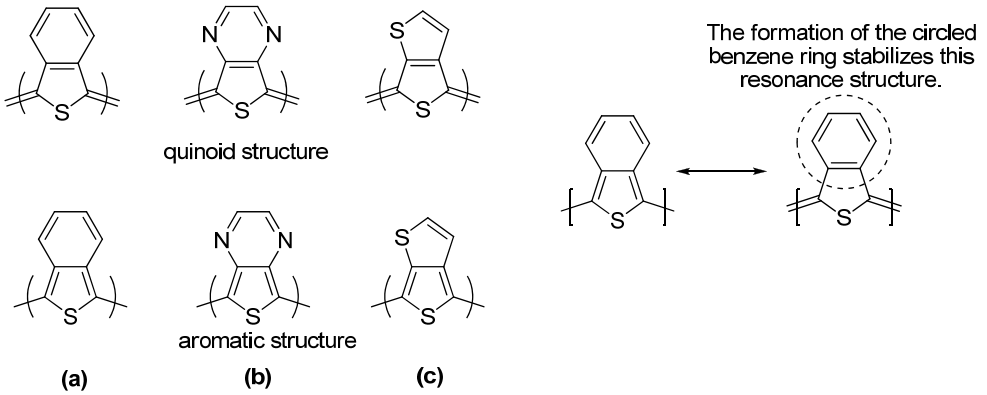

Figure 1-7. Aromatic and quinoid forms of poly(benzo[c]thiophene) (a), poly(thieno[3,4-b]pyrazine (b), and poly(thieno[3,4-b]-thiophene) (c)[8]. (Reprinted with permission. Copyright 2010 American Chemical Society.)

Rather than inserting electron-deficient acceptor moieties into the conjugated backbone to lower the band gap, the bridge polymer attaches them as the pendant groups to the backbone, aiming to optimize the absorption and conserve/promote the isotropic charge transport without any interruption by these acceptor moieties.[81,82] There are only a few examples of these bridge polymers with limited success.[81-83] One challenge for this type of polymers is the understanding and control of the active layer morphology.

Instead of blending electron donor materials with electron acceptor materials to form solar cell active layer in hope of obtaining well-defined nanostructure, a so-called "double-cable" approach was smartly designed, in which acceptors such as fullerenes (acceptor cable) are covalently connected to p-type conjugated backbones (donor cable). The advantages of this design include (i) a larger donor-acceptor interfacial area compared with BHJ structure; (ii) unwanted large phase separation and clustering are prevented, (iii) relatively stable morphology and (iv) variation of the chemical structures

of the donor and acceptor moieties and length of the spacer connecting them allows tuning the electronic interaction of the double-cable components.[84,85] In solar cell devices made from "double-cable" materials, electrons generated by the dissociation of excitons are transported by hopping between the pendent acceptor moieties, leaving holes on the p-type backbones. Several double cable materials have been demonstrated in polymer solar cells.[86-91] However, the PCE of such devices is still at a low level, which is probably due to fast recombination, ineffective interchain transport and low acceptor content.[92,93]

Due to the aforementioned advantages, the versatility in design, and the popularity of the D-A polymers, *we will focus on the design of donor-acceptor polymers in this disseration*. And we are going to study the polymer structure-property relationship and to rationally design polymers to achieve the properties discussed in section 1.6, which are (1) good solubility, (2) high molecular weight, (3) HOMO level around – 5.4eV, (4) LUMO level around – 3.9 eV and (5) high hole mobility, (6) optimal morphology, and (7) long term stability.

CHAPTER 2

DONOR-ACCEPTOR POLYMERS INCORPORATING ALKYLATED DITHIENYL BENZOTHIADIAZOLE FOR BULK HETEROJUNCTION SOLAR CELLS: PRONOUNCED EFFECT OF POSITIONING ALKYL CHAINS

Huaxing Zhou, Liqiang Yang, Shengqiang Xiao, Shubin Liu and Wei You

Adapted with permission from *Macromolecules* 2010, 43, (2), 811-820

2.1. Introduction

For conjugated polymers used in organic solar cells, solubilizing side chains are required to allow solution processability, which is the key feature for future low-cost mass production of these flexible solar cells. Without solubilizing chains, the conjugated backbone would adopt a more planar structure, thereby facilitating the chain-chain interactions among polymers and leading to unprocessable "bricks". Besides the function to improve solubility, side chains were once considered to have negligible effect on the performance of conjugated polymers by many people. Thus, the attaching position, shape and length of side chains haven't caught much research attention until recently. People start to discover that in addition to imparting the solubility to conjugated polymers, side chains play important roles in certain key properties of conjugated polymers, such as molecular weight, inter- and intra-molecular interactions, charge transport and active layer morphology.[94] And we are among the first groups to unveil the importance of polymer side chains for the polymer solar cell efficiency. In this chapter, we will discuss

a pronounced effect of alkyl chain position on BHJ solar cell efficiency by systematically investigating a series of donor-acceptor (D-A) type conjugated polymers with additional alkyl side chains on different positions of acceptor unit.

As discussed in **chapter 1**, "donor-acceptor" approach is a typical way to construct low band gap polymers, in which the intramolecular charge transfer between alternating electron-rich units (donor units) and electron-deficient units (acceptor units) lowers the band gap.[95] The development of D-A type polymers recently lead to a boost on power conversion efficiency. One common feature of these successful D-A low band gap polymers is the predominant employment of 2,1,3-benzothiadiazole (**BT**)[96-98] or di-2-thienyl-2,1,3-benzothiadiazole (**DTBT**)[5,47,99-103] as the acceptor units. Compared with the **BT** unit, **DTBT** has a few advantages. First, the two flanking thienyl units relieve the otherwise possibly severe steric hindrance between the acceptor – **BT** unit and donor aromatic units (especially when benzene based aromatics are used). Thus, the synthesized donor-acceptor polymers would adopt a more planar structure, thereby reducing the band gap by enhancing the D-A conjugation. In addition, a more planar conjugated backbone would facilitate the chain-chain interactions among polymers, improving the charge carrier (usually hole) mobility. Second, while the electron accepting **BT** unit maintains the low band gap, the two electron rich, flanking thienyl units would help improve the hole mobility, since thiophene based polymers (such as P3HT) have shown very high hole mobility.[104] Due to these advantages, the widespread usage of the **DTBT** unit has resulted in a number of polymers with high BHJ solar cell efficiencies.[5,47,99-103,105-107]

Unfortunately, the strong stacking ability of polymers incorporating the **DTBT** unit also introduces several concomitant technical difficulties. For example, the additional thiophene rings could result in polymers which are poorly soluble.[105] This low solubility can lead to low molecular weight of the polymer, and unnecessary difficulty in processing the polymer. For BHJ solar cells, high molecular weight polymers are desirable, which have been shown to help enhance the efficiency of related BHJ devices, presumably by improved inter-polymer interaction to enhance the current.[108-110] Even if one could manage to obtain high molecular weight polymers, the excessive stacking may result in aggregation of polymers upon spin casting of the film. This aggregation leads to polymer-only domains on a micron scale, in contrast to the desired morphology: nanometer sized, separated phases of donor polymers and fullerenes.[111] In order to fully utilize the aforementioned merits of **DTBT** units, it is important to search for new strategies to modify the structure of **DTBT** so as to improve the solubility and molecular weight of polymers incorporating **DTBT** units. In addition, such modification of **DTBT** units should also have minimum impact on the band gap and energy levels one would obtain from "conventional" polymers incorporating un-modified **DTBT** units.

There have been attempts to incorporate alkyl or alkoxy chains on the **DTBT** unit in order to enhance both the solubility and molecular weight of resulting polymers. In one study, Shi *et al.* copolymerized alkylated fluorene with **DTBT** modified with alkoxy chains on the 3 position of these thienyl units, resulting in a polymer with much higher molecular weight (number average molecular weight, *Mn*, 68 kg/mol) and better solubility[112] than those of original polymers without any soluble chains on the **DTBT** unit.[105] However, these electron-donating alkoxy groups on the **DTBT** unit caused the

HOMO level of the resulting polymer to increase, which led to a lower V_{oc}. More recently, Wang *et al.* attempted to add additional alkylated thiophene units to extend the **DTBT** unit.[113] The resulting D-A polymer with alkylated fluorene as the donor unit showed a smaller band gap, higher molecular weight and better solubility compared with the original copolymer that incorporated alkylated fluorene and **DTBT (PF-DBT)**.[105,114] Unfortunately, the overall efficiency of this new polymer (**PFO-M3**) was smaller (2.63%) than that of the original **PF-DBT** (up to 3.5%),[102] in spite of a lower band gap and a similar HOMO energy level of **PFO-M3**. In another study, Song *et al.* prepared polymers incorporating a **DTBT** unit modified with either alkyl chains on the 4 position of these thienyl units or alkoxy chains on the 3 postion.[115] Compared with polymers incorporating **DTBT** without any decorated chains, these modified ones were more soluble. Again, the overall BHJ device efficiencies of polymers with such modified **DTBT** were lower than that of the corresponding **DTBT** based polymer without alkoxy/alkyl chains, mainly due to the lower J_{sc} in the former case. Computational simulation revealed that a severe steric hindrance was introduced by these alkyl/alkoxy chains, leading to a twisted conjugated backbone in both polymers with such modified **DTBT** units.[115] Therefore the hole mobilities of the polymers incorporating such modified **DTBT** units were noticeably lower than that of polymers with unmodified **DTBT** unit, which accounted for a smaller J_{sc} in the former case.[115] In an earlier study, Jayakannan *et al.* prepared the homopolymers of alkylated **DTBT** by varying alkyl chains on either 3 or 4 positions of thienyl groups.[116] Though relatively high molecular weight polymers were obtained, the steric hindrance introduced by these alkyl chains in these polymers led to much larger band gaps than that of the homopolymer of unmodified

DTBT.[117] All these studies acknowledged the advantage of employing **DTBT** units in constructing D-A low band gap polymers for BHJ solar cells. More importantly, these previous studies underscored the importance of the functionalization of **DTBT** units to reach high molecular weight and good solubility of resulting polymers, which should lead to PV devices with higher efficiencies. Unfortunately, no improvements on BHJ devices efficiency were observed from these reported polymers that incorporated modified **DTBT** units.

Previously we have demonstrated that by incorporating a donor – bithiophene fused with a benzene moiety (benzo[2,1-*b*:3,4-*b'*]dithiophene, **BDT**) and an acceptor – benzothiadiazole (**BT**), a low band gap polymer (**PBDT-BT**) was obtained together with a low HOMO energy level.[118] However, an efficiency of only 0.6 % was obtained for **PBDT-BT**, mainly due to a small J_{sc} of 2.06 mA/cm^2. This low current was ascribed to a low hole mobility (4.21×10^{-6} cm^2/V·s) and a low molecular weight (M_n: 10.1 kg/mol), both of which would be alleviated by introducing the modified **DTBT** units. Thus a library of polymers incorporating **BDT** as the donor and modified **DTBT** as the acceptor unit was envisioned and synthesized (**Figure 2-1**). Alkyl chains, rather than alkoxy chains, were used to mitigate the possible elevation of the HOMO energy levels of the resulting polymers. Three variations of modified **DTBT** units were prepared: alkyl side chains at (a) the 5 and 6 positions of 2,1,3-benzothiadiazole (**DTsolBT**), (b) 3 positions of the flanking thienyl groups (**3DTBT**), and (c) 4 positions (**4DTBT**). For comparison, the polymer with unmodified **DTBT** (**PBDT-DTBT**) was also synthesized.

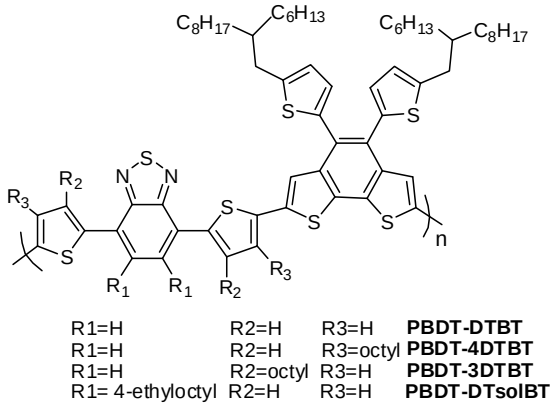

Figure 2-1. Chemical structures of **PBDT-DTBT**, **PBDT-4DTBT**, **PBDT-3DTBT** and **PBDT-DTsolBT**

As expected, much higher molecular weights (~ 30 kg/mol) and better solubility in processing solvents were observed for all three polymers with alkylated **DTBT** units than those of **PBDT-DTBT** (9 kg/mol). Interestingly, contrary to results from previous studies, optical and electrochemical studies disclose almost identical band gap and energy levels between **PBDT-4DTBT** and **PBDT-DTBT**. These results indicate that anchoring solubilizing alkyl chains on the 4 positions of **DTBT** only introduces a minimum steric hindrance within **PBDT-DTBT**, thereby maintaining the extended conjugation of the fundamental structural unit (**PBDT-DTBT**). Furthermore, the polymer containing the "properly" modified **DTBT** unit, **PBDT-4DTBT**, shows an improved hole mobility of 9.2×10^{-6} $cm^2/V{\cdot}s$ than that of **PBDT-DTBT** (3.9×10^{-6} $cm^2/V{\cdot}s$) or **PBDT-BT** (4.21×10^{-6} $cm^2/V{\cdot}s$). This noticeably higher mobility of **PBDT-4DTBT**, together with its low band gap and relatively low HOMO energy level inherited from **PBDT-DTBT**, leads to a significantly improved efficiency of related BHJ solar cells (up to 2.2 % has been observed), triple the efficiency obtained from BHJ devices fabricated from either **PBDT-**

DTBT (0.72 %) or **PBDT-BT** (0.6 %).[118] A thorough investigation of this library of structurally related polymers unveils a complete picture of the influence of alkyl chains on different positions of **DTBT** units on the optical, electrical and photovoltaic properties of resulting polymers.

2.2. Monomer Synthesis

In order to obtain a high molecular weight polymer with good solubility, long, branched alkyl chains were attached at the central **BT** unit during the synthesis of **DTsolBT** (**M1** in **Figure 2-2**). 4-ethyloct-1-yne was prepared from commercially available 2-ethylhexyl bromide with overall yield of > 60%. A Sonogashira coupling was employed to attach the 4-ethyloct-1-yne to 1,2-dibromo-4,5-dinitrobenzene (**2**) obtained by nitration of 1,2-dibromo benzene (**1**), leading to the alkylated dinitrobenzene (**3**). Both triple bonds and nitro groups were reduced simultaneously via Pd/H_2, yielding alkylated diaminobenzene (**5**). Treating (**5**) with thionyl chloride under basic condition afforded compound (**6**), the alkylated benzothiadiazole (**solBT**), which then underwent several conventional halogenations and coupling reaction to monomer **A1**, the brominated **DTsolBT**.

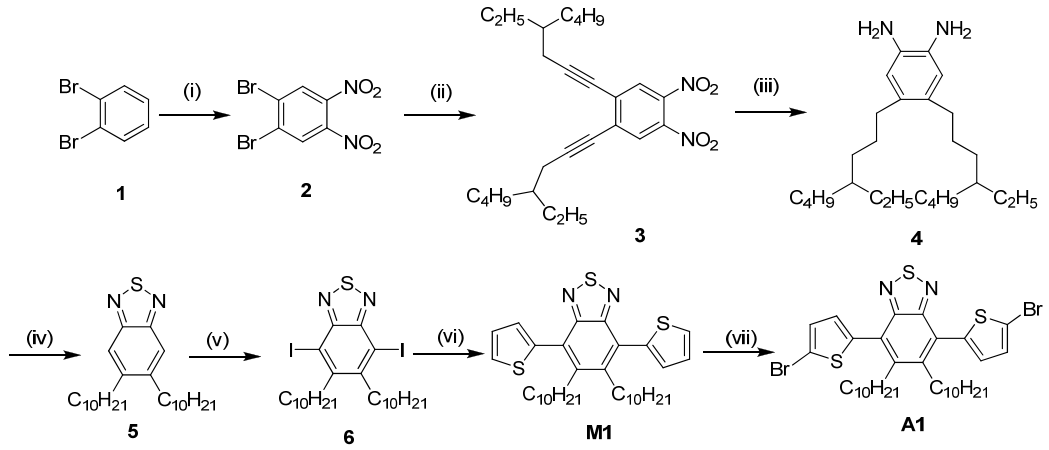

Reagents and conditions: (i) fuming H_2SO_4, fuming HNO_3, overnight; (ii) 4-ethyloct-1-yne, Et_3N, $Pd(PPh_3)_2Cl_2$, CuI, 3 h; (iii) Pd/C(10%Pd), ethyl acetate:methanol 2:1, H_2; (iv) $SOCl_2$, Et_3N, CH_2Cl_2, refulx 5 h; (v) I_2, $NaIO_3$, H_2SO_4, HOAc, H_2O, reflux overnight; (vi) thiophene,BuLi, $ZnCl_2$, 30 min; $Pd(OAc)_2$, PPh_3, THF, reflux 16 h; (vii) NBS, $CHCl_3$:HOAc=2:1, r.t, overnight

Figure 2-2. Synthesis of monomer A1 (brominated **DTsolBT**)

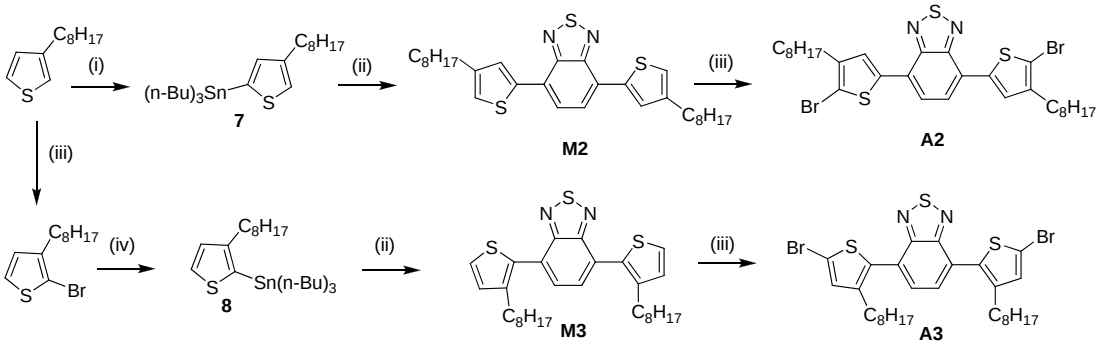

Reagents and conditions: (i) LDA, 0°C, 1 h, $(n\text{-}Bu)_3SnCl$, 0°C, 30 min; (ii) $Pd(PPh_3)_2Cl_2$, THF, reflux overnight; (iii) NBS, THF, r.t. overnight; (iv) BuLi, -78°C, 2 h, $(n\text{-}Bu)_3SnCl$, -78°C, 30 min

Figure 2-3. Synthetic route for **A2** and **A3 (**brominated **3DTBT** and **4DTBT**)

Synthesis of **A2**, **A3** is depicted in **Figure 2-3**. They were synthesized via slightly modified literature procedures (shown in **Experimental Section**).[116,119] It is worth noting that the deprotonation of 3-octyl thiophene selectively occurred at the more acidic 5 position, followed by stannylation to yield (**7**). The other isomer (**8**), with tributyl tin anchored at 2 position was obtained via 2-bromo-3-octyl thiophene as the intermediate, since the bromination via NBS was selective at the more nucleophilic 2 position. Then

halogen exchange with *n*-BuLi led to lithiated 2 position, which was subsequently quenched by $(n\text{-}Bu)_3SnCl$ to yield the 2-stannylated (**8**). The unmodified **DTBT** monomer was synthesized following a literature report.[120]

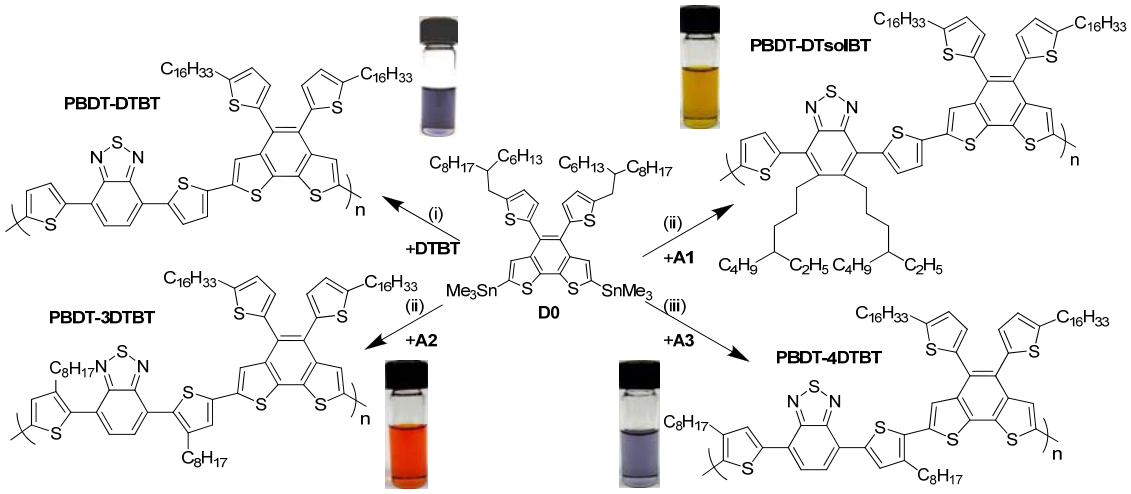

Figure 2-4. Polymerization of conjugated polymers by Stille coupling reaction

2.3. Polymer synthesis

Four polymers were therefore prepared by a palladium catalyzed Stille cross coupling polycondensation of benzo[2,1-*b*:3,4-*b*′]dithiophene (**BDT**) distannane (**D0**) with brominated **DTBT** and its derivatives (**Figure 2-4**). The polymerization of **PBDT-DTBT** was stopped after 18 hours when precipitation was observed. The crude polymer was then precipitated from methanol and extracted via a Soxhlet apparatus with acetone, hexane, and finally chloroform. Only the chloroform soluble portion was collected in order to obtain a high molecular weight, solution processable polymer. A noticeable amount of residue remained in the extraction thimble after the extraction with chloroform. This presumably high molecular weight portion was discarded since it would not be

solution processable, which consequently led to a relatively low yield (51%) of the polymerization. Not surprisingly, the measured molecular weight of **PBDT-DTBT** is low: number average (M_n) is only 9 kg/mol and weight average (M_w) is 12 kg/mol, mainly due to the poor solubility of **PBDT-DTBT**.

On the other hand, adding solubilizing chains to the **DTBT** unit significantly increases the molecular weight of the resulting polymers and improves their solubility in commonly employed solvents such as THF and chloroform. Both of these features, high molecular weight and good solubility, also explain the high yields of these polymerizations even after crude polymers were extensively purified (**Table 2-1**). The structures of these purified polymers were confirmed by ^{1}H-NMR (**Appendix 2**). Microwave-assisted polymerization was ultilized in synthesizing PBDT-4DTBT because it has been reported to yield high molecular weight in a much shortened polymerization time, half an hour comparing with days in conventional polymerization[121,122].

Table 2-1. Polymerization results for polymers

	Yield [%]	M_n[a] [kg/mol]	M_w[a] [kg/mol]	PDI[a]	T_d[b] [°C]
PBDT-DTBT	51%	9	12	1.31	270
PBDT-4DTBT	75%	27	54	1.80	420
PBDT-3DTBT	88%	37	84	3.07	436
PBDT-DTsolBT	87%	30	92	2.44	440

[a] Determined by GPC in tetrahydrofuran (THF) using polystyrene standards. [b] The temperature of degradation corresponding to a 5% weight loss determined by TGA at a heating rate of 10 °C/min.

2.4. Optical and Electrochemical Properties

The positioning of attached solubilizing alkyl chains on the **DTBT** unit seemingly has little impact on the molecular weight and solubility of related polymers: high molecular weight and good solubility have been unanimously obtained for polymers incorporating alkylated **DTBT** units. However, dramatic effects were observed on the optical and electrochemical properties of polymers incorporating alkylated **DTBT** units, depending upon where these alkyl chains are attached on the **DTBT** units. It is surprising to discover that anchoring these alkyl chains on the 4 positions of these thienyl groups on the **DTBT** unit have negligible impact on the absorption and band gap of **PBDT-4DTBT** compared with those of **PBDT-DTBT** in solution (**Figure 2-5a**). In thin films, the un-substituted **PBDT-DTBT** has a strong tendency to π-stack: a pronounced absorption increase was observed from about 550 nm, extending up to almost 800 nm. The alkylated **PBDT-4DTBT** shows similar behavior of strong stacking, though the absorption edge is slightly blue shifted compared with that of **PBDT-DTBT** (735 nm vs. 761 nm) (**Table 2-2**), indicative of a slight steric hindrance from these extra alkyl chains in the solid state. Nevertheless, similarly small band gaps (< 1.7 eV) have been observed for both polymers. These results suggest that anchoring alkyl chains on the 4 positions of the thienyl groups (i.e. **4DTBT**) introduces minimum steric hindrance to the original

conjugated backbone of **PBDT-DTBT**, maintaining the electron delocalization from D-A structures.

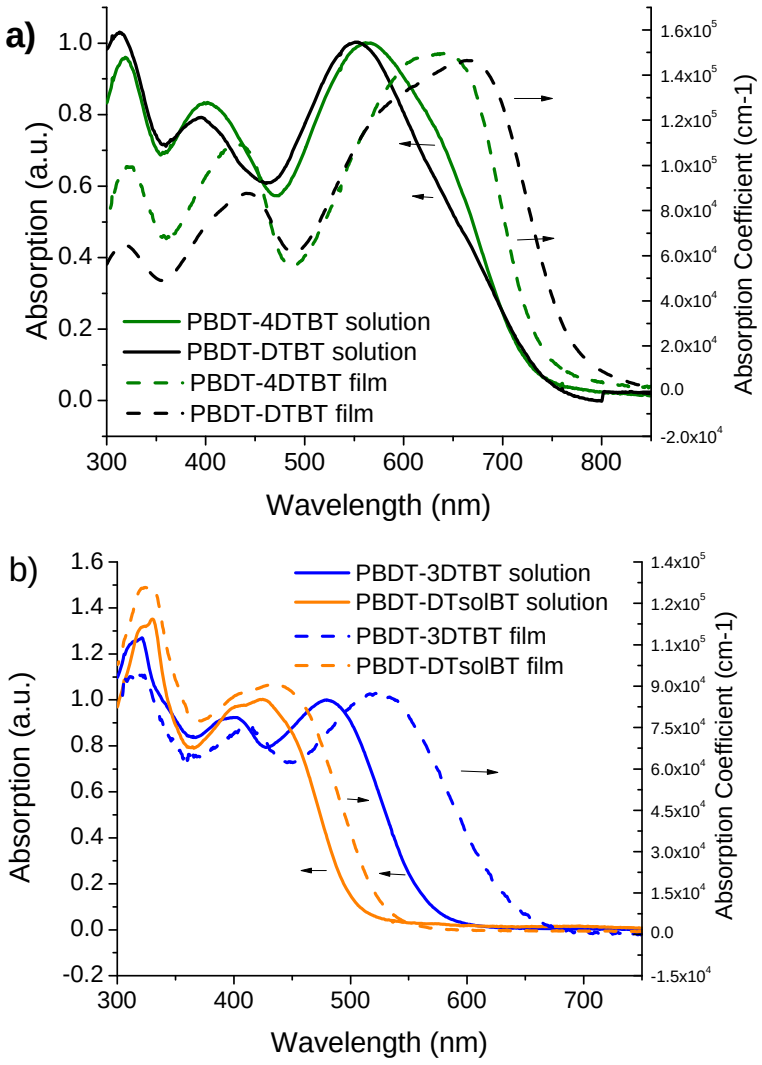

Figure 2-5. UV-Vis spectra of all the polymers: a) **PBDT-DTBT** and **PBDT-4DTBT** polymers in chloroform solution (solid line) and in solid film (dash line) and b) **PBDT-DTsolBT** and **PBDT-3DTBT** polymers in chloroform solution (solid line) and in solid film (dash line)

Table 2-2. Optical and electrochemical data of all polymers

	UV-Vis Absorption						PL	Cyclic Voltammetry		DFT
	$CHCl_3$ solution			Film			$CHCl_3$ Solution	E^{ox}_{onest} (V)	E^{red}_{onest} (V)	Calculated HOMO [eV]
polymer	λ_{max} [nm]	λ_{onset} [nm]	$E_g{}^a$ [eV]	λ_{max} [nm]	λ_{onset} [nm]	$E_g{}^a$ [eV]	λ_{max} [nm]	HOMO [eV]	LUMO [eV]	
PBDT-DTBT	550	738	1.68	666	761	1.63	628	0.47/-5.27	-1.64/-3.16	-5.22
PBDT-DTsolBT	425	500	2.48	435	528	2.35	580	0.89/-5.69	-1.79/-3.01	-5.43
PBDT-3DTBT	475	560	2.21	520	628	1.97	654	0.58/-5.38	-1.67-3.13	-5.33
PBDT-4DTBT	567	726	1.70	641	735	1.69	619	0.41/-5.21	-1.82-2.98	-5.19

[a] Calculated from the intersection of the tangent on the low energetic edge of the absorption spectrum with the baseline.

When these alkyl chains are located at either the 3 positions of the thienyl groups (**3DTBT**) or the 5 and 6 positions of the 2,1,3-benzothiadiazole (**DTsolBT**), severe steric hindrance is introduced between the flanking thienyl groups and the central **BT** unit. The conjugated backbone is thereby twisted at the D-A linkage, significantly affecting the effective conjugation between the donor and the acceptor (**BT**). Large band gaps were observed for these two polymers (2.21 eV for **PBDT-3DTBT** and 2.48 eV for **PBDT-DTsolBT**). The even larger band gap of **PBDT-DTsolBT** implies much stronger steric hindrance (thereby twisting of the conjugated backbone) is introduced when alkyl chains are located at the central **BT** unit. The twisting of the backbone due to the **DTsolBT** unit also explains the fact that nearly negligible stacking was observed for **PBDT-DTsolBT** in

thin film, while an appreciable red shift in thin film was still observed for **PBDT-3DTBT**. Finally, both **PBDT-DTBT** and **PBDT-4DTBT** are much more absorptive in the solid state than either **PBDT-3DTBT** or **PBDT-DTsolBT**: similar absorption coefficients of about 1.5×10^{-5} cm^{-1} for the former two polymers at their maximum absorption wavelength, significantly greater than those of the latter two (up to 0.9×10^{-5} cm^{-1}) at their maxima.

Probing this library of polymers with identical conjugated backbone via cyclic voltammetry provides direct evidence on how the difference in positioning these alkyl chains affects the energy levels of these related polymers. The lowest unoccupied molecular orbital (LUMO) is essentially dominated by the common acceptor unit (**BT**), which explains why all four polymers show similar reduction potential and LUMO energy levels (**Figure 2-6** and **Table 2-2**). However, the HOMO energy levels disclose dramatic differences. The HOMO energy levels of **PBDT-4DTBT** and **PBDT-DTBT** differ only slightly (– 5.27 eV vs. – 5.21 eV), further indicating that anchoring alkyl chains at the 4 positions of thienyl groups has almost negligible influence on the extended conjugation of the D-A polymer. The introduction of two electron rich thienyl groups to the original **PBDT-BT** increases the electron density of the conjugated backbone, leading to an elevated HOMO energy level of **PBDT-DTBT** (– 5.21 eV) compared with that of **PBDT-BT** (– 5.34 eV).[118] Shifting these alkyl chains to the 3 positions of thienyl groups (**PBDT-3DTBT**) leads to an appreciable conjugation twisting at the linkage of thienyl groups with the central **BT** unit. The apparently reduced electron delocalization renders a lowered HOMO energy level of – 5.38 eV. In the case of **PBDT-DTsolBT**, a very low HOMO level of – 5.69 eV was observed, strikingly similar to that of the homopolymer of

BDT (**HMPBDT**, – 5.70 eV).[118] This apparent coincidence implies that the severe steric hindrance from **DTsolBT** may disrupt the conjugation between the "donor" and the "acceptor" in **PBDT-DTsolBT**. Thus the HOMO is essentially localized at the **BDT** unit (and partially on thienyls), which explains similar HOMO levels of **PBDT-DTsolBT** and **HMPBDT**.

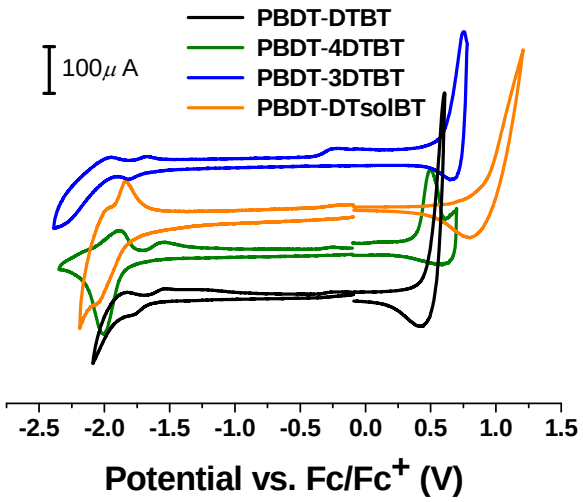

Figure 2-6. Cyclic voltammograms of the oxidation and reduction behavior of thin films of **PBDT-DTBT**, **PBDT-4DTBT**, **PBDT-3DTBT** and **PBDT-DTsolBT**

2.5. Computational Study

Computational study of this series of polymers provides insightful information to account for the observed difference of optical and electrochemical properties. To simplify the calculation, only one repeating unit of each polymer was subject to the calculation, with alkyl chains replaced by CH_3 groups. The optimized geometry, HOMO and LUMO energy levels and their electron density distributions were calculated at the

B3LYP/6-311+G* level of theory [123,124] using density functional theory and Gaussian 03 package (**Figure 2-7**).[125]

The dihedral angles between two thienyl groups with central **BT** unit as well as the donor **BDT** unit quantitatively measure the steric hindrance introduced by these alkyl chains. All three dihedral angles for **PBDT-DTBT** are small (**Table 2-3**), indicative of complete conjugation of all participating aromatic units. The electron density is well delocalized along the conjugated backbone, as displayed by the isosurface of the HOMO energy level of **PBDT-DTBT** (**Figure 2-7**). There is only a slight increase of the dihedral angle between the 4-substituted thienyl group and **BDT** unit in **PBDT-4DTBT**, confirming the minimum steric hindrance introduced by the **4DTBT**. The electron density is also delocalized in the HOMO of **PBDT-4DTBT**, though slightly biased towards the **BDT** unit compared with that of **PBDT-DTBT**. These very similar – however slightly different – HOMO isosurfaces explain that only a slight difference (0.06 eV) was observed for the HOMO energy levels of **PBDT-DTBT** and **PBDT-4DTBT**. Furthermore, the electron density of LUMO energy levels of both **PBDT-DTBT** and **PBDT-4DTBT** are essentially localized on the **DTBT** unit, supporting observed similar LUMO energy levels. All these similarities contribute to the similar UV-Vis absorptions and band gaps of **PBDT-DTBT** and **PBDT-4DTBT**.

Moving these alkyl chains away from the vicinity of **BDT** unit in the case of **PBDT-3DTBT** and **PBDT-DTsolBT** relieves the steric hindrance between substituted **DTBT** and **BDT** unit, recovering small numbers on dihedral angle 3 (**Table 2-3**). However, greater steric hindrance is formed between thienyl groups and central **BT** unit, as shown by a dramatic numerical increase in dihedral angles 1 and 2. For example, over 50°

angles have been calculated for the dihedral angels between thienyl groups and **BT** in **PBDT-DTsolBT**. This severe steric hindrance essentially breaks the conjugation at the linkages between thienyl groups and **BT**, thereby rendering the HOMO of **PBDT-DTsolBT** localized at the donor **BDT** unit. Compared with **PBDT-DTsolBT**, smaller torsional angles between thienyl groups and **BT** unit are calculated in the case of **PBDT-3DTBT**. Therefore the electron density is slightly extended to the **BT** unit in the HOMO of **PBDT-3DTBT**. Comparing the isophases of all three polymers incorporating modified **DTBT** unit clearly explains why the measured HOMO energy level of **PBDT-3DTBT** is between that of **PBDT-4DTBT** and that of **PBDT-DTsolBT**.

Table 2-3. Calculated dihedral angels of polymers [a]

Polymer	Dihedral angle 1 (°)	Dihedral angle 2 (°)	Dihedral angle 3 (°)
PBDT-DTBT	4.1	10.9	14.1
PBDT-4DTBT	5.2	14.3	30.2
PBDT-3DTBT	50.7	36.2	17.7
PBDT-DTsolBT	58	55.2	19.9

[a] Calculations were carried out for one repeating unit of each polymer, in gas phase, at temperature 0 K and in vacuum.

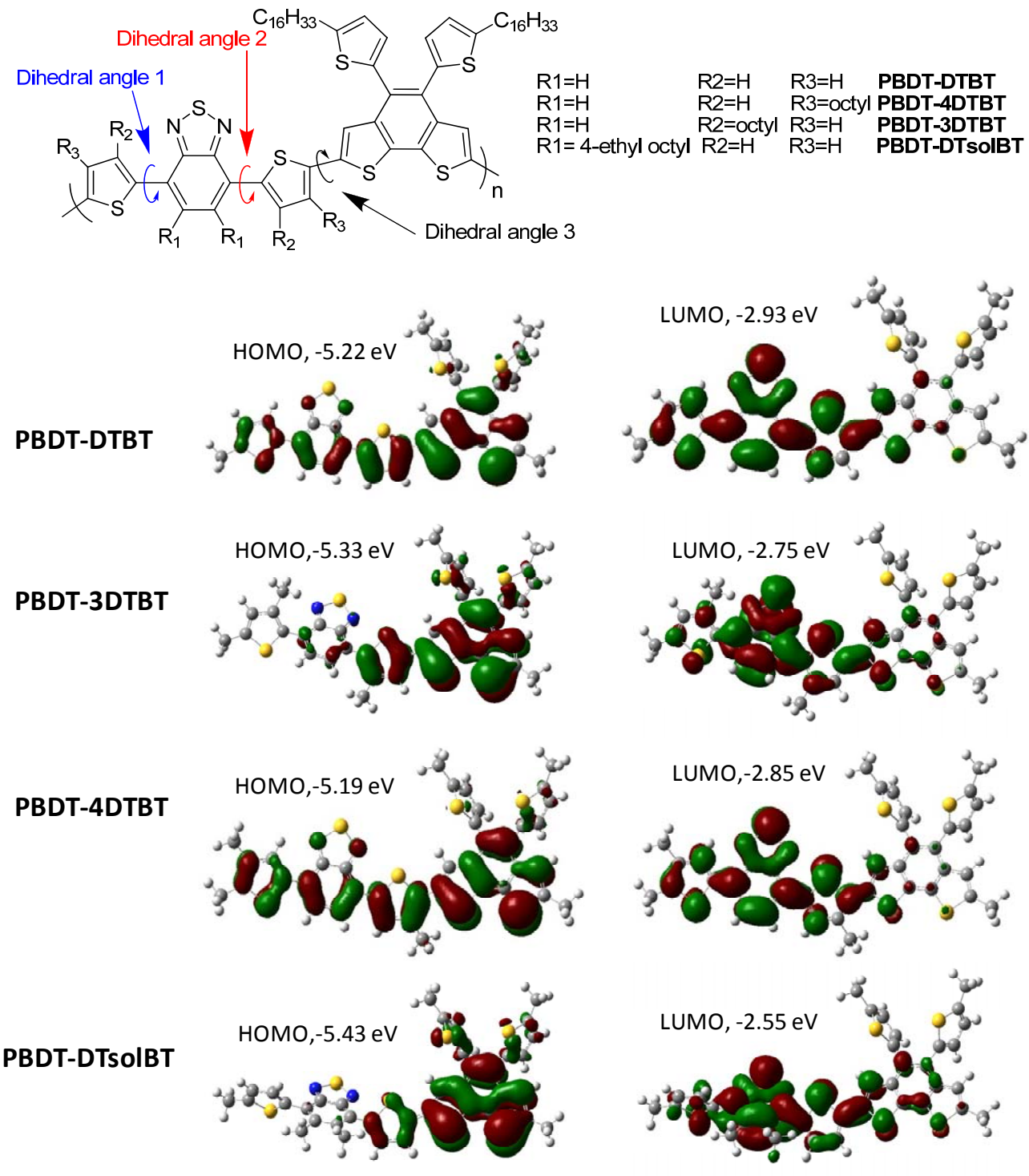

Figure 2-7. Calculation of HOMO (left) and LUMO (right) orbitals of polymers

2.6. Photovoltaic Properties

Bulk heterojunction photovoltaic devices were constructed to investigate the influence on photovoltaic properties introduced by the subtle change in positioning alkyl chains. For fair comparison, care was taken during the processing to maintain similarly structured devices: (a) because this series of polymers have the identical conjugated backbone with only variations on the size and position of side chains, all polymers were blended with $PC_{61}BM$ at 1:1 weight ratio in chloroform at 5 mg/mL; (b) identical spin rate (1100 RPM) and time (1 min) were employed to achieve similar film thicknesses. A typical fabricated solar cell has a configuration of glass/ITO/PEDOT:PSS(40 nm)/polymer:$PC_{61}BM$ blend (~100 nm)/Ca(30 nm)/Al(70 nm) (**Experimental Section**). The current-voltage characteristics of solar cells based on these four polymers blended with $PC_{61}BM$ are shown in **Figure 2-8**. Representative performance parameters of solar cells are listed in **Table 2-4**.

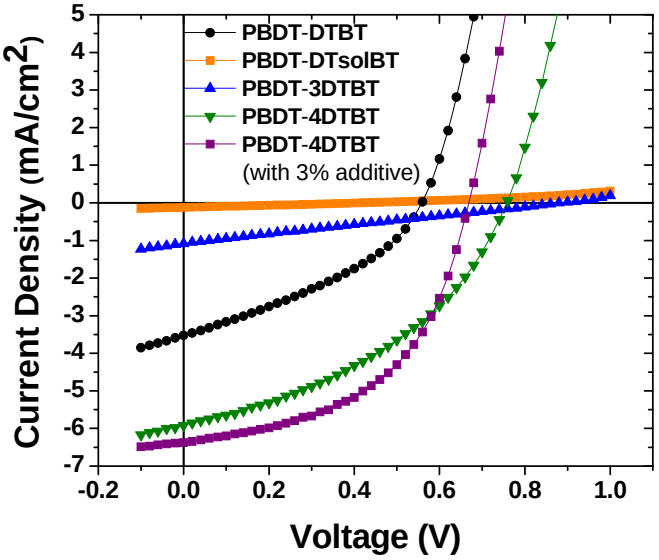

Figure 2-8. Characteristic J-V curves of the optimized devices of polymer based BHJ solar cells under 1 Sun condition (100 mW/cm^2)

Table 2-4. PV performances of polymers

Polymer	Polymer: $PC_{61}BM$	Thickness (nm)	V_{oc} (V)	J_{sc} (mA/cm^2)	*FF*	η (%)
PBDT-4DTBT **(3% DIO)**	1:1	95	0.67	6.38	50.79%	2.17%
PBDT-4DTBT	1:1	100	0.75	5.92	41.27%	1.83%
PBDT-3DTBT	1:1	85	0.89	0.94	24.74%	0.21%
PBDT-DTsolBT	1:1	80	0.43	0.12	26.35%	0.01%
PBDT-DTBT	1:1	65	0.55	3.53	36.8%	0.72%

Due to its low solubility, **PBDT-DTBT** was dissolved into chloroform at high temperature (~ 60 °C). Polymers noticeably aggregated when the solution cooled. Therefore, the solution of **PBDT-DTBT** and $PC_{61}BM$ was sonicated during cooling, which precipitated the polymer, resulting in a processable dispersion.[126] Films of **PBDT-DTBT**:$PC_{61}BM$ are the thinnest (65 nm) among all the polymer:$PC_{61}BM$ films, which is attributed to the low viscosity of the dispersion. A relatively low V_{oc} of 0.55 V was observed, likely due to the elevated HOMO energy level of **PBDT-DTBT** in the aggregated state. Excessive aggregation would also likely lead to form polymers-only domains so large that excitons cannot reach a donor/acceptor interface before they decay to the ground state.[127] Thus the measured J_{sc} is only 3.53 mA/cm^2 despite the low band gap (1.63 eV) of **PBDT-DTBT**. Together with a *FF* of 0.37, an overall conversion efficiency of 0.72% is obtained for **PBDT-DTBT**. Not surprisingly, attaching these alkyl chains greatly improved the solubility of resulting polymers; however, the anchoring positions significantly impact the photovoltaic properties of related polymer based BHJ

PV cells. As discussed earlier, anchoring solubilizing chains at 4 positions of these thienyl groups (**PBDT-4DTBT)** has a minimum impact on the band gap and energy levels, compared with those of **PBDT-DTBT**. More importantly, the newly acquired solubility/processibility of **PBDT-4DTBT** renders a much improved intermixing with $PC_{61}BM$ without severe aggregation of polymers. Therefore, the BHJ solar cell of **PBDT-4DTBT**:$PC_{61}BM$ displays a V_{oc} of 0.75 V (0.2 V higher than that of **PBDT-DTBT** based solar cell). The low band gap (1.69 eV) leads to a much higher J_{sc} (5.92 mA/cm^2), leading to an overall efficiency of 1.83%. By applying 3% 1,8-diiodoocane as an additive into the processing solvent (chloroform) to modify the film morphology,[127,128] a higher efficiency of 2.17% is achieved, mainly due to the noticeably increased *FF* (**Table 2-4**). Adding additives appears to promote more ordering in the polymer domains, as indicated by a ~ 50 nm red shift in the absorption maximum of blends processed with additive (**Figure 2-9**).[128] This noticeable red shift in the absorption maximum might account for the improved J_{sc} of the devices processed with additives.

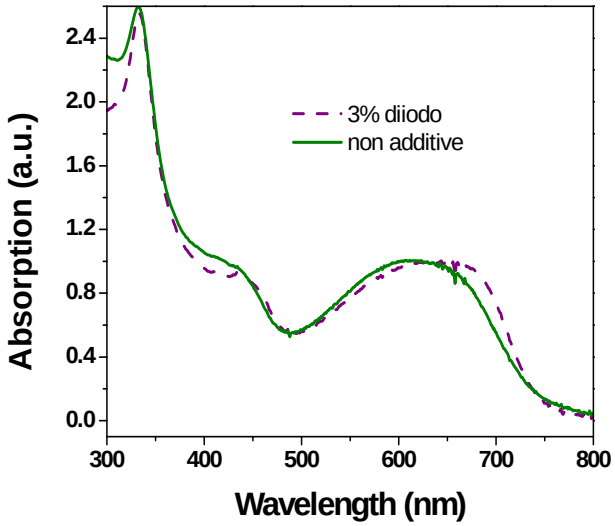

Figure 2-9. Comparison of absorption of **PBDT-4DTBT**:$PC_{61}BM$ (1:1) thin films with and without additive

Shifting alkyl chains to the inner core of **DTBT** introduces significant steric hindrance between the aromatic units on the conjugated backbone, leading to much increased band gaps. The severe steric hindrance would also weaken the interaction between polymer chains, leading to low hole mobilities. Furthermore, the electron density of HOMO energy levels of **PBDT-3DTBT** and **PBDT-DTsolBT** are essentially localized at the **BDT** unit (**Figure 2-7**). The lack of delocalization would reduce the possibility of excitons moving to donor/acceptor interface and increase the geminate recombination of the recently dissociated excitons. Therefore low efficiencies were observed for both **PBDT-3DTBT** (0.21%) and **PBDT-DTsolBT** (0.01%). The very small efficiency of **PBDT-DTsolBT** is largely due to severely disrupted conjugation between thienyl groups and the **BT** unit (**Table 2-3** and **Figure 2-7**).

The BHJ devices of **PBDT-DTBT** and **PBDT-4DTBT** were further tested for their incident photon to current efficiency (IPCE). For comparison, the IPCE data are shown together with the absorption of blended thin films (**Figure 2-10**). These two films absorb light rather equally when the absorption is normalized by film thickness, though the **PBDT-DTBT** based film has slightly more absorption in the near IR region. The IPCE curves follow individual film absorptions, with maxima at 430 nm and 600 nm. However, the maximum IPCE value of **PBDT-4DTBT** based device is almost twice as much as that of **PBDT-DTBT** based device (29% vs. 16% at 600 nm). Since the film thickness of **PBDT-4DTBT** based device is only about 50% thicker than that of **PBDT-DTBT** (100 nm vs. 65 nm), these indicate that charges have much greater chance to reach

the electrodes in the case of **PBDT-4DTBT** based device, possibly due to a higher hole mobility in **PBDT-4DTBT** devices.

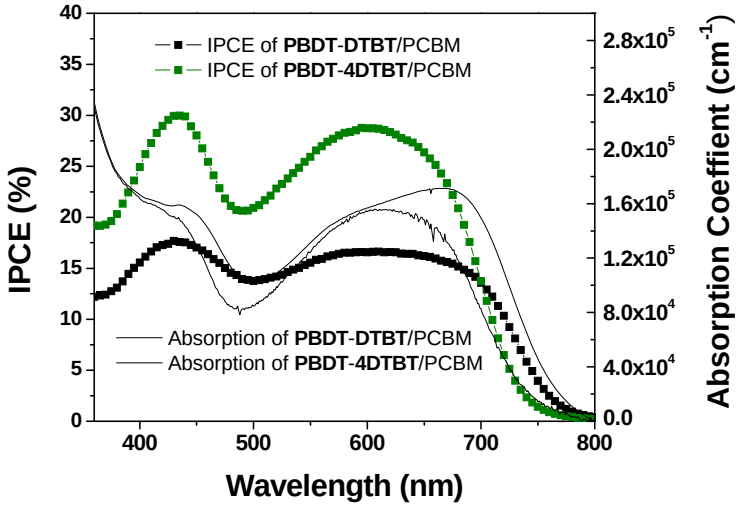

Figure 2-10. IPCE and absorption of **PBDT-DTBT** and **PBDT-4DTBT** (absorption is normalized by film thickness)

In order to further understand the dramatically different PV performance of these two polymers, **PBDT-DTBT** and **PBDT-4DTBT**, hole mobility values were estimated via space-charge limit current (SCLC) by fabricating hole-only devices (**Appendix 2**).[129,130] For pure polymers, the measured mobilities are similar for both polymers (**Table 2-4**), with **PBDT-4DTBT** having slightly higher hole mobility. The hole mobility difference is more noticeable in the polymer/$PC_{61}BM$ blend. **PBDT-4DTBT**/$PC_{61}BM$ blend demonstrates a much higher mobility, double that of **PBDT-DTBT**/$PC_{61}BM$ blend (**Table 2-5**). As indicated earlier, **PBDT-DTBT** has a strong tendency to stack, which is desirable in improving mobility within a polymer-only domain. However, these low

molecular weight polymers, i.e. short chains, limit the interaction between different domains, leading to an overall suppressed mobility.[104] On the other hand, the properly positioned alkyl chains offer the excellent solubility and high molecular weight of **PBDT-4DTBT**. The high molecular weight of **PBDT-4DTBT** (i.e. long polymer chains) would connect locally ordered individual domains, thereby improving the hole mobility in the polymer only devices.[131] Furthermore, the good solubility of **PBDT-4DTBT** ensures a good miscibility with $PC_{61}BM$ in the processing solvent. The clustering of $PC_{61}BM$ during solvent evaporation could help further aggregation of **PBDT-4DTBT** while maintaining the connection between polymer only domains, further improving the hole mobility. In addition, using additives appears to improve the film morphology with more ordering in the polymer domains, which explains an even higher hole mobility (1.60×10^{-6} $cm^2/V{\cdot}s$). These observations signify the importance of high molecular weight and good solubility of polymers in improving device efficiencies.

Table 2-5. Mobility of polymers under SCLC condition

Polymer only	Thickness (nm)	Mobility ($cm^2/V{\cdot}s$)	Polymer: $PC_{61}BM$	Thickness (nm)	Mobility ($cm^2/V{\cdot}s$)
PBDT-4DTBT	55	4.36×10^{-6}	1:1 + 3% diiodooctane	75	1.60×10^{-5}
			1:1	75	9.20×10^{-6}
PBDT-DTBT	55	2.91×10^{-6}	1:1	65	3.94×10^{-6}

2.7. Conclusions

It has been demonstrated that introducing alkyl chains onto various positions of the dithienyl benzothiadiazole (**DTBT**) can significantly increase the molecular weight and solubility of related polymers. However, the anchoring positions of these alkyl chains have strong influence on the optical and electrochemical properties of these structurally similar polymers with identical conjugated backbones. Contrary to previous reports, our study indicates that attaching alkyl chains on the 4 positions of these thienyl groups (i.e., **4DTBT**) only introduces minimum steric hindrance into the related D-A polymer (**PBDT-4DTBT**). Therefore **PBDT-4DTBT** maintains almost identical band gap and energy levels compared with **PBDT-DTBT** (unmodified **DTBT**). More importantly, the additional high molecular weight and excellent solubility of **PBDT-4DTBT** leads to a more uniform mixture with $PC_{61}BM$, with better control on the film morphology. All these features of **PBDT-4DTBT** contribute to a much enhanced efficiency (up to 2.2%) of **PBDT-4DTBT**, significantly higher than that of **PBDT-DTBT** based devices (0.7%). Our discovery reinforces the importance of high molecular weight and good solubility of donor polymers for BHJ solar cells, in addition to a low band gap and a low HOMO energy level, in order to further enhance the device efficiencies. Finally, we believe the strategy of "properly" modifying the acceptor unit can be applied to other D-A polymers as well. For example, **4DTBT** can be employed in conjugation with other fused bithiophene based polycyclic aromatics to construct D-A polymers with low band gap and low HOMO energy levels. If a higher mobility together with better controlled morphology can be achieved by these new polymers, an even higher efficiency can be expected.

2.8. Experimental Section

For the experimental details about electrochemistry, spectroscopy and SCLC mobility measurements please check **Appendix 1**. And please check **Appendix 2** for supporting information.

Polymer solar cell fabrication and testing:

Glass substrates coated with patterned indium-doped tin oxide (ITO) were purchased from Thin Film Devices, Inc. The 150 nm sputtered ITO pattern had a resistivity of 15Ω/□. Prior to use, the substrates were ultrasonicated for 20 minutes in acetone followed by deionized water and then 2-propanol. The substrates were dried under a stream of nitrogen and subjected to the treatment of UV-Ozone over 30 minutes. A filtered dispersion of PEDOT:PSS in water (Baytron PH500) was then spun cast onto clean ITO substrates at 4000 rpm for 60 seconds and then baked at 140 °C for 10 minutes to give a thin film with a thickness of 40 nm. A blend of polymer and $PC_{61}BM$ (1:1 w/w, 10 mg/mL for polymers) was dissolved in chloroform with heating at 60 °C for 6 hours. All the solutions (except in the case of **PBDT-DTBT**, which has a poor solubility) were filtered through a 0.45 μm poly(tetrafluoroethylene) (PTFE) filter, spun cast at 1100 rpm for 60 seconds onto PEDOT:PSS layer. The substrates were then dried at room temperature in the glovebox under nitrogen atmosphere for 12 hours. The thicknesses of films were recorded by a profilometer (Alpha-Step 200, Tencor Instruments). The devices were finished for measurement after thermal deposition of a 30 nm film of calcium and a 70 nm aluminum film as the cathode at a pressure of $\sim 1\times10^{-6}$ mbar. There are 8 devices per substrate, with an active area of 12 mm^2 per device. Device

characterization was carried out under AM 1.5G irradiation with the intensity of 100 mW/cm^2 (Oriel 91160, 300 W) calibrated by a NREL certified standard silicon cell. Current versus potential (I-V) curves were recorded with a Keithley 2400 digital source meter. EQE were detected under monochromatic illumination (Oriel Cornerstone 260 ¼ m monochromator equipped with Oriel 70613NS QTH lamp) and the calibration of the incident light was performed with a monocrystalline silicon diode. All fabrication steps after adding the PEDOT:PSS layer onto ITO substrate, and characterizations were performed in gloveboxes under nitrogen atmosphere.

Reagents and Instrumentation:

All reagents and chemicals were purchased from commercial sources (Aldrich, Acros, Strem, Fluka) and used without further purification unless stated otherwise. Reagent grade solvents were dried when necessary and purified by distillation. Microwave assisted polymerizations were conducted in a CEM Discover Benchmate microwave reactor. Gel permeation chromatography (GPC) measurements were performed on a Waters 2695 Separations Module apparatus with a differential refractive index detector with tetrahydrofuran (THF) as eluent. The obtained molecular weight is relative to the polystyrene standard. Thermogravimetric analysis (TGA) measurements were carried out with a PerkinElmer thermogravimetric analyzer (Pyris 1 TGA) at a heating rate of 10 °C min^{-1} under a nitrogen atmosphere. The temperature of degradation (T_d) is correlated to a 5% weight loss. ^1H nuclear magnetic resonance (NMR) measurements were recorded either with a Bruker Avance 300MHz AMX or Bruker 400 MHz DRX spectrometer. ^{13}C nuclear magnetic resonance (NMR) measurements were carried out with a Bruker 400 MHz DRX spectrometer. Chemical shifts were expressed in parts per million (ppm), and

splitting patterns are designated as s (singlet), d (doublet), and m (multiplet). Coupling constants *J* are reported in Hertz (Hz).

Synthesis of Monomers and Polymers

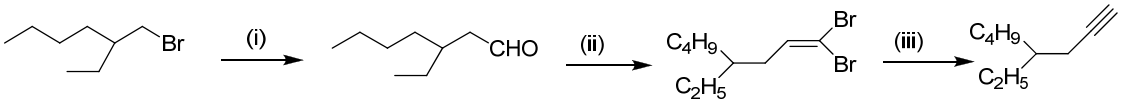

Reagents and conditions: (i) Bouveault Mg, ethyl ether, Ar, overnight; DMF, 1hour; (ii) PPh_3, CBr_4, CH_2Cl_2; (iii) BuLi, 3equiv., 0 ^oC, quenched with water.

Figure 2-11. Synthetic scheme from 2-ethylhexyl bromide to 4-ethyloct-1-yne

3-ethylheptanal: Magnesium (1.95 g, 80 mmol) and anhydrous THF 150 mL were added into a flame-dried two-necked RB flask equipped with stir bar, condenser and addition funnel under argon. 2-Ethylhexyl bromide (13.51 g, 70 mmol) was added dropwise into vigorously stirred solution through the addition funnel (a few crystals of I_2 can be added to initiate the reaction). The reaction mixture was then refluxed overnight. Subsequently, the reaction mixture was cooled to 0 °C and anhydrous DMF (5.85 g, 80 mmol) was directly injected into reaction mixture under stirring. The reaction mixture was kept at stirring for another 30 min and was poured into 250 mL HOAc/H_2O (1:10) solution. The mixture was extracted with hexane and the organic layer was washed with brine, dried over $MgSO_4$. After solvent removal under reduced pressure, the residue was purified by column chromatography (20:1, ethyl acetate:hexane) to offer the product as a colorless clear liquid. Yield: 8.06g (81%). ^{1}H NMR (300 MHz, $CDCl_3$): δ 9.75 (t, 1H, *J*=1.75Hz), 2.32-2.35 (dd, 2H, *J*=1.57Hz, 4.9Hz), 1.86-1.92 (m,1H), 1.26-1.45 (m, 8H), 0.87-0.89 (m, 6H).

1,1-dibromo-4-ethyloct-1-ene: A flame-dried two-neck RB flask was charged with anhydrous CH_2Cl_2 800 mL under argon. After the solution was cooled in an ice-bath, CBr_4 (81.90 g, 248 mmol) and PPh_3 (130.43 g, 497 mmol) were added under argon. Reaction mixture was stirred at 0 °C for 20 min, then 3-ethylheptanal (17.7 g, 124.3 mmol) was added. The mixture was maintained with stirring at room temperature for 2 hours. Then 400 mL water was added to quench the reaction. Organic layer was separated, washed with brine, and dried over $MgSO_4$. After solvent removal under reduced pressure, the resulting colorless liquid was collected and purified by column chromatography on silica gel using ethyl acetate: hexane (1:8) as eluent. Yield: 33.0 g (90%). ^{1}H NMR (300MHz, $CDCl_3$): δ 6.39 (t, 1H, *J*=7.5 Hz), 2.07 (t, 2H, *J*=6.9Hz), 1.45-1.41 (m, 1H), 1.38-1.18 (m, 8H), 0.92-0.81 (m, 6H).

4-ethyloct-1-yne: A flame-dried, two-necked RB flask was added with 1,1-dibromo-4-ethyloct-1-ene (20 g, 67.1 mmol) and anhydrous THF 300 mL. The reaction mixture was cooled to – 78 °C, then n-BuLi (2.5 M, 60 mL, 150 mmol) was added via syringe over 30 min. Reaction mixture was stirred under – 78 °C for another 30 min, then H_2O (200 mL) was added to quench the reaction. Organic layer was separated, washed with brine, and dried over $MgSO_4$. After removing the THF, the crude product was further purified via distillation at reduced pressure to yield the pure product as a colorless liquid. Yield: 7.7 g (83%). ^{1}H NMR (300MHz, $CDCl_3$): δ 2.19 (t, 2H, *J*=2.4Hz), 1.93 (t, 1H, *J*=2.4Hz), 1.45-1.28 (m, 11H), 0.92-0.86 (m, 6H). ^{13}C NMR (400MHz, CDCl3): 84.66, 68.78, 38.46, 32.64, 29.00, 25.87, 22.90, 22.24, 14.02, 11.01.

1,2-dibromo-4,5-dinitrobenzene (**2**): Concentrated H_2SO_4 (30.3 mL), fuming H_2SO_4 (46.6 mL), and fuming nitric acid (25.6 mL) were added successively into a 250 mL 2-neck RB flask under 0 °C (via an ice-bath). 1,2-dibromo benzene (17 g, 72 mmol) was added dropwise at room temperature. The reaction mixture was stirred overnight and poured into 900 g ice. The crude product was collected as a solid via filtration. Pure product was achieved through recrystallization from methanol as yellow cubic crystals. Yield: 7.1 g (30 %). ^{1}H NMR (400MHz, $CDCl_3$): δ 8.18 (s, 2H). ^{13}C NMR (400MHz, CDCl3): 141.5, 130.9, 129.7.

1,2-bis(4-ethyloct-1-ynyl)-4,5-dinitrobenzene (3): 1,2-dibromo-4,5-dinitrobenzene (1.90 g, 5.8 mmol) was dissolved by 150 mL triethyl amine (TEA) in a 250 mL 3-neck RB flask equipped with condenser and 100 mL addition funnel. The reaction mixture was purged by argon for 20min. Bis(triphenyl phosphine) palladium(II) dichloride (0.24 g) and CuI (0.10 g) were added under argon flow. The resulting mixture was heated to 80 °C. 4-ethyl oct-1-yne (1.7 g , 13 mmol) dissolved in argon-purged TEA 30 mL was then added dropwise into the reaction flask. The as formed mixture was stirred for 10 hours. Distilled water 100 mL was added to stop the reaction. The reaction mixture was extracted with ethyl acetate (3 × 100 ml). Organic layer was combined and solvent was removed under reduced pressure. The residue was purified by column chromatography (8:1, hexane: ethyl acetate) to yield the product as a red liquid. Yield: 1.97 g (77 %).

^{1}H NMR (400MHz, $CDCl_3$): δ 7.85 (s, 2H), 2.49 (t, 4H), 1.55-1.32 (m, 18H), 0.95-0.92 (m, 12H). ^{13}C NMR (400MHz, CDCl3): δ 140.73, 131.87, 128.08, 101.36, 78.12, 38.66, 32.89, 29.06, 26.13, 23.72, 22.89, 14.06, 11.11.

4,5-bis(4-ethyloctyl)benzene-1,2-diamine (**4**): Under argon atmosphere, **3** (1.64 g, 3.7 mmol) was dissolved in 200 mL of a degassed mixture of ethyl acetate and methanol (2:1). Reaction mixture was purged with argon for another 20 min, then 530 mg of Pd/C (10% Pd) was added. The flask was first flushed with hydrogen gas for 10 min then maintained under hydrogen gas. The mixture was stirred at room temperature for 4 days. Reaction mixture was filtered under argon and the solvent was removed under reduced pressure. The final product was given as yellow sticky oil by column chromatography on silica gel using ethyl acetate: hexane (1:3) as eluent. Yield: 1.2 g (80%). ^{1}H NMR (300MHz, $CDCl_3$): δ 6.52 (s, 2H), 3.26 (b, 4H), 2.42 (t, *J*=7.8Hz), 1.57-1.47 (m, 4H), 1.33-1.23 (m, 22H), 0.91-0.83 (m, 12H). ^{13}C NMR (400MHz, CDCl3): δ 132.46, 132.22, 117.84, 38.82, 33.46, 32.91, 32.66, 29.04, 28.97, 25.93, 23.17, 14.17, 10.90.

5,6-bis(4-ethyloctyl)benzo[c][1,2,5]thiadiazole (**5**): To a flask were added **4** (1.144 g, 2.95 mmol), CH_2Cl_2 (10 mL) and triethyl amine (12 mmol). Thionyl chloride (0.72 g, 6 mmol) was then added dropwise very slowly. The reaction mixture was refluxed for 5 hours. Solvent was removed under reduced pressure and water was added. The mixture was extracted with methylene chloride and dried over $MgSO_4$. After solvent removal, the residue was purified by column chromatography on silica gel using ethyl acetate: hexane (1:8) as eluent to afford the pure compound as pale yellow oil. Yield: 1.05g (85%). ^{1}H NMR (300MHz, $CDCl_3$): δ 7.76 (s, 2H), 2.74 (t,4H, J=7.8Hz), 1.67 (m, 4H), 1.42-1.26 (m, 22H), 0.91-0.83 (m, 12H). ^{13}C NMR (400MHz, CDCl3): δ 154.3, 144.75, 119.40, 38.80, 33.57, 33.29, 32.85, 28.99, 27.67, 25.91, 23.13, 14.14, 10.88.

5,6-bis(4-ethyloctyl)-4,7-diiodobenzo[c][1,2,5]thiadiazole (**6**): Compound **5** (9.9 g, 23.7 mmol) was added to a mixture of iodine (6.62 g, 26 mmol), sodium iodate (2.35 g,

11.8 mmol), sulfuric acid (4.96 mL), HOAc (80.4 mL), H_2O (0.6mL) in a 250 mL one-neck RB flask. The mixture was refluxed overnight. Excess saturated NaS_2O_4 solution was added to consume un-reacted I_2. The reaction mixture was extracted with CH_2Cl_2. The organic layer was washed with brine and dried over $MgSO_4$. Target product as yellow oil was obtained by removing solvent followed by column chromatography on silica gel using ethyl acetate: hexane (1:8) as eluent. Yield: 12.4g (78%). ^{1}H NMR (400MHz, $CDCl_3$): δ 3.05 (t, 4H, *J*=7.2Hz), 1.55-1.48 (m, 4H), 1.34-1.27 (m, 22H), 0.96-0.87 (m, 12H). ^{13}C NMR (400MHz, CDCl3): δ 153.21, 147.78, 93.87, 40.61, 38.56, 33.55, 32.83, 28.99, 26.96, 25.92, 23.14, 14.19, 10.91

5,6-bis(4-ethyloctyl)-4,7-di(thiophen-2-yl)benzo[c][1,2,5]thiadiazole (**M1**): In a flame-dried one-neck RB flask, anhydrous THF 20 mL and thiophene (0.67 g, 18 mmol) were added. After cooling the mixture down to 0 °C, n-BuLi (2.5 M, 4 mL, 10 mmol) was added. After 20 min, $ZnCl_2$ solution in hexane 0.5 M (20 mL, 10 mmol) was added slowly. The reaction mixture was allowed to react for 30 min at room temperature. The resulting thien-2-yl-zinc chloride solution was added via a cannula to a stirred mixture of compound **6** (2.67 g, 4 mmol), palladium acetate (30 mg) and PPh_3 (78 mg) at room temperature under argon flow. The reaction mixture was further stirred at room temperature for 2 hours. Then it was heated to 50 °C and maintained with stirring overnight. Solvent was removed under reduced pressure, and a bright orange liquid was isolated by column chromatography using hexane: ethyl acetate of 20:1 as eluent. Yield: 1.37 g (59%). ^{1}H NMR (400MHz, $CDCl_3$): δ 7.53 (d, 2H, *J*=1.2Hz), 7.22-7.24 (m, 2H), 7.19-7.21 (m, 2H), 2.77(t, 4H, *J*=8.4Hz), 1.55(m, 4H), 1.40-1.19 (m, 22H), 0.90-0.78 (m,

12H). ^{13}C NMR (400MHz, CDCl3): δ 154.30, 144.40, 137.32, 128.41, 127.01, 126.49, 126.13, 38.39, 33.62, 32.73, 31.66, 29.17, 28.91, 25.84, 23.16, 14.21, 10.89.

4,7-bis(5-bromothiophen-2-yl)-5,6-bis(4-ethyloctyl)benzo[c][1,2,5]thiadiazole (**A1**):

M1 (0.91 g, 1.57 mmol) was dissolved in 100 mL $CHCl_3$:HOAc (2:1) in a one-neck RB flask. Then NBS (0.71 g, 4mmol) was added and reacted overnight. The reaction mixture was then washed with distilled water, NaOH solution and distilled water to pH near 7. Yellow solid was obtained by removing solvent followed by purification by column chromatography using hexane: ethyl acetate (8:1) as eluent. Yield: 0.93g (80%) ^{1}H NMR (400MHz, $CDCl_3$): δ 7.23 (d, 2H, *J*=4.8Hz), 6.94 (d, 2H, *J*=3.6Hz), 2.78 (t, 4H, *J*=8Hz), 1.54-1.51 (m, 4H), 1.39-1.19 (m, 22H), 0.99-0.82 (m, 12H). ^{13}C NMR (400MHz, CDCl3): δ 153.88, 144.67, 138.77, 129.92, 128.87, 125.53, 113.37, 38.36, 33.57, 32.71, 31.59, 29.25, 28.91, 25.83, 23.16, 14.22, 10.87.

Following compounds were prepared from the literature procedures:

4,7-dibromo-2,1,3-benzothiadiazole (BT) Mancilha, F. S.; Da Silveira Neto, B. A.; Lopes, A. S.; Moreira Jr., P. F.; Quina, F. H.; Goncalves, R. S.; Dupont, J. *Eur. J. Org. Chem.* **2006**, *21*, 4924-4933

4,7-Bis(5-bromothien-2-yl)-2,1,3-benzothiadiazole (DTBT) Zhang, C. U.S. Pattent, 2004229925, 2004

4,7-bis(5-bromo-4-octylthiophen-2-yl)benzo[c][1,2,5]thiadiazole (M2) Jayakannan, M.; Van Hal, P. A.; Janssen, R. A. J. *J. Polym. Sci., Part A: Polym. Chem.* **2002**, *40*, 251-261.

Synthesis of A2: 4,7-Di(3-octyl-2-thienyl)-2,1,3-benzothiadiazole (**M2**) (0.0 91g, 0.157 mmol) and N-bromosuccinimide (NBS) (55.7mg, 0.314mmol) were added into THF under stirring. The reaction mixture was stirred at a room temperature for 2 h, then hexane was added into the mixture. The precipitate formed was filtered, and the filtrate was extracted with ether. The organic layer was washed with brine and dried over anhydrous sodium sulfate. The solvent was removed at a reduced pressure to give the product as a red solid. Yield: 93 mg (80%). ^{1}H NMR (400MHz, $CDCl_3$): δ 7.64 (s, 2H), 7.44 (d, 2H, *J*= Hz), 7.11 (d, 2H, *J*= Hz), 2.66 (m, 4H), 1.63 (m, 4H), 1.33-1.40 (m, 20H), 0.86 (t, 6H). ^{13}C NMR (400MHz, CDCl3): δ 153.94, 142.44, 133.60, 131.99, 129.68, 126.66, 113.20, 31.80, 30.51,29.43,29.35, 29.14, 22.62, 14.06.

M4 and **A4** was synthesized according to the procedure from Jayakannan, M.; Van Hal, P. A.; Janssen, R. A. J. *J. Polym. Sci., Part A: Polym. Chem.* **2002**, *40*, 2360-2372.

4,7-di(4-octyl-2-thienyl)-2,1,3-benzothiadiazole (M3): ^{1}H NMR (400MHz, $CDCl_3$): δ 7.97 (dd, 2H), 7.82 (s, 2H), 7.04 (dd, 2H), 2.67(m, 4H), 1.70 (m, 4H), 1.25-1.53 (m, 20H), 0.90 (t, 6H). ^{13}C NMR (400MHz, CDCl3): δ 126.15, 126.38, 127.21, 127.90, 128.42, 139.75, 153.02, 31.80, 29.70, 29.43, 29.35, 29.03, 22.62, 14.06.

4,7-Bis(5-bromo-4-octyl-2-thienyl)-2,1,3-benzothiadiazole (A3). ^{1}H NMR (400MHz, $CDCl_3$): δ 7.78 (s, 2H), 7.77 (s, 2H), 2.64 (m, 4H), 1.67 (m, 4H), 1.33-1.40 (m, 20H), 0.90 (t, 6H). ^{13}C NMR (400MHz, CDCl3): δ 151.99, 142.98, 138.45, 127.94, 125.02, 124.51, 111.59, 31.80, 29.70, 29.43, 29.35, 29.03, 22.62, 14.06.

Synthesis of polymers via Stille coupling polymerization.

A representative procedure is as follows. To a 25mL two-necked round bottom flask equipped with a condenser was added **D0** (352mg, 0.312 mmol), **A1 (**230 mg, 0.312

mmol) and 20 mL of anhydrous DMF: toluene 1:5 v/v. The mixture was then evacuated and refilled with argon for three cycles to remove oxygen. Subsequently, $Pd_2(dba)_3$ (7.13 mg, 2.5%) and $P(o\text{-}toyl)_3$ (19 mg, 20%) was added under argon stream. The mixture was heated under reflux over 2 days. After cooling the reaction mixture to room temperature, the organic solution was added dropwise to 200 mL of methanol to obtain precipitate, which was collected by filtration and washed with methanol and dried. The crude polymer was then extracted subsequently with methanol, acetone, hexane and CHCl3 in a Soxhlet's extractor. The fraction from chloroform was concentrated under reduced pressure and precipitated into methanol to give the polymer **PBDT-DTsolBT** as a yellow solid. Yield: 0.37 g (87%).

PBDT-DTBT and **PBDT-3DTBT** are synthesized according to the same procedure as **PBDT-DTsolBT** with respective monomers.

PBDT-4DTBT was synthesized via microwave assisted polymerization:

To a 10 mL Microwave pressurized vial equipped with a stir bar, **D0** (108 mg, 0.096 mmol),**A3** (65 mg, 0.096 mmol), $Pd_2(dba)_3$ (2.2 mg, 2.5%) and $P(o\text{-}tol)_3$,(6mg, 20%) was added. Then the tube was sealed and evacuated and refilled with argon for three cycles and then chlorobenzene was added in a glovebox. Reaction tube was put into microwave reactor and heated to 150 °C under 300watt microwave for 20 min. After cooling to room temperature, the organic solution was added dropwise to 200 mL of methanol to obtain precipitate, which was collected by filtration and washed with methanol and dried. The crude polymer was then extracted subsequently with methanol, acetone, hexane and $CHCl_3$ in a Soxhlet's extractor. The fraction from chloroform was concentrated under

reduced pressure and precipitated into methanol to give the polymer **PBDT-4DTBT** (95 mg, 75%) as a dark green solid.

PBDT-DTBT: ^{1}HNMR (400 MHz, CDCl2CDCl2, 400K): δ0.77-1.10 (12H, br), 1.11-1.77 (50H, br), 2.76-2.98 (4H,br), 6.76 (2H, br) 6.88 (2H, br), 7.44(2H, br), 7.61 (2H, br), 7.91 (2H, br), 8.13 (2H, br) Elemental analysis: C: 68.41%, H: 6.94%, N: 2.79%

PBDT-4DTBT: ^{1}HNMR (400 MHz, CDCl2CDCl2, 400K): δ0.79-1.10 (12H, br), 1.13-1.60 (72H, br), 1.60-1.82 (2H, br), 2.76-3.03 (8H,br), 6.73 (2H, br) 6.89 (2H, br), 7.59 (2H, br), 7.91 (2H, br), 8.07 (2H, br) Elemental analysis: C: 68.02%, H: 8.36% N: 2.04%

PBDT-3DTBT: ^{1}HNMR (400 MHz, CDCl3): δ0.70-0.95 (18H, br), 0.96-1.38 (72H, br), 1.48-1.77 (2H, br), 2.60-2.81 (8H, br) 6.65 (2H, br), 6.81(2H, br), 7.32 (2H, br), 7.53 (2H, br), 7.70 (2H, br) Elemental analysis: C: 71.65%, H: 8.43%, N: 2.19%

PBDT-DTsolBT: ^{1}HNMR (400 MHz, CDCl3): δ0.67-0.96 (12H, br), 1.01-1.78 (74H, br), 2.66-2.98 (8H,br), 6.63 (2H, br), 6.79 (2H, br), 7.14 (2H, br), 7.41 (2H, br), 7.51 (2H, br) Elemental analysis: C: 70.45%, H: 8.28%, N: 2.14%

CHAPTER 3

A WEAK DONOR-STRONG ACCEPTOR STRATEGY TO DESIGN IDEAL POLYMERS FOR ORGANIC SOLAR CELLS

Huaxing Zhou, Liqiang Yang, Sarah Stoneking, and Wei You

Adapted with permission from *ACS Applied Materials & Interfaces* 2010, 2, 1377

3.1. Introduction

Synthesizing conjugated polymers for use in organic solar cells is an exceptionally difficult structure property optimization problem that requires two balancing acts. First, the gap between the HOMO and the LUMO energy levels of the polymer should be as narrow as possible, in order to absorb the maximum amount of light. However, any low band gap polymer suitable for PV applications should also maintain a relatively low HOMO energy level to avoid any loss in the $V_{oc.}$

Fullerene derivatives (such as $PC_{61}BM$) have been extensively used as the n-type semiconductor in BHJ solar cells due to their superior electron accepting and transporting behavior. However, these fullerene derivatives are usually poor light absorbers, thereby leaving the task of light absorbing to the conjugated polymers. Moreover, fullerene derivatives usually have fixed energy levels (e.g., a LUMO of – 4.3 eV), which largely dictate the appropriate energy levels of the conjugated polymers in order to construct the required type II heterojunction alignment (i.e., polymer and fullerene with staggered band

energies) for effective exciton splitting.**(Figure 3-1)** These stringent requirements set the proposed "ideal" conjugated polymer with an estimated low HOMO energy level of – 5.4 eV and a small band gap of 1.5 eV. [28,52,132]

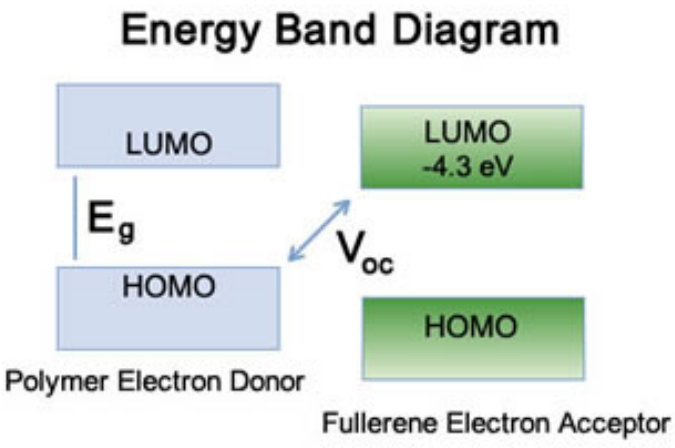

Figure 3-1. Energy diagrams showing the HOMO and LUMO levels of polymer donor and fullerene acceptors

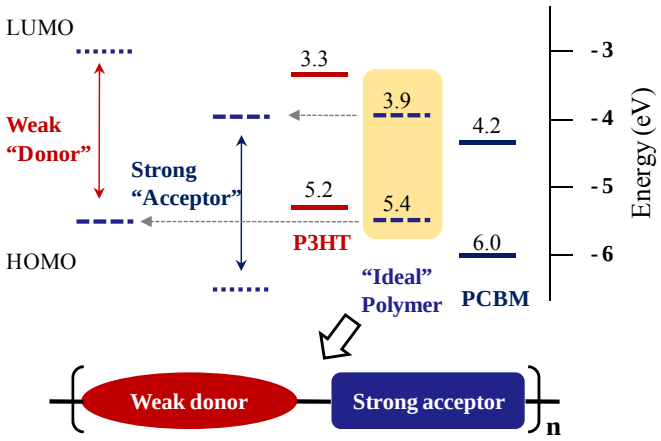

Figure 3-2. The "weak donor-strong acceptor" strategy

Alternating donor and acceptor units in copolymers has been proven to be an effective approach to lowering the band gap of copolymers via internal charge transfer

(ICT).[59] In order to ***concurrently*** lower the HOMO energy level and the band gap, we propose to modify the donor-acceptor low band gap polymer strategy by constructing alternating copolymers incorporating a *"weak donor"* and a *"strong acceptor"* (**Figure 3-2**). The "weak donor" should help maintain a low HOMO energy level, while a "strong acceptor" should reduce the band gap via ICT. Assuming a fill factor of 0.65, an external quantum efficiency of 65%, and an optimal morphology, one can estimate the overall power conversion efficiency from the optical band gap and the LUMO/HOMO of donor polymers in a polymer:$PC_{61}BM$ BHJ solar cell (**Figure 1-4**).[52] The ideal donor polymer in the BHJ device would theoretically be able to offer efficiency as high as 10%; double the efficiency (5%) of P3HT based BHJ PV cells.

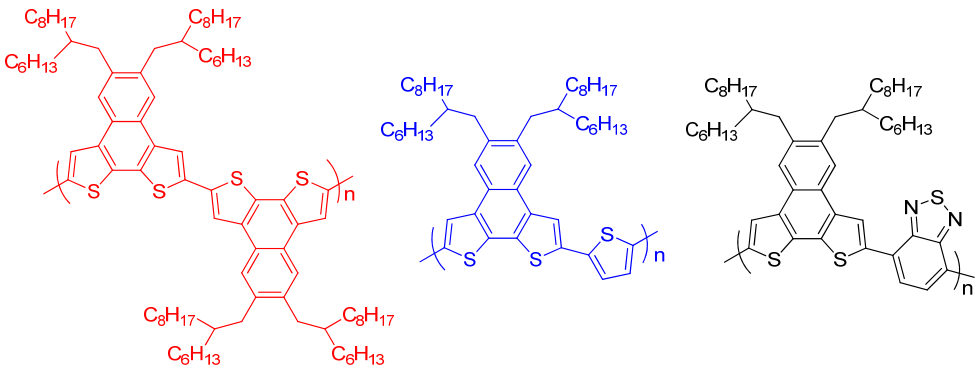

Figure 3-3. Chemical structures of **HMPNDT**, **PNDT-T** and **PNDT-BT**

One method to design such a "weak donor" is to judiciously fuse different aromatics into polycyclic aromatics with extended conjugation. For example, one can decrease the electron-richness of the thiophene unit by fusing it with a less electron-rich benzene unit. A few such polycyclic aromatics have already been successfully applied as the weak donor in conjugated polymers yielding open circuit voltages (V_{oc}) over 0.7 V in related

BHJ devices.[118,133] In this paper, another such weak donor, naphtho[2,1-*b*:3,4-*b'*]dithiophene (**NDT**) was copolymerized with a strong acceptor, benzothiadiazole (**BT**) to explore the proposed "weak donor – strong acceptor" concept. (**Figure 3-3**) The **NDT** monomer contains a naphthalene core, which was incorporated to decrease the electron-richness of the flanked bithiophene unit. For comparison, two other polymers, the homopolymer (**HMPNDT**) and "weak donor – strong donor" polymer (**PNDT-T**) were also synthesized. All three polymers were thoroughly characterized and their photovoltaic properties were carefully investigated. As expected, the "weak donor – strong acceptor" polymer – **PNDT-BT** – demonstrated both a low HOMO energy level of – 5.35 eV and a low band gap of 1.59 eV. A noticeably high V_{oc} of 0.83 V and a moderate J_{sc} of 2.90 mA/cm^2 were obtained from the BHJ device of **PNDT-BT** blended with $PC_{61}BM$, resulting in a total energy conversion efficiency of 1.27% (with a 70 nm thin film).

3.2. Polymer Synthesis

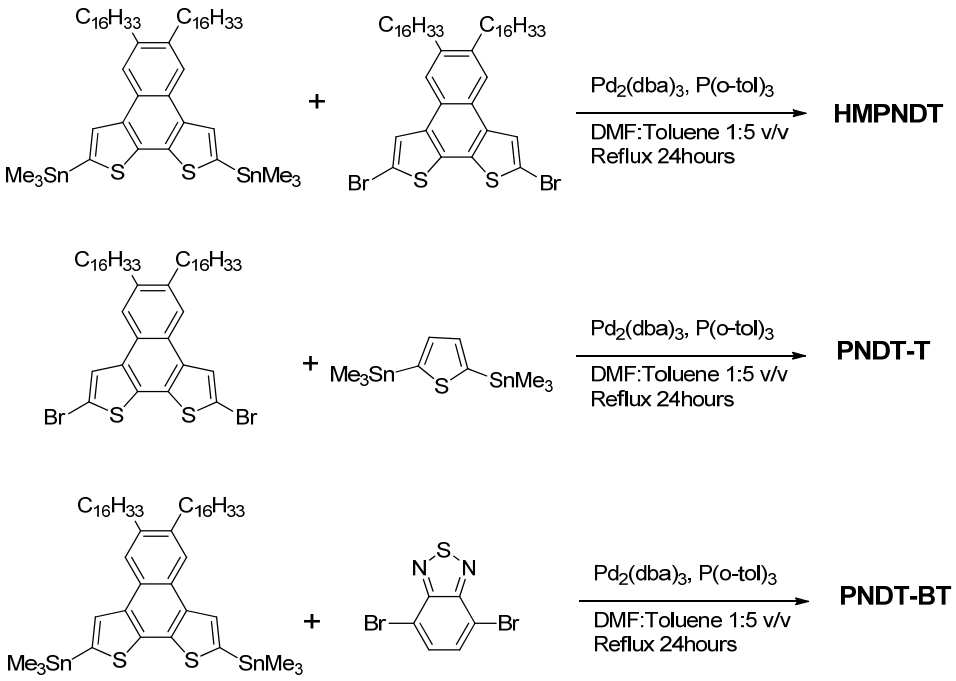

Figure 3-4. Polymerization of **HMPNDT**, **PNDT-T** and **PNDT-BT**

Synthesis of the **NDT** monomer was described elsewhere and in the experimental section.[134] Standard Stille coupling reactions were used to synthesize all three polymers (**Figure 3-4**). The resulting polymers were collected by directly precipitating polymerization solutions in methanol followed by filtration. The crude polymers were extracted via a Soxhlet apparatus by methanol, followed by sequential extractions with ethyl acetate and hexane. There was no remaining polymer residue observed in the extraction thimble following hexane extraction. Hexane fractions were collected, concentrated, re-precipitated in methanol, and dried under vacuum overnight to offer the pure polymer. All purified polymers have thermal stability up to 420 °C (**Table 3-1**), and are soluble in common organic solvents such as THF and chloroform. The molecular structures of all the polymers synthesized were confirmed by NMR (**Experimental**

Section) and element analysis (**Appendix 3**). Yields and molecular weights of each polymer are summarized in **Table 3-1**. Though decent yields were obtained for all three polymerizations, the molecular weight of each polymer was noticeably different. The molecular weight of **PNDT-BT** is much lower than that of **HMPNDT** or **PNDT-T**, which is assumed to be a direct result from the low reactivity of brominated benzothiadiazole in the Stille coupling polymerization.[135] Therefore, further optimization of the polymerization conditions are necessary to achieve high molecular weight polymers.[6]

Table 3-1. Polymerization results and thermo stability of polymers.

	Yield [%]	M_n[a] [kg/mol]	M_w[a] [kg/mol]	PDI[a]	T_d[b] [°C]
HMPNDT	82	16	34	2.11	426
PNDT-T	90	37	251	6.66	428
PNDT-BT	80	9	10	1.06	445

[a] Determined by GPC in tetrahydrofuran (THF) using polystyrene standards. [b] The temperature of degradation corresponding to a 5% weight loss determined by TGA at a heating rate of 10 °C/min.

3.3. Optical and Eletrochemical Properties

The UV-Vis absorption spectra were acquired in both chloroform solution and solid state as thin films (**Figure 3-6**). The absorption coefficient of each polymer was calculated from the thin film absorption and the film thickness. HOMO and LUMO energy levels of all three polymers were estimated from cyclic voltammograms of

polymer thin films drop-cast from chloroform solutions and calculated from the oxidative potential and reductive potential respectively (**Figure 3-5**). Compared with the **NDT** unit, the thiophene (**T**) unit is more electron-rich which raises the HOMO energy level of **PNDT-T** to – 5.20 eV compared with that of **HMPNDT** (– 5.33 eV). Since the other common unit, **NDT**, dictates similar LUMO energy levels of **HMPNDT** and **PNDT-T**, the band gap of **PNDT-T** is slightly smaller than that of **HMPNDT** (**Table 3-2**). In similar studies, incorporating thiophene units into the polymer backbone has also shown band gap decreasing and HOMO energy level increasing.[72,136] In contrast, **PNDT-BT**, designed by the "weak donor – strong acceptor" concept, successfully demonstrates both a low HOMO energy level of – 5.35 eV and a low band gap of 1.59 eV. The "weak donor" – **NDT** – determines the HOMO energy level of **PNDT-BT**, explaining why a similar HOMO energy level to that of **HMPNDT** was observed.

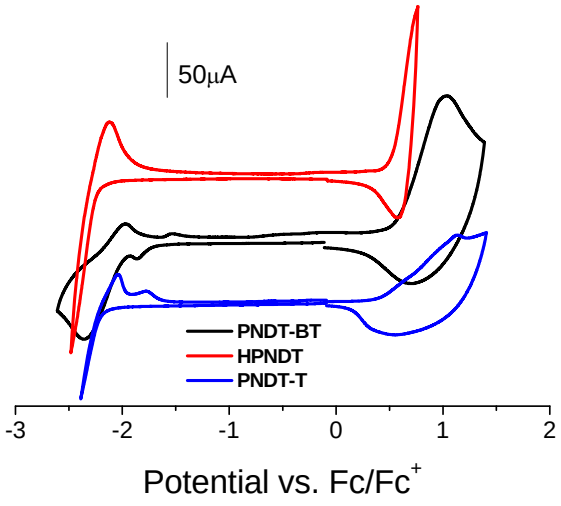

Figure 3-5. Cyclic voltammograms of the oxidation and reduction behavior of thin films of **HMPNDT, PNDT-T** and **PNDT-BT**. (HOMO and LUMO levels are calculated from the onset of the oxidation and reduction peaks respectively).

Replacing the electron-rich thiophene unit (**T**) with the highly electron-deficient benzothiadiazole unit (**BT**) effectively lowers the band gap of **PNDT-BT** to 1.59 eV via ICT. In addition, this strong internal charge transfer interaction between **NDT** and **BT** would encourage the polymer backbone to adopt a more planar structure, thereby enhancing the inter-chain stacking of polymers[26]. As seen from **Figure 3-6**, a red shift in solid state absorption of **PNDT-BT** is observed compared with that of the solution absorption. Furthermore, the intensity of the "shoulder" around 680nm noticeably increased, indicative of a pronounced inter-chain interaction in the solid state.

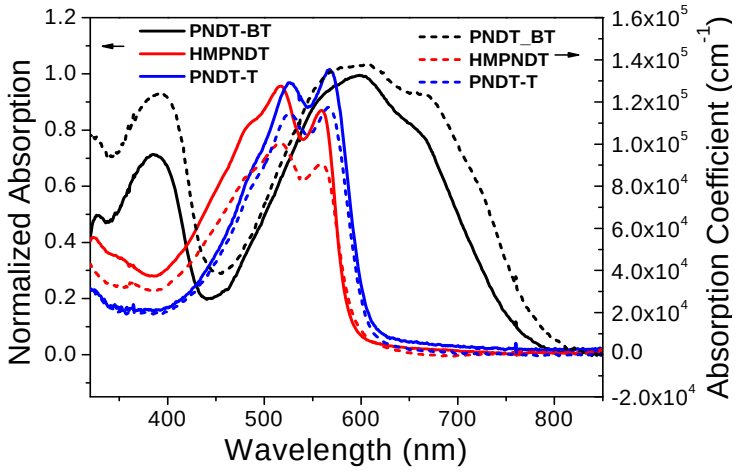

Figure 3-6. UV-vis absoption spectra of polymers in solution (solid lines) and in solid state (dash lines). The polymer films were spun coat from 5 mg/mL chloroform solution onto glass substrates.

Table 3-2. Optical and electrochemical data of all polymers.

	UV-Vis Absorption						PL	Cyclic Voltammetry	
	$CHCl_3$ solution			Film			$CHCl_3$ Solution	E^{ox}_{onest} (V)	E^{red}_{onest} (V)
polymer	λ_{max} [nm]	λ_{onset} [nm]	$E_g{}^a$ [eV]	λ_{max} [nm]	λ_{onset} [nm]	$E_g{}^a$ [eV]	λ_{max} [nm]	HOMO [eV]	LUMO [eV]
HMPNDT	516,561	587	2.11	515,559	592	2.12	543,573	0.53/–5.33	-2.23/–2.57
PNDT-T	526,567	606	2.05	524,567	607	2.05	544	0.40/–5.20	-2.17/–2.63
PNDT-BT	597	765	1.62	602	778	1.59	636	0.55/–5.35	-1.70/–3.1

[a] Calculated from the intersection of the tangent on the low energetic edge of the absorption spectrum with the baseline.

3.4. Photovoltaic Properties

The photovoltaic performance of all three polymers were probed by fabricating BHJ solar cells with the configuration of ITO/PEDOT:PSS/polymer:$PC_{61}BM$/Ca/Al. Device optimizations were conducted by varying solvents, ratios of polymer vs. $PC_{61}BM$, and film thicknesses (**Appendix 3**). Representative results for each polymer are summarized in **Table 3-3**.

Table 3-3. PV performances of polymers in optimized conditions

Polymer	Polymer: $PC_{61}BM$	Processing solvent	Thickness (nm)	V_{oc} (V)	J_{sc} (mA/cm^2)	*FF*	η (%)	*IPCE*	*Rs* (Ω)
HMPNDT	1:1	$CHCl_3$	65	0.83	1.42	0.47	0.56	13.3	78.5
PNDT-T	1:2	CB	55	0.73	3.25	0.50	1.18	20.1	133
PNDT-BT	1:4	CB	70	0.83	2.90	0.53	1.27	16.8	68.5

Clearly, a lower HOMO energy level provides a higher open circuit voltage (V_{oc}). For example, the measured difference (0.15 eV) of the HOMO energy levels between **PNDT-T** and **PNDT-BT** almost completely translated into the observed difference in V_{oc} (~ 0.1 V), re-emphasizing the importance of a low HOMO energy level towards a higher V_{oc}. **HMPNDT** has a similar HOMO level (– 5.33 eV) to that of **PNDT-BT** (– 5.35 eV), leading to a similar V_{oc} (0.83 V) in its BHJ devices.

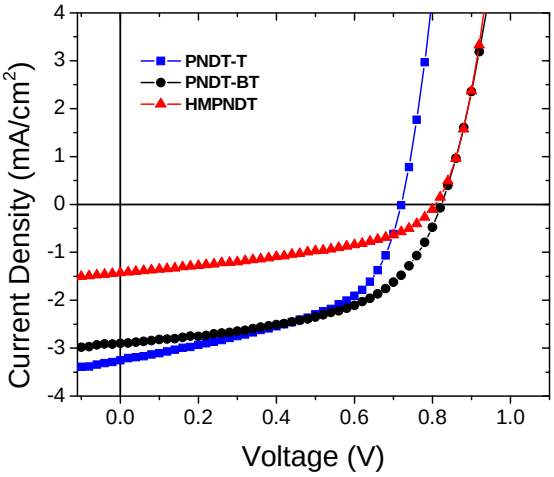

Figure 3-7. Characteristic J-V curves of the optimized devices of all polymers based BHJ solar cells under 1 Sun condition (100 mW/cm^2)

The short circuit current (J_{sc}) is a more complicated issue. Lower band gap, in theory, should harvest more light and generate higher current. However, there are other important influencing factors in BHJ devices such as the molecular weight of the polymers,[6] charge carrier mobility, [137,138] and device morphology.[139] Compared to **HMPNDT**, the J_{sc} of **PNDT-T** is noticeably higher, partly due to its smaller band gap. More importantly, the molecular weight of **PNDT-T** is significantly higher than that of

HMPNDT (**Table 3-1**), which should contribute positively to the observed higher current.[6] With a small band gap of 1.59 eV, **PNDT-BT** should have offered the highest J_{sc} among three polymers. However, the maximum J_{sc} obtained through device optimization was 3 mA/cm^2. Two possible reasons account for such a low current: (a) there is only 20 wt% of **PNDT-BT** in the optimized device with a very thin active layer of 70 nm. Such a low loading of light absorbing polymers cannot absorb the incident light effectively (**Figure 3-8**); (b) the molecular weight of **PNDT-BT** is the lowest (M_n: 9 kg/mol). Usually low molecular weight polymers are not able to achieve the maximum current as promised by their optical band gap.[108-110,140] This observation reiterates the necessity of a high molecular weight polymer in achieving a high J_{sc}.

These optimized devices were subsequently characterized for the incident photon to current efficiency (IPCE). In addition, UV-vis measurements of the active layers were performed on glass substrates coated with blends of polymer/$PC_{61}BM$ prepared under the same conditions as the optimized devices. Both the UV-vis and IPCE curves are displayed together in **Figure 3-8** to show their correlation. The high loading of $PC_{61}BM$ in the **PNDT-BT**:$PC_{61}BM$ blend essentially dominates the IPCE and the film absorption, resulting a peak external quantum efficiency (EQE) of 16% around 440 nm where $PC_{61}BM$ absorbs most of the solar influx. The EQE is only about 10% in the longer wavelength region where **PNDT-BT** absorbs. On the other hand, the UV-vis spectra of **HMPNDT** and **PNDT-T** based devices with much lower loading of $PC_{61}BM$ clearly show characteristic absorption from polymers. Still, the maximum EQE of the **PNDT-T** based device is about 20% at 400 nm, falling into the absorption region of $PC_{61}BM$, though higher EQE (~ 16%) was observed in the absorption region of **PNDT-T** (450 –

600 nm). With an equal weight percentage, the **HMPNDT**/$PC_{61}BM$ (1:1) device achieves an EQE of roughly 10% across its absorption region (350 – 600 nm).

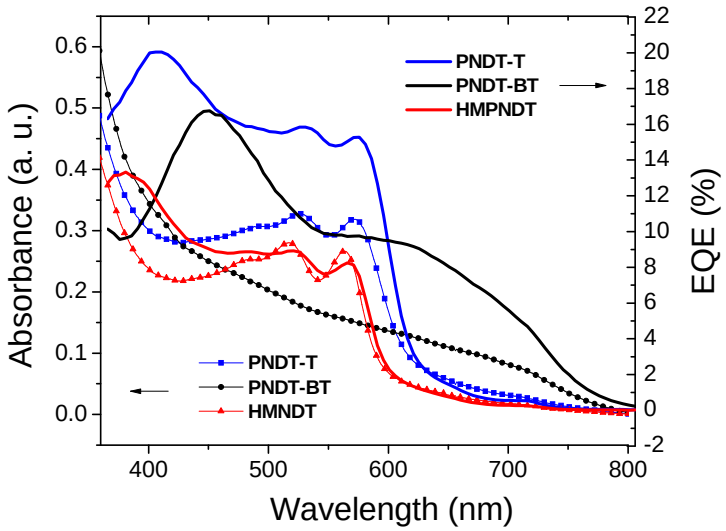

Figure 3-8. IPCE and absorption of **HMNDT, PNDT-T** and **PNDT-BT** (absorption is normalized by film thickness)

Table 3-4. Mobility of polymers under SCLC condition

Polymer only	Thickness (nm)	Mobility ($cm^2/V{\cdot}s$) [a]	Polymer: $PC_{61}BM$	Thickness (nm)	Mobility ($cm^2/V{\cdot}s$) [b]
HMPNDT	45	1.81×10^{-6}	1:1	75	6.87×10^{-6}
PNDT-T	60	4.35×10^{-6}	1:2	70	5.55×10^{-6}
PNDT-BT	50	2.60×10^{-6}	1:4	70	6.23×10^{-6}

[a] Measured with polymers only devices with Al as the top electrode. [b] Measured with BHJ devices with Pd as the top electrode.

The investigation of the hole mobility of all these polymers provides further insights in understanding their PV performance. The space charge limited current (SCLC)

method was employed to probe the vertical hole transport through the device by fabricating hole-only devices. The hole mobility of all three polymers (either in the blend or in pure polymer) are generally very low; on the order of 10^{-6} $cm^2/V{\cdot}s$ (**Table 3-4**). Such low hole mobilities require a thin film (< 100 nm) to be used, in order to effectively transport generated charges.[118] Additionally, the low hole mobility of **PNDT-BT** may also explain why a much higher $PC_{61}BM$ loading (80 wt%) is required to improve the morphology and (possibly) increase the hole mobility in the **PNDT-BT**/$PC_{61}BM$ blend, similar to what was observed for MDMO-PPV.[41,42] The results on the mobility study indicate that the hole mobility needs to be much improved to match the electron mobility of $PC_{61}BM$ (~ 10^{-3} $cm^2/V{\cdot}s$). A balanced charge transport (electrons and holes) would minimize the build-up of space charges, thereby enhancing the observed J_{sc}. [137]

3.5. Conclusions

We have demonstrated that the proposed "weak donor-strong acceptor" strategy is an effective method to achieve low band gap polymers coupled with low HOMO energy levels. This strategy takes us one step closer towards the development of ideal donor polymers to be used in conjunction with $PC_{61}BM$ to improve the efficiency of BHJ PV cells. The "weak donor" can be prepared by judiciously fusing different aromatic units, as shown in the case of naphtho[2,1-*b*:3,4-*b'*]dithiophene (**NDT**), while the "strong acceptor" is usually supplied by electron-withdrawing conjugated aromatics, such as benzothiadiazole (**BT**). For example, **PNDT-BT**, designed under the "weak donor-strong acceptor" strategy, was able to achieve a low HOMO energy level of – 5.35 eV and a narrow band gap of 1.59 eV, leading to an impressive open circuit voltage of 0.83 V.

However, the short circuit current (~ 3 mA/cm^2) was significantly lower than the maximum achievable current from such a low band gap, which limited the observed efficiency to 1.27%. Therefore, new strategies need to be actively pursued in order to (a) increase molecular weight[141] and (b) improve the hole mobility,[133] in addition to maintaining a low HOMO energy level and a narrow band gap of these donor polymers.

3.6. Experimental Section

For the experimental details about electrochemistry, spectroscopy and SCLC mobility measurements please check **Appendix 1**. And please check **Appendix 3** for supporting information.

Reagents and Instrumentation

All reagents and chemicals were purchased from commercial sources (Aldrich, Acros, Strem, Fluka) and used without further purification unless stated otherwise. Reagent grade solvents were dried when necessary and purified by distillation. Gel permeation chromatography (GPC) measurements were performed on a Waters 2695 Separations Module apparatus with a differential refractive index detector with tetrahydrofuran (THF) as eluent. The obtained molecular weight is relative to the polystyrene standard. Thermogravimetric analysis (TGA) measurements were carried out with a PerkinElmer thermogravimetric analyzer (Pyris 1 TGA) at a heating rate of 10 °C min^{-1} under a nitrogen atmosphere. The temperature of degradation (T_d) is correlated to a 5% weight loss. Differential scanning calorimetry (DSC) measurements were carried out with a module Q 200 from TA Instruments under a nitrogen atmosphere. ^{1}H nuclear magnetic resonance (NMR) measurements were recorded either with a Bruker Avance 300MHz

AMX or Bruker 400 MHz DRX spectrometer. ^{13}C nuclear magnetic resonance (NMR) measurements were carried out with a Bruker 400 MHz DRX spectrometer. Chemical shifts were expressed in parts per million (ppm), and splitting patterns are designated as s (singlet), d (doublet), and m (multiplet). Coupling constants *J* are reported in Hertz (Hz). Element analysis was performed in Atlantic Microlab, Inc. with ±0.3% error limits for both accuracy and precision.

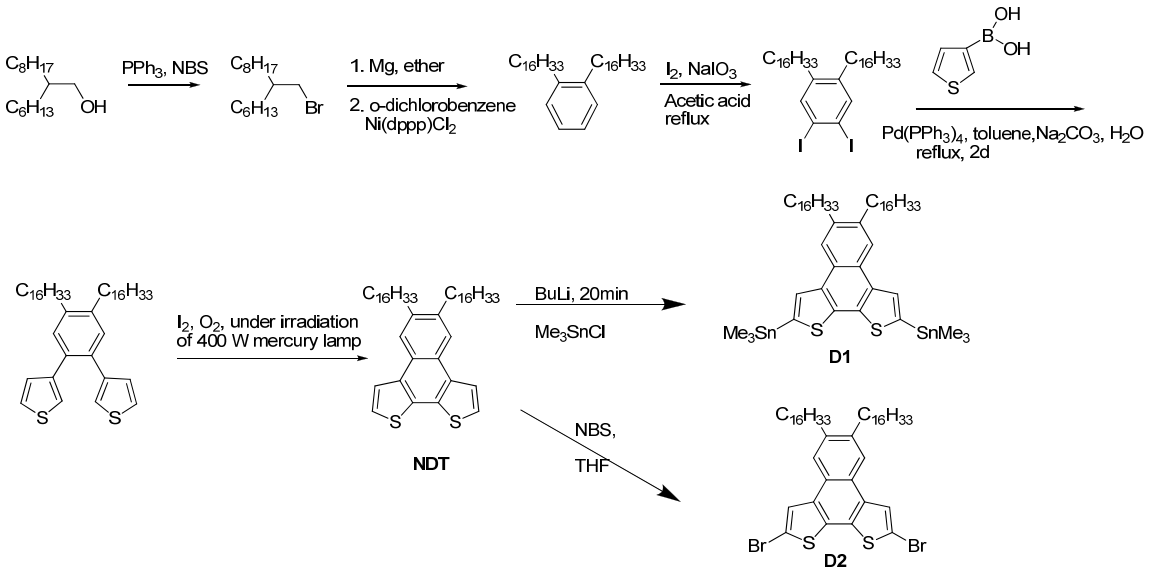

Figure 3-9. Synthesis of **D1** and **D2**

Synthetic procedures

NDT and **D2** were prepared with slightly modified literature procedure. [134]

NDT: ^{1}H NMR (400MHz, $CDCl_3$): δ 8.08 (s, 2H), 7.97 (d, 2H, J=5.2Hz), 7.48 (d, 2H, J=5.2Hz), 2.80 (d, 4H, J=7.2Hz), 1.78(m, 2H), 1.4-1.15 (m, 48H), 0.89-0.85 (m, 12H)

^{13}C NMR (400MHz, $CDCl_3$): δ 138.64, 134.20, 131.27, 125.89, 125.22, 123.41, 122.76, 39.18, 38.09, 33.46, 33.37, 32.00, 31.94, 30.12, 29.82, 29.70, 29.40, 26.70, 22.73, 22.70, 14.13

D2: ^{1}H NMR (400MHz, $CDCl_3$): δ 7.90 (s, 2H), 7.89(s, 2H), 2.75 (d, 4H, J=7.2Hz), 1.73 (m, 2H), 1.39-1.23 (m, 48H), 0.90-0.84 (m, 12H)

^{13}C NMR (400MHz, $CDCl_3$): δ 139.84, 133.84, 130.90, 125.51, 124.90, 123.64, 111.98, 39.02, 37.30, 33.50, 31.94, 30.12, 29.78, 29.67, 29.36, 26.70, 26.65, 22.68, 14.09

Synthesis of D1.

To a solution of **NDT** (120 mg, 0.17 mmol) in anhydrous THF (5 mL) at 0 °C, n-BuLi 2.5M in hexane (0.21mL, 0.52 mmol) was added dropwise and the mixture was stirred at room temperature under argon for 30 min. Then trimethyl tin chloride 1M solution in hexane (0. 6mL, 0.6 mmol) was added, and the mixture was stirred at room temperature for 20 min. The mixture was poured into saturated aqueous sodium bicarbonate, and the organic phase was separated and washed with saturated brine and then dried over an anhydrous sodium sulfate. The solvent was removed at a reduced pressure, and the product was used without further purification. Yield: 167mg (95%). ^{1}H NMR (400MHz, $CDCl_3$): δ 8.11 (s, 2H), 8.01(s, 2H), 2.80 (d, 4H, *J* = 6.8Hz), 1.78 (m, 2H), 1.38-1.25 (m, 48H), 0.90-0.84 (m, 12H), 0.52 (s, 18H)

Following compounds were prepared according to the literature procedures

4,7-dibromo-2,1,3-benzothiadiazole (**BT**) [142]

2,5-bis(trimethylstannyl)thiophene [72]

Synthesis of polymers via Stille coupling polymerization

A representative procedure is as follows. To a 25 mL two-necked round bottom flask equipped with a condenser was added **D1** (241mg, 0.237 mmol), 4,7-dibromo-2,1,3-benzothiadiazole (70 mg, 0.237 mmol) and 12 mL of anhydrous DMF: toluene (1:5 v/v). The mixture was then evacuated and refilled with argon for three cycles to remove oxygen. Then $Pd_2(dba)_3$ (7.13mg, 2.5%) and $P(o\text{-}tol)_3$ (19mg, 20%) were added under argon stream. The mixture was heated under reflux over 2 days. After cooling to room temperature, the organic solution was added dropwise to 200 mL of methanol to obtain precipitate, which was collected by filtration and washed with methanol and dried. The crude polymer was then extracted subsequently with methanol, and hexane in a Soxhlet extractor. The fraction from hexane was concentrated under reduced pressure and precipitated into methanol to give the polymer **PNDT-BT** as a dark blue solid (156 mg, 80%).

HMPNDT: Yield: 188 mg (82%). ^{1}H NMR (400MHz, $CDCl_2CDCl_2$): δ 8.21 (2H, br), 7.93 (2H, br), 2.95(4H, br), 1.99(2H, br), 1.80-1.10(48H, br), 1.10-0.70(12H, br).

PNDT-T: Yield: 220 mg (90%). ^{1}H NMR (400MHz, $CDCl_2CDCl_2$): δ 8.05(2H, br), 7.69(2H, br), 6.87 (2H, br), 2.95 (4H, br), 2.05 (2H, br), 1.73-1.10 (48H, br), 1.10-0.78 (12H, br).

PNDT-BT: Yield: 156 mg (80%). ^{1}H NMR (400MHz, $CDCl_2CDCl_2$): δ 8.26-6.95 (6H, br), 3.53-2.95 (4H, br), 2.25-1.11 (50H, br), 1.11-0.79 (12H, br)

Polymer solar cell fabrication and testing

Glass substrates coated with patterned indium-doped tin oxide (ITO) were purchased from Thin Film Devices, Inc. The 150 nm sputtered ITO pattern had a resistivity of 15Ω/□. Prior to use, the substrates were ultrasonicated in acetone followed by deionized water and then 2-propanol for 20min each. The substrates were dried under a stream of nitrogen and subjected to the treatment of UV-Ozone over 30 minutes. A 0.45 μm-filtered dispersion of PEDOT:PSS in water (Baytron PH500) was then spun cast onto clean ITO substrates at 4000 rpm for 60 seconds and then baked at 140 °C for 15 minutes to give a thin film with a thickness of 40 nm. A blend of polymer and $PC_{61}BM$ with varied concentration and feed ratio were dissolved in organic solvent with heating at 90 °C for 6 hours. All the solutions were filtered through a 0.45 μm poly(tetrafluoroethylene) (PTFE) filter, spun cast at different rpm for 60 seconds onto PEDOT:PSS layer. The substrates were then dried under vacuum at room temperature for 12 hours. The thicknesses of films were recorded by a profilometer (Alpha-Step 200, Tencor Instruments). The devices were finished for measurement after thermal deposition of a 25 nm film of calcium and a 80 nm aluminum film as the cathode at a pressure of ~ 1×10^{-6} mbar. There are 8 devices per substrate, with an active area of 12 mm^2 per device. Device characterization was carried out under AM 1.5G irradiation with the intensity of 100 mW/cm^2 (Oriel 91160, 300 W) calibrated by a NREL certified standard silicon cell. Current versus potential (I-V) curves were recorded with a Keithley 2400 digital source meter. EQE were detected under monochromatic illumination (Oriel Cornerstone 260 ¼ m monochromator equipped with Oriel 70613NS QTH lamp) and the calibration of the incident light was performed with a monocrystalline silicon diode. All

fabrication steps after adding the PEDOT:PSS layer onto ITO substrate, and characterizations were performed in gloveboxes under nitrogen atmosphere.

CHAPTER 4

A TALE OF CURRENT AND VOLTAGE: INTERPLAY OF BAND GAP AND ENERGY LEVELS OF CONJUGATED POLYMERS TOWARDS HIGHLY EFFICIENT BULK HETEROJUNCTION SOLAR CELLS

Huaxing Zhou, Liqiang Yang and Wei You

Adapted From *Macromolecules* 2010, 43, 10390

4.1. Introduction

Perhaps the most important parameters in determining the efficiency of any given solar cell are open circuit voltage (V_{oc}) and short circuit current (J_{sc}). In polymer BHJ solar cells, the V_{oc} and J_{sc} are determined by the energy level and band gap of the conjugated polymers. As the benchmark for BHJ solar cells, poly(3-hexylthiophene) (P3HT) provides a V_{oc} of ~ 0.6 V with a HOMO level of – 5.1 eV, and a J_{sc} of ~ 11 mA/cm^2 at a band gap of 1.9 eV.[25] In order to increase the V_{oc} of P3HT, structural units with a high oxidation potential (weak donors) such as carbazole,[5] fluorene,[47] ladder-type *p*-phenylene,[48] and silafluorene[101] have been employed to construct low band gap polymers via the donor-acceptor approach. This has successfully yielded V_{oc} as high as 1 V in related BHJ devices.[47,48] Unfortunately, their relatively large band gaps (> 1.8 eV) limit the J_{sc} to less than 11 mA/cm^2, even with internal quantum efficiency approaching 100%.[5] Alternatively, by constructing polymers with much smaller band gaps through structural moieties (strong donors) such as cyclopentadithiophene (or its silol version)[6]

and thienothiophene,[143] the J_{sc} can be enhanced to as high as 17 mA/cm^2.[6] However, the V_{oc} of related devices is often lower than 0.6 V[6,143] due to an elevated HOMO energy level.

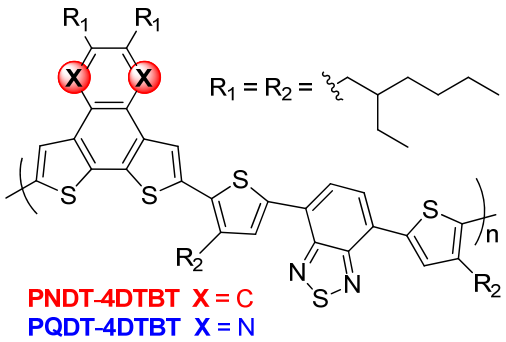

Figure 4-1. Structure of polymers. (i) Naphthalene/quinoxaline center ring lowers oxidation potential, and planarity of **NDT/QDT** unit encourages crystallinity. (ii) Additional alkylated positions (R_2) ensure high molecular weight and soluble polymers without introducing severe steric hindrance between donor (**NDT/QDT)** and acceptor **(4DTBT)**. *Note: the structures of the two polymers only differ by two atoms.*

Recognizing the importance of achieving both a high V_{oc} and a high J_{sc}, we proposed to construct "weak donor-strong acceptor" copolymers to *concurrently* lower the HOMO energy level and the band gap.[144] (as discussed in **Chapter 3**) One such copolymer, **PNDT-BT**, incorporated naphtho[2,1-*b*:3,4-*b'*]dithiophene (**NDT**) and benzothiadiazole (**BT**), and indeed demonstrated both a low HOMO energy level of – 5.35 eV and a low band gap of 1.64 V. Though a noticeably high V_{oc} of 0.83 V was obtained from the BHJ device of **PNDT-BT** blended with $PC_{61}BM$, the J_{sc} was only 2.90 mA/cm^2, attributed to the low molecular weight and low hole mobility of **PNDT-BT**. Fortunately, we have discovered that 4,7-di(4-hexyl-2-thienyl)-2,1,3-benzothiadiazole (**4DTBT**) can impart

low band gap polymers with additional solubility and (thereby) high molecular weight.[141] (as discussed in **Chapter 2**) Therefore, a new polymer, **PNDT-4DTBT**, was envisioned and synthesized (**Figure 4-1**) in hope of achieving desired energy levels, high molecular weight and good solubility. BHJ solar cells based on the blend of this polymer and $PC_{61}BM$ demonstrated a V_{oc} of 0.67 V, a J_{sc} of 14.20 mA/cm^2, and a *FF* of 0.54, yielding an overall efficiency of 5.1 % under 1 sun condition(AM 1.5, 100 mW/cm^2). In order to improve the V_{oc} by further lowering the HOMO energy level (to make a weaker donor), we substituted the two C atoms of the center naphthalene unit within **NDT** with two N atoms, converting **NDT** into an even *weaker* donor, dithieno[3,2-*f*:2',3'-*h*]quinoxaline (**QDT**).[134] As expected, **PQDT-4DTBT** offered a much improved V_{oc} of 0.83 V. Interestingly, a similar overall efficiency was obtained (4.31 %), largely due to a noticeably deceased J_{sc} (11.4 mA/cm^2). Comparison of these two structurally related polymers has set an excellent example to demonstrate the delicate interplay between the HOMO energy level (affecting V_{oc}) and the band gap (deciding J_{sc}).

4.2. Polymer Synthesis

Both polymers were synthesized by microwave-assisted Stille coupling reaction[6,121,122] of distannylated **NDT** or **QDT** and dibrominated **4DTBT** as shown in **Figure 4-2**. Same alkyl chains were anchored on the PNDT-4DTBT and PQDT-4DTBT polymer backbones to avoid the possible chain effects on polymer properties. Both polymers are readily soluble in common solvents such as chloroform, chlorobenzene (CB), and dichlorobenzene (DCB). The high solubility and high molecular weight of these two polymers highlight the benefits of incorporating a soluble acceptor (e.g.,

4DTBT) in constructing low band gap polymers.[141] The structures of these purified polymers were confirmed by ^{1}H NMR (**Appendix 4**). Gel permeation chromatography (GPC) results using tetrahydrofuran (THF) as eluent at room temperature and using 1,2,4-trichlorobenzene (TCB) at 135°C are shown in **Table 4-1**. Molecular weights and PDI measured in high temperature GPC were noticeably smaller than measured in THF GPC. Moreover, symmetrical and single GPC peaks were obtained in high temperature GPC but multiple peaks were shown in THF GPC curves These differences on GPC measurements indicate strong polymer tangling and aggregation at room temperature. (**Appendix 4**)

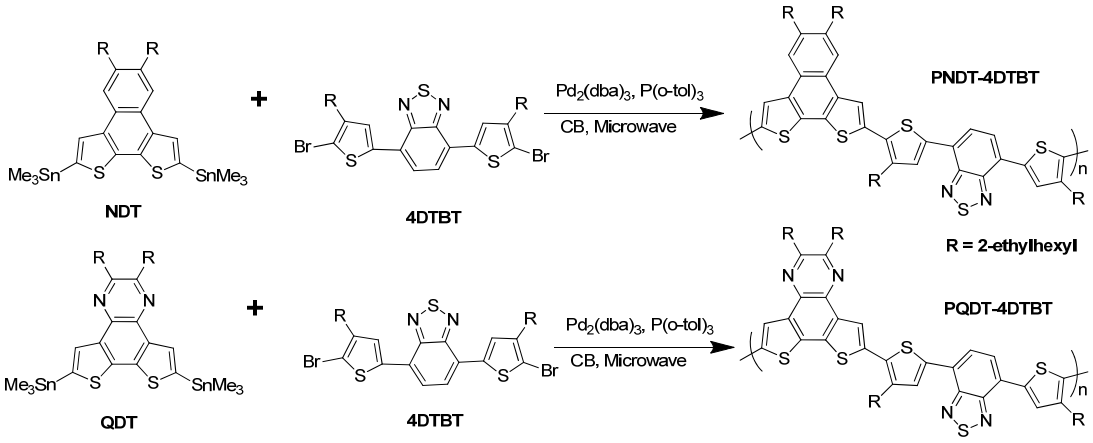

Figure 4-2. Polymerization of **PNDT-4DTBT** and **PQDT-4DTBT**

Table 4-1. Polymerization results of **PNDT-4DTBT** and **PQDT-4DTBT.**

Polymer	Mn[a] [kg/mol]	PDI[a]	Mn[b] [kg/mol]	PDI[b]
PNDT-4DTBT	25.7	3.93	6.8	2.07
PQDT-4DTBT	12.9	2.26	5.2	1.90

[a] Determined by GPC in tetrahydrofuran (THF) using polystyrene standards. [b] Determined by high-temperature GPC using 1,2,4-trichlorobenzene as the eluent (stabilized with 125 ppm BHT) at 135 °C with polystyrene standards.

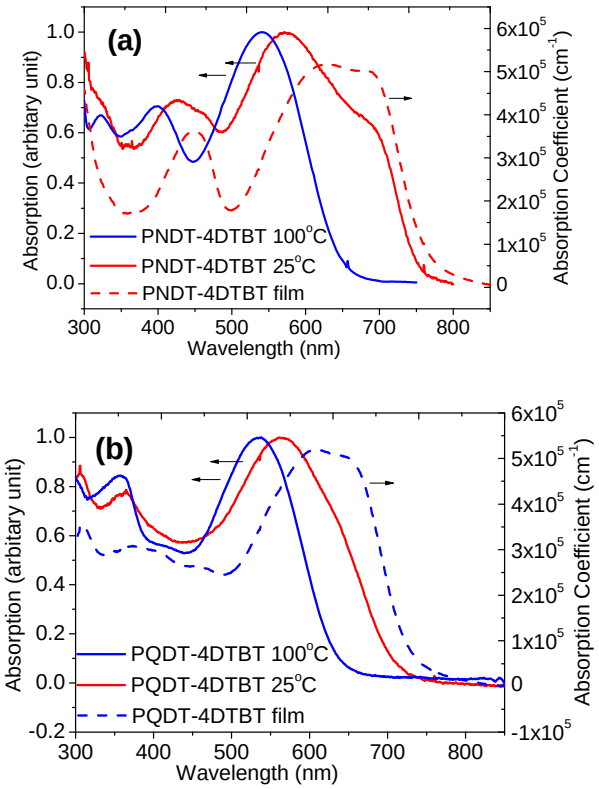

Figure 4-3. UV-vis absorption of PNDT-4DTBT (a) and PQDT-4DTBT (b) in various conditions: in chlorobenzene solution at 100 °C (blue solid line), at room temperature (red solid line) and in solid films (dotted line)

4.3. Optical Properties

The absorption spectra of the polymers in chlorobenzene (CB) solution at different temperatures and in solid films are shown in **Figure 4-3** and the related data are summarized in **Table 4-2**. Solution UV-vis spectra in CB solution at various temperatures showed similar absorption maximum for both **PNDT-4DTBT** and **PQDT-4DTBT**. In CB solution at room temperature, **PNDT-4DTBT** also showed signs of

aggregation via strong inter-chain π-π interaction, which is suggested by an additional absorption shoulder around 700 nm (**Figure 4-3**). This absorption shoulder is much weaker in **PQDT-4DTBT** absorption spectrum, suggesting reduced aggregation for **PQDT-4DTBT**. These additional absorpotion shoulders disappear when measuring the solution at 100°C. Absorption shoulder is more pronounced in the solid state for both polymers indicating strong π-stacking and polymer chain re-organization.[6] Again, **PNDT-4DTBT** showed further red shift, extending beyond 800 nm. A band gap of 1.61 eV was estimated from the onset of the film absorption for **PNDT-4DTBT**, smaller than that of **PQDT-4DTBT** (1.70 eV). The narrower band gap should lead to more light absorption and a higher current.

4.4. Electrochemical Properties

Cyclic voltammograms were recorded from thin films of PNDT-4DTBT and PQDT-4DTBT drop-casted from chloroform solutions as described in the experimental section. The potentials were internally calibrated using the ferrocene/ferrocenium redox couple (Fc/Fc^+). The CV curves of both polymers are shown in **Figure 4-4a** and the HOMO levels calculated from onset of the oxidation and reduction peaks and LUMO levels calculated calculated from the HOMO level and the optical band gap of each polymer are illustrated in **Figure 4-4b**. Both electrochemical characterizations of polymers via cyclic voltammetry (CV) of their thin films and calculated using optical band gaps reveal that these two polymers share similar LUMO energy levels. This similarity is expected since the LUMO of donor-acceptor copolymers is largely determined by the acceptor moiety.[118,144] However, substituting naphthalene unit with more electron deficient

quinoxaline in the donor part weakens the electron donating ability of **QDT**, leading to the observed lower HOMO energy level of – 5.46 eV (**PQDT-4DTBT**) compared with – 5.34 eV (**PNDT-4DTBT**) (**Figure 4-4**). The difference of 0.12 eV in HOMO energy levels, together with a near identical LUMO energy level, explains the observed difference of 0.09 eV in the band gaps of **PNDT-4DTBT** and **PQDT-4DTBT**. The lower HOMO energy level suggests that a higher voltage can be obtained in the BHJ devices.

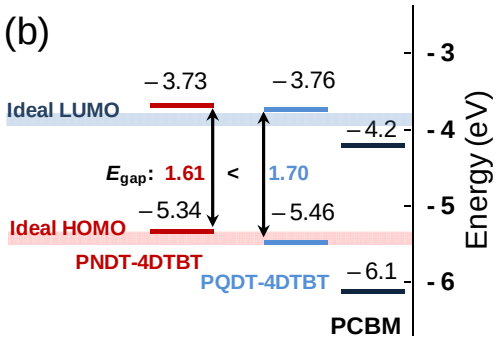

Figure 4-4. (a) Cyclic voltammograms of the oxidation and reduction behavior of **PNDT-4DTBT** and **PQDT-4DTBT** thin films. (The arrows indicate where the onsets of the oxidation and reduction peaks are. Note the LUMO levels of the two polymers are nearly identical) (b) Energy band diagram. The LUMO level was calculated from the HOMO level and the optical band gap of each polymer. Ideal LUMO and HOMO levels were adapted from reference 3.

4.5. Computational Simulation

Computational study of **PNDT-4DTBT** and **PQDT-4DTBT** provides insightful information to account for the observed difference of optical and electrochemical properties. To simplify the calculation, only one repeating unit of each polymer was subject to the calculation, with alkyl chains replaced by CH_3 groups. The optimized geometry, HOMO and LUMO energy levels and their electron density distributions were calculated at the B3LYP/6-311+G* level of theory [123,124] using density functional theory and Gaussian 03 package.[125] The simulated electron density distributions are shown in **Figure 4-5** and the calculated HOMO and LUMO levels are shown in **Table 4-2**.

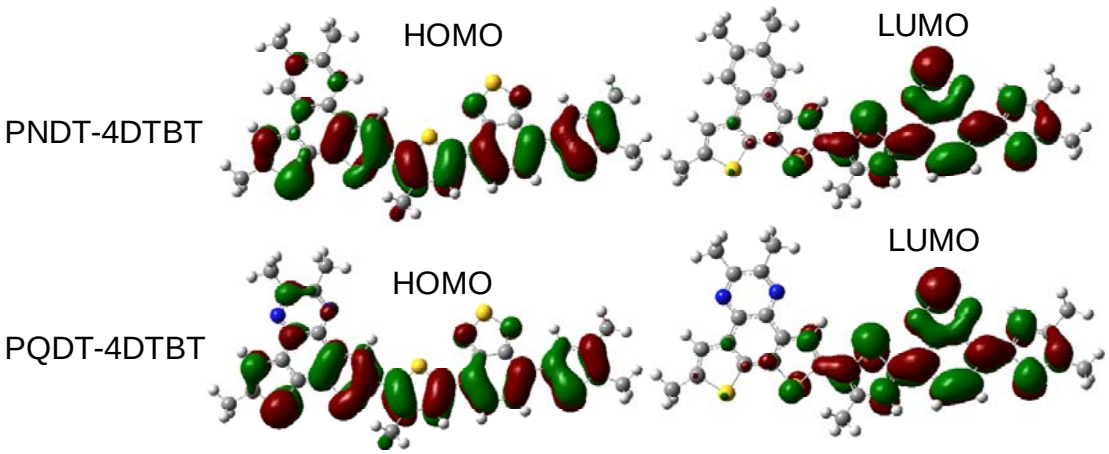

Figure 4-5. Calculation of HOMO (left) and LUMO (right) electron density distributions of **PNDT-4DTBT** and **PQDT-4DTBT**

The electron density distributions of LUMO levels for both polymers are nearly identical and both localized on DTBT unit only. Thus the change of donor units has little effect on LUMO levels. However, the electron density distributions of HOMO levels are

delocalized which indicates donor and acceptor units determine HOMO levels of the resulting polymers together. By changing NDT unit to the "weaker donor" QDT unit, both calculated and measured HOMO levels of **PQDT-4DTBT** decreased but LUMO levels did not change because both polymers have the same acceptor unit, **4DTBT**.

Table 4-2. Energy levels and optical data of **PNDT-4DTBT** and **PQDT-4DTBT.**

Polymer	HOMO [a] [eV]	LUMO [a] [eV]	Calculated HOMO [b] [eV]	Calculated LUMO [b] [eV]	UV-vis Absorption				
					CB solution		Film		
					λ_{max} [c] [nm]	λ_{max} [d] [nm]	λ_{max} [nm]	λ_{onset} [nm]	E_g [e] [eV]
PNDT-4DTBT	- 5.34	-3.29	-5.09	-2.86	573	540	629, 681	766	1.61
PQDT-4DTBT	- 5.46	-3.28	- 5.18	-2.86	563	533	609,647	728	1.70

[a] HOMO and LUMO levels are calculated from onset of the oxidation and reduction peaks of Cyclic voltammograms, respectively. [b] HOMO and LUMO levels calculated by density functional theory (DFT). [c] Absorption maxima at room temperature. [d] Absorption maxima at 100 °C. [e] Calculated from the intersection of the tangent on the low energetic edge of the absorption spectrum with the baseline.

4.6. Photovoltaic Properties

Photovoltaic properties of both polymers were probed on typical BHJ solar cell with a configuration of ITO/PEDOT:PSS (40 nm)/polymer:$PC_{61}BM$/Ca (40 nm)/Al (70 nm). Representative *J-V* curves are shown in **Figure 4-6a** and their photovoltaic performances are summarized in **Table 4-3**. In the case of **PNDT-4DTBT**, a thin film of ~ 95 nm were

fabricated by spin-coating a polymer:$PC_{61}BM$ (1:0.8 w/w) solution in DCB onto a PEDOT:PSS layer. The active layer of **PQDT-4DTBT** BHJ cells has a thickness of ~ 85 nm, processed from a blend of polymer:$PC_{61}BM$ (1:1.2 w/w) in DCB. Indeed, the smaller band gap of **PNDT-4DTBT** produces a short circuit current of 14.20 mA/cm^2, which is one of the highest J_{sc} generated by polymer/$PC_{61}BM$ BHJ *without* applying any additives.[143] Along with an open circuit voltage of 0.67 V and a fill factor of 53.95 %, a power conversion efficiency of 5.13 % is achieved. Conversely, the lower HOMO energy level of **PQDT-4DTBT** translates into a much higher V_{oc} of 0.83 V. However, the slightly larger band gap limited the J_{sc} to only 11.38 mA/cm^2. With a fill factor of 45.6 %, smaller efficiency (4.31 %) is obtained for **PQDT-4DTBT** based devices.

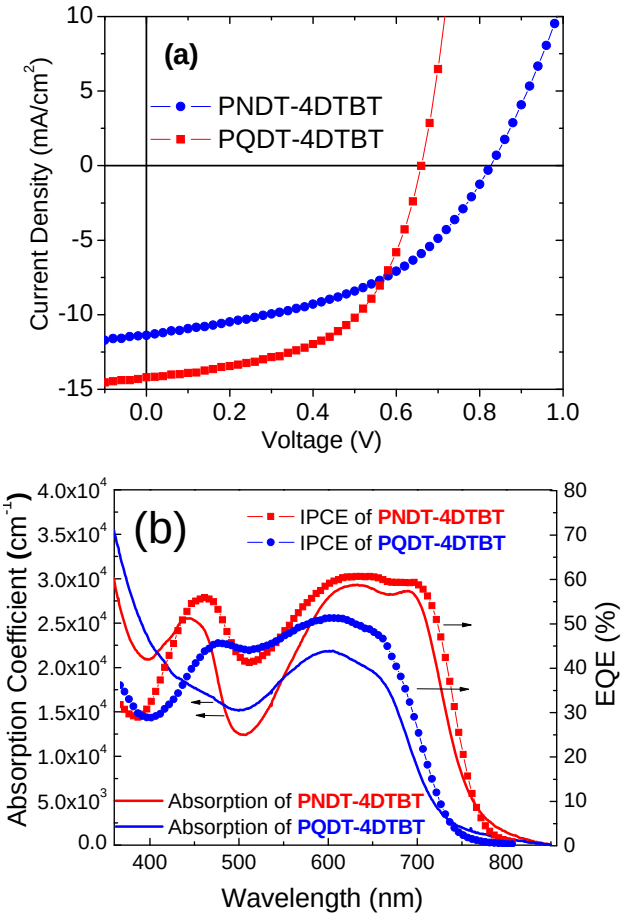

Figure 4-6. (a) Characteristic *J-V* curves of the devices of polymer based BHJ solar cells under 1 Sun condition (100 mW/cm^2). (b) IPCE and absorption of semi-optimized devices

Table 4-3. PV performances of polymers

Polymer	Polymer: $PC_{61}BM$	Processing Solvent	Thickness (nm)	V_{oc} (V)	J_{sc} (mA/cm^2)	*FF*	η (%)
PNDT-4DTBT	1:0.8	DCB	95	0.67	14.20	53.95%	5.13%
PQDT-4DTBT	1:1.2	DCB	85	0.83	11.38	45.64%	4.31%

Figure 4-6b shows the incident photo to current efficiency (IPCE) of related BHJ devices, together with their individual film absorption. Both BHJ devices show significant photo-to-current response in nearly the entire visible range (400 nm to 800 nm). For the **PNDT-4DTBT**/$PC_{61}BM$ solar cell, an IPCE of ~ 60 % was observed spanning from 620 nm to 720 nm. Due to the larger band gap of **PQDT-4DTBT**, its BHJ solar cell exhibits a decent IPCE over 40 % from 450 nm to 680 nm. The calculated J_{sc} by integrating the spectral response of the cells agrees well with photocurrent obtained by *J-V* measurements. Mobility measurements via space charge limited current (SCLC) is summarized in **Table 4-4**. A hole mobility of 7.17×10^{-5} cm^2/V·s was observed for the **PNDT-4DTBT**:$PC_{61}BM$ device, more than double that of the **PQDT-4DTBT**:$PC_{61}BM$ device (1.79×10^{-5} cm^2/V·s). The relatively low hole mobility partially explains why increasingly thin films need to be employed in both cases.[118]

Table 4-4. Mobility of polymers under SCLC condition

Polymer Only	Thickness (nm)	Mobility ($cm^2/V{\cdot}s$)	Polymer: $PC_{61}BM$	Thickness (nm)	Mobility ($cm^2/V{\cdot}s$)
PNDT-4DTBT	70	1.73×10^{-5}	1:0.8	95	7.17×10^{-5}
PQDT-4DTBT	45	7.24×10^{-6}	1:1.2	70	1.79×10^{-5}

4.7. Morphological Properties

The impact on the morphology by this small structural modification of similar polymers was studied using atomic force microscopy (AFM). Surface topography and phase images were acquired for each polymer/$PC_{61}BM$ film as shown in **Figure 4-7** and **Figure 4-8**, respectively. Relatively smooth surfaces with similar roughness observed for both polymer/$PC_{61}BM$ films suggest similar solubility of these two polymers in the processing solvent (DCB), due to the structural similarity of these two polymers with identical solubilizing alkyl chains. However, noticeable difference was observed in the phase images: phase separated domains of similar sizes can be clearly observed in the BHJ film of **PNDT-4DTBT**/$PC_{61}BM$, whereas no clear evidence of such phase separation was obtained in the blend film of **PQDT-4DTBT**/$PC_{61}BM$. The differences on the morphologies indicate a stronger inter-chain π-π interaction in **PNDT-4DTBT** than that in **PQDT-4DTBT**, which is consistent with the results of UV-vis spectra as previously discussed. A strong inter molecular π-π interaction in the conjugated polymer/$PC_{61}BM$ blend typically correlates to a high short circuit current of BHJ solar cells (e.g., in widely studied P3HT solar cells[145-147]), which further supports the observed larger J_{sc} in the **PNDT-4DTBT** based solar cell than in the case of **PQDT-4DTBT**.

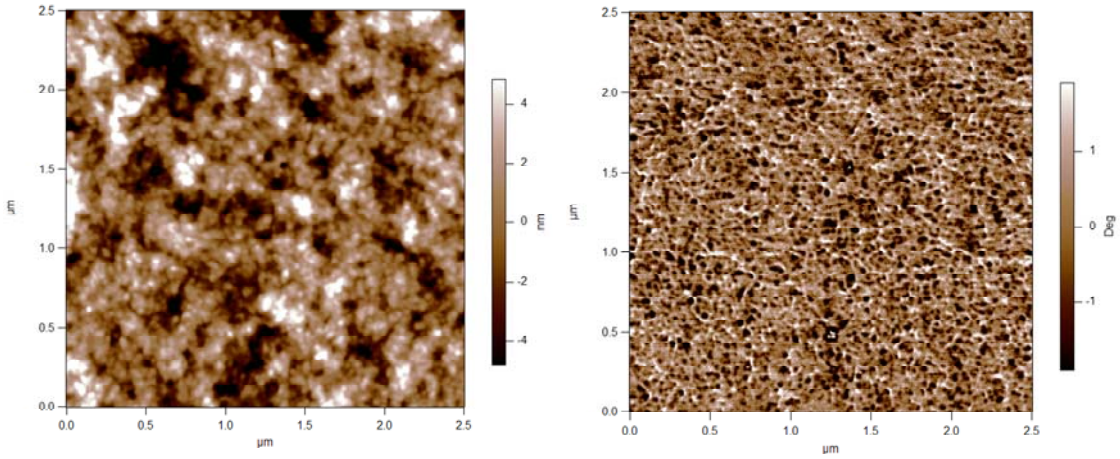

Figure 4-7. AFM images of **PNDT-4DTBT**:$PC_{61}BM$ film in a 1:0.8 ratio blend. (left: height image; right: phase image).

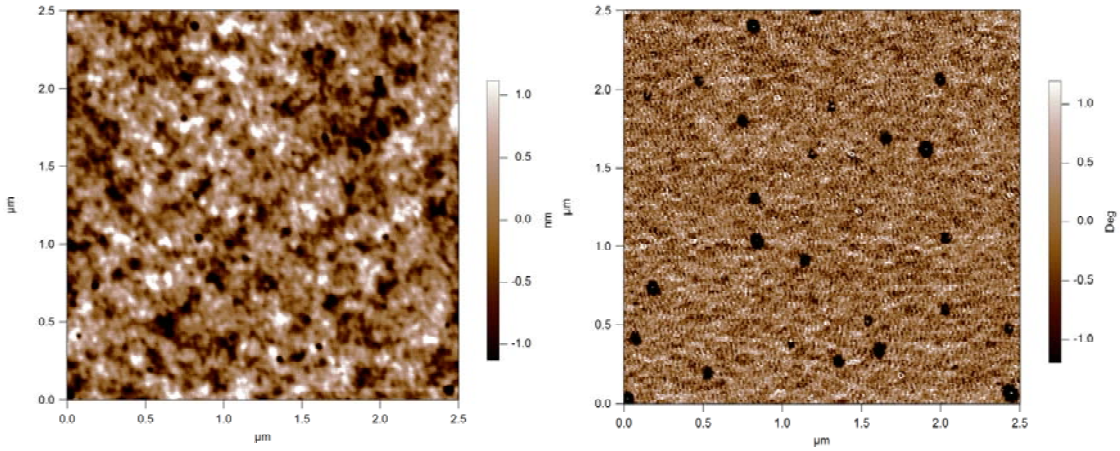

Figure 4-8. AFM images of **PQDT-4DTBT**:$PC_{61}BM$ film in a 1:1.2 ratio blend. (left: height image; right: phase image).

4.8. Conclusions

This study signifies the importance of fine tuning polymers structure via chemical modification. The conjugated backbones of these two polymers *differ by only two atoms*; however, this subtle change on the donor structure leads to a pronounced effect on the HOMO energy level and the band gap of resulting polymers. Future research will be focused on employment of even weaker donor and stronger acceptors via innovative

structural modification, in order to *concurrently* achieve a higher V_{oc} and a higher J_{sc}. In the meantime, new strategies to further improve the hole mobility also need to be pursued.

Finally, we want to highlight that an overall efficiency of 5.1 % and 4.3 % has been achieved for **PNDT-4DTBT** and **PQDT-4DTBT** *without* any special treatment, respectively. Further efficiency enhancement is expected by employing additional optimization methods. For example, replacing $PC_{61}BM$ with $PC_{71}BM$ can increase the J_{sc} by up to 20%.[5,143] In addition, processing additives and interfacial materials can also help improve the film morphology,[127,148-150] leading to a higher J_{sc} and *FF*.

4.9. Experimental Section

For the experimental details about electrochemistry, spectroscopy and SCLC mobility measurements please check **Appendix 1**. And please check **Appendix 4** for supporting information.

Instrumentation. Microwave assisted polymerizations were conducted in a CEM Discover Benchmate microwave reactor. Gel permeation chromatography (GPC) measurements of **PNDT-4DTBT** and **PQDT-4DTBT** were performed on a Waters 2695 Separations Module apparatus with a differential refractive index detector with tetrahydrofuran (THF) as eluent. The obtained molecular weight is relative to the polystyrene standard. Asylum Research MFP3D Atomic Force Microscope was used for taking AFM images. Differential Scanning Calorimeters (DSC) curves were acquired with TA Q200 instrument. ^{1}H nuclear magnetic resonance (NMR) measurements were recorded either with a Bruker Avance 300MHz AMX or Bruker 400 MHz DRX

spectrometer. ^{13}C nuclear magnetic resonance (NMR) measurements were carried out with a Bruker 400 MHz DRX spectrometer. Chemical shifts were expressed in parts per million (ppm), and splitting patterns are designated as s (singlet), d (doublet), m (multiplet) and br (broad). Coupling constants *J* are reported in Hertz (Hz).

Materials. All reagents and chemicals were purchased from commercial sources (Aldrich, Acros, Strem, Fluka) and used without further purification unless stated otherwise. Reagent grade solvents were dried when necessary and purified by distillation. Naphtho[2,1-*b*:3,4-*b'*]dithiophene (**NDT**) and dithieno[3,2-*f*:2',3'-*h*]quinoxaline (**QDT**) were synthesized according to our previous paper with slightly modified procedures.[134] The synthesis of 4,7-di(4-2-ethylhexyl-2-thienyl)-2,1,3-benzothiadiazole were described elsewhere.[141,151]

4,7-Bis(5-bromo-4-(2-ethylhexyl)-2-thienyl)-2,1,3-benzothiadiazole (4DTBT). 4,7-di(4-2-ethylhexyl-2-thienyl)-2,1,3-benzothiadiazole (0.091g, 0.157 mmol) and N-bromosuccinimide (NBS) (55.7mg, 0.314mmol) were added into THF under stirring. The reaction mixture was stirred at a room temperature for 2 h, then hexane was added into the mixture. The precipitate formed was filtered, and the filtrate was extracted with ether. The organic layer was washed with brine and dried over anhydrous sodium sulfate. The solvent was removed at a reduced pressure to give the product as a red solid. Yield: 93 mg (80%). ^{1}H NMR (300MHz, $CDCl_3$): δ 7.74 (s, 2H), 7.73 (s, 2H), 2.59 (m, 4H), 1.73 (m, 2H), 1.33-1.40 (m, 16H), 0.92 (m, 12H). ^{13}C NMR (400MHz, $CDCl_3$): δ 152.20, 142.26, 138.35, 128.65, 125.37, 124.86, 112.26, 40.02, 33.94, 32.55, 28.81, 25.78, 23.06, 14.08, 10.86.

Synthesis of Polymers. PNDT-4DTBT and **PQDT-4DTBT** were syntheized via Microwave-assisted Stille Coupling Polymerization shown in **Figure 4-2**. A representative procedure is as follows. To a 10 mL Microwave pressurized vial equipped with a stirring bar, **NDT** (160 mg, 0.202 mmol), **4DTBT** (138 mg, 0.202 mmol), $Pd_2(dba)_3$ (4.6 mg, 2.5%) and $P(o\text{-}tol)_3$ (12.7mg, 20%) were added. Then the tube was sealed, evacuated and refilled with argon for three cycles. Then chlorobenzene was added into the same reaction tube inside a glovebox. Reaction tube was put into microwave reactor and heated to 150 °C under 300 watt microwave for 20 min. After cooling to room temperature, the organic solution was added dropwise to 200 mL of methanol to obtain precipitate, which was collected by filtration and washed with methanol and dried. The crude polymer was then extracted subsequently with methanol, ethyl acetate, hexane and $CHCl_3$ in a Soxhlet's extractor. The fraction from chloroform was concentrated under reduced pressure and precipitated into methanol to give the polymer **PNDT-4DTBT** (151 mg, 76%) as a dark green solid.

PQDT-4DTBT was synthesized according to the same procedure as **PNDT-4DTBT** with respective monomers.

PNDT-4DTBT: ^{1}HNMR (400 MHz, $CDCl_2CDCl_2$, 400K): δ0.79-1.12 (24H, br), 1.27-1.67 (32H, br), 1.79-2.02 (4H, br), 2.83-3.09 (8H,br), 7.94 (2H, br), 7.99 (2H, br), 8.13 (2H, br), 8.19 (2H, br)

PQDT-4DTBT: ^{1}HNMR (400 MHz, $CDCl_2CDCl_2$, 400K): δ0.82-1.25 (24H, br), 1.27-1.83 (32H, br), 1.94 (2H,br), 2.32 (2H, br), 3.02 (4H, br), 3.11 (4H, br), 7.96 (2H, br), 8.08 (2H, br), 8.44(2H, br)

Polymer solar cell fabrication and testing. Glass substrates coated with patterned indium-doped tin oxide (ITO) were purchased from Thin Film Devices, Inc. The 150 nm sputtered ITO pattern had a resistivity of 15Ω/□. Prior to use, the substrates were ultrasonicated in acetone followed by deionized water and then 2-propanol for 20min each. The substrates were dried under a stream of nitrogen and subjected to the treatment of UV-Ozone over 30 minutes. A 0.45 μm-filtered dispersion of PEDOT:PSS in water (Baytron PH500) was then spun cast onto clean ITO substrates at 4000 rpm for 60 seconds and then baked at 140 °C for 15 minutes to give a thin film with a thickness of 40 nm. A blend of polymer and $PC_{61}BM$ with varied concentration and feed ratio were dissolved in dichlorobenzene with heating at 110 °C for 6 hours. All the solutions were filtered through a 1 μm poly(tetrafluoroethylene) (PTFE) filter, spun cast at different rpm for 60 seconds onto PEDOT:PSS layer. The substrates were then dried under nitrogen atmosphere at room temperature for 12 hours. The thicknesses of films were recorded by a profilometer (Alpha-Step 200, Tencor Instruments). The devices were finished for measurement after thermal deposition of a 40 nm film of calcium and a 70 nm aluminum film as the cathode at a pressure of ~ 1×10^{-6} mbar. There are 8 devices per substrate, with an active area of 12 mm^2 per device. Device characterization was carried out under AM 1.5G irradiation with the intensity of 100 mW/cm^2 (Oriel 91160, 300 W) calibrated by a NREL certified standard silicon cell. Current density versus potential (J-V) curves were recorded with a Keithley 2400 digital source meter. IPCE were detected under monochromatic illumination (Oriel Cornerstone 260 ¼ m monochromator equipped with Oriel 70613NS QTH lamp) and the calibration of the incident light was performed with a monocrystalline silicon diode. All fabrication steps after adding the PEDOT:PSS layer

onto ITO substrate, and characterizations were performed in gloveboxes under nitrogen atmosphere.

CHAPTER 5

ENHANCED PHOTOVOLTAIC PERFORMANCES OF LOW BAND GAP POLYMERS WITH DEEP LUMO LEVELS

Huaxing Zhou, Liqiang Yang, Samuel C. Price, Kelly Jane Knight, and Wei You

Adapted from *Angew. Chem. Int. Ed.* 2010, 49, 7992

5.1 Introduction

Most of the conjugated polymers developed so far have either high-lying HOMO levels compared with ideal energy levels or large band gap in spite of low-lying HOMO levels, which prevents the enhancement on PCE.[32] In order to concurrently lower the HOMO energy level and the band gap as required by the ideal polymer, we proposed the "weak donor-strong acceptor" strategy to construct alternating D-A copolymers (**Chapter 3**).[144] In D-A polymers, the HOMO and LUMO energy levels are largely localized on the donor moiety and the acceptor moiety, respectively.[144,152] This feature offers an important advantage of *individually* tuning the band gap and energy levels of the conjugated polymer. For example, smaller band gap can be obtained by copolymerizing a more electron-rich donor moiety and a more electron-deficient acceptor moiety, whereas the HOMO and LUMO levels can also be adjusted by varying the electron donating ability of the donor moiety and the electron affinity of the acceptor moiety.[144] As exemplified in **Chapter 3**, by incorporating weak donor moieties based on

fused benzodithiophene, and a strong acceptor based on benzothiadiazole (BT), we have successfully demonstrated this weak donor-strong acceptor strategy with high efficiency in typical BHJ devices.[51,151] In these conjugated polymers, close to ideal HOMO energy levels were achieved (e.g., – 5.46 eV), which lead to the observed open circuit voltage (V_{oc}) as high as 0.85 V.[51] However, the band gaps of these materials were still larger than the proposed 1.5 eV of ideal polymers, which explains why mediocre short circuit currents (J_{sc}) were obtained. Logically, in order to further improve the efficiency, a smaller band gap is needed to achieve a higher short circuit current (J_{sc}) while the low HOMO energy level should still be maintained. Thus, copolymers with lower LUMO levels should be designed. Fortunately, our previous study on "weak donor – strong acceptor" strategy indicated that the LUMO of donor-acceptor copolymers is mostly controlled by the acceptor moiety.[118,133,141] Therefore, we envisioned that copolymerizing a more electron deficient acceptor (strong acceptor) with "weak donors" would lead to a smaller band gap and maintain the low HOMO energy level in these newly designed materials.

5.2. Strong Acceptor Design

Compared with benzene, pyridine is π-electron deficient. Therefore if we replaced the benzene in the BT unit with pyridine, the new acceptor, thiadiazolo[3,4-*c*]pyridine (PyT), would be one such stronger acceptor. A similar strategy has been demonstrated by Leclerc *et al.*;[100] the copolymer (PCDTPT) indeed showed a much lower LUMO level compared with that of PCDTBT. However, low efficiencies were obtained when compared with benzothiadiazole, presumably due to the low molecular weight and low

solubility ofthe thiadiazolo[3,4-*c*]pyridine based polymers. To solve these issues, we employed the strategy of a "soluble" acceptor,[141,151] by flanking the PyT moiety with two alkylated thienyl units, which converted the PyT into the new soluble stronger acceptor, DTPyT. As demonstrated in **Chapter 2**,[141] anchoring alkyl chains to the 4 position of the thienyl units of DTPyT would only introduce minimum steric hindrance, while significantly improve the molecular weight and solubility of resulting polymers.

Figure 5-1. Molecular structure of PNDT-DTPyT, PQDT-DTPyT and PBnDT-DTPyT

Herein we report the synthesis of a series of "weak donor-strong acceptor" polymers PNDT-DTPyT, PQDT-DTPyT and PBnDT-DTPyT by copolymerizing various donor moieties, NDT (naphtho[2,1-*b*:3,4-*b′*]dithiophene), QDT (dithieno[3,2-*f*:2',3'-*h*]quinoxaline), BnDT (benzo[1,2-*b*:4,5-*b′*]dithiophene) with the soluble DTPyT acceptor

moiety (**Figure 5-1**). Our preliminary investigation on the photovoltaic properties of these polymers in typical BHJ devices using $PC_{61}BM$ as the electron acceptor showed highly respectable power conversion efficiencies (PCE) over 5.5% for PQDT-DTPyT, and over 6% for PBnDT-DTPyT and PNDT-DTPyT.

5.3. Monomers and Polymer Synthesis

The synthesis of the alkylated DTPyT is modified from the reported procedure[100] (experimental details in **Experimental Section**). The other co-monomers – alkylated NDT, QDT and BnDT – used established literature procedures.[72,134,151] Three polymers, PNDT-DTPyT, PQDT-DTPyT and PBnDT-DTPyT were synthesized via the microwave-assisted Stille polycondensation[6] between alkylated dibrominated DTPyT and corresponding distannane monomers. Crude polymers were purified by Soxhlet extraction with methanol, ethyl acetate, hexane and chloroform. The chloroform fraction was concentrated and re-precipitated in methanol to afford the purified polymers. Gel permeation chromatography (GPC) studies of these three polymers were conducted in trichlorobenzene at high temperature (135°C). All three polymers showed high molecular weights, especially in the case of PBnDT-DTPyT (**Table 5-1**), underscoring the importance of introducing the "soluble" acceptor.

Table 5-1. Polymerization results and energy levels of PNDT-DTPyT, PQDT-DTPyT and PBnDT-DTPyT.

Polymers	Yield	Mw [kg/mol][a]	PDI	HOMO [eV][b]	LUMO [eV][b]
PNDT-DTPyT	92%	17.1	2.14	5.36	3.42
PQDT-DTPyT	88%	21.7	2.27	5.50	3.44
PBnDT-DTPyT	53%	104.4	3.64	5.47	3.44

[a] Determined by GPC in TCB at 135°C using polystyrene standards. [b] HOMO and LUMO levels were calculated from the onsets of oxidation peaks and reduction peaks, respectively.

5.4. Optical and Electrochemical Properties

The solution absorption spectra of the three polymers at high temperature (100°C) are almost identical as shown in **Figure 5-2a**, containing two absorption maxima as typically observed for donor-acceptor low band gap materials. However, these polymers tend to aggregate, indicated by a large bathochromic shift (ca. 25-90 nm) in the solution spectra at room temperature (**Figure 5-2b**). The absorption spectra in the solid state are quite different for these three polymers, indicating different polymer chain organization and interaction in thin films.[6] For example, the absorption of PBnDT-DTPyT has the largest redshift when transitioning from solution to the film, presumably due to the symmetric molecular structure of the BnDT unit which helps molecular stacking in the solid state. A larger redshift of the absorption spectrum of PNDT-DTPyT than that of PQDT-DTPyT was observed, suggesting PNDT-DTPyT adopts a more planar polymer chain conformation and more effective chain-chain stacking in the solid state. The estimated

optical band gaps of PNDT-DTPyT, PQDT-DTPyT and PBnDT-DTPyT are 1.53 eV, 1.56 eV and 1.51 eV respectively, noticeably reduced (ca. 0.09-0.19eV) compared with the band gaps of their 2,1,3-benzothiadiazole counterparts.[51,151]

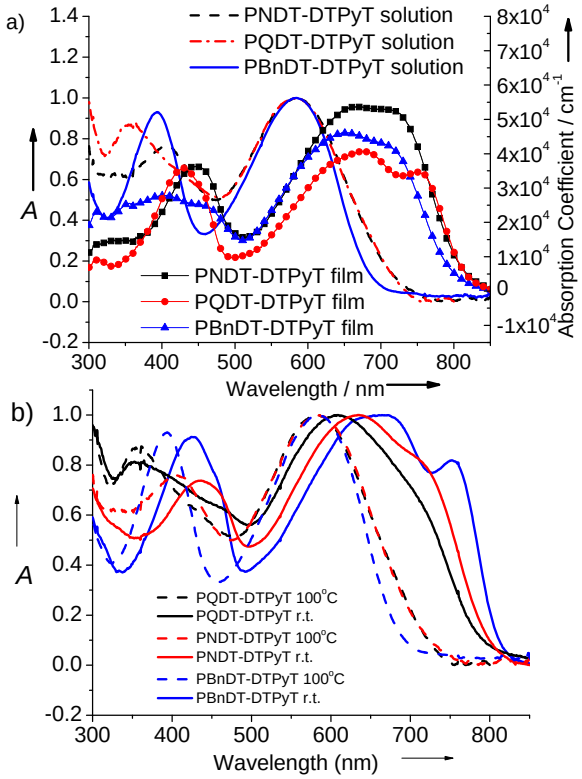

Figure 5-2. a) The UV-vis absorption spectra of PNDT-DTPyT, PQDT-DTPyT and PBnDT-DTPyT in chlorobenzene solution at 100°C and in solid films. b) UV-vis Absorption spectra of **PNDT-DTPyT**, **PQDT-DTPyT** and **PBnDT-DTPyT** in chlorobenzene (CB) solution at room temperature and 100°C.

The HOMO and LUMO energy levels of each polymer were estimated via cyclic voltammograms and tabulated in **Table 5-1**. The LUMO levels of all three polymers, calculated from the onset of the reduction potential, are almost identical within the

experimental error, indicative of the identical acceptor unit (DTPyT). This agrees well with the previous discovery that LUMO of donor-acceptor polymer is primarily located in the acceptor unit.[100,141,144] More importantly, replacing 2,1,3-benzothiadiazole with the stronger acceptor DTPyT in these three polymers lowered the LUMO energy levels by ~ 0.2 eV compared with the benzothiadiazole analogs.[51,151] It is also worth noting that all three weak donors – NDT, QDT and BnDT – were able to maintain low HOMO energy levels around the ideal HOMO energy level of – 5.4 eV.

Table 5-2. Optical data of **PNDT-DTPyT, PQDT-DTPyT** and **BnDT-DTPyT**

Polymer	UV-Vis Absorption								
	CB solution at 100°C			CB solution at room temp.			Film		
	λ_{max} [nm]	λ_{onset} [nm]	Eg^a [eV]	λ_{max} [nm]	λ_{onset} [nm]	Eg^a [eV]	λ_{max} [nm]	λ_{onset} [nm]	Eg^a [eV]
PNDT-DTPyT	583	727	1.71	635	800	1.55	667,712	812	1.53
PQDT-DTPyT	583	717	1.73	607	790	1.57	654	797	1.56
PBnDT-DTPyT	583	682	1.82	670	810	1.53	676	819	1.51

[a] Calculated from the intersection of the tangent on the low energetic edge of the absorption spectrua with the baseline.

5.5. Photovoltaic Properties

BHJ PV devices were fabricated with a typical configuration of ITO/PEDOT:PSS(40nm)/polymer:$PC_{61}BM$/Ca(40nm)/Al(70nm). All PV devices were tested under simulated AM1.5G illumination (100mW/cm^2). Typical current density-voltage (*J-V*) characteristics are shown in **Figure 5-3a** and summarized in **Table 5-3**. All devices showed promising efficiency over 5.5% with one of these three polymers as the

donor material and $PC_{61}BM$ as the electron acceptor in our initial trials. The highest current of 14.2 mA/cm^2 was obtained for PNDT-DTPyT based devices, which is among the highest J_{sc} obtained for BHJ device consisting of a donor polymer and $PC_{61}BM$ as the acceptor.[143] The high J_{sc} along with a V_{oc} of 0.71V and a high fill factor (FF) of 0.61, yields an impressive PCE of 6.20% for PNDT-DTPyT:$PC_{61}BM$ based BHJ solar cells. When PQDT-DTPyT or PBnDT-DTPyT with deeper HOMO levels is used in BHJ solar cells, we observe higher V_{oc} than that of PNDT-DTPyT based devices. Though PQDT-DTPyT based devices generate smaller J_{sc} than that of PNDT-DTPyT devices, presumably due to the slightly larger band gap of PQDT-DTPyT, a PCE of 5.57% is still achieved because the increased V_{oc} partially compensates for the decreased J_{sc}. Interestingly, the J_{sc} of PBnDT-DTPyT based device is smaller than those of the other two polymer devices, despite PBnDT-DTPyT having the smallest band gap. Two possible reasons are proposed to explain this observation. First, PBnDT-DTPyT has the longest solubilizing chains among all three studies polymers. Therefore the effective chromophore density in the solid state is the lowest in the case of PBnDT-DTPyT, as corroborated by its relatively low absorption coefficient. Second, such long alkyl chains could increase the inter-conjugated backbone distance and lower the hole mobility.[26] However, a noticeably high V_{oc} of 0.85 V was obtained, which helps reach a respectable PCE of 6.32% in PBnDT-DTPyT based BHJ devices.

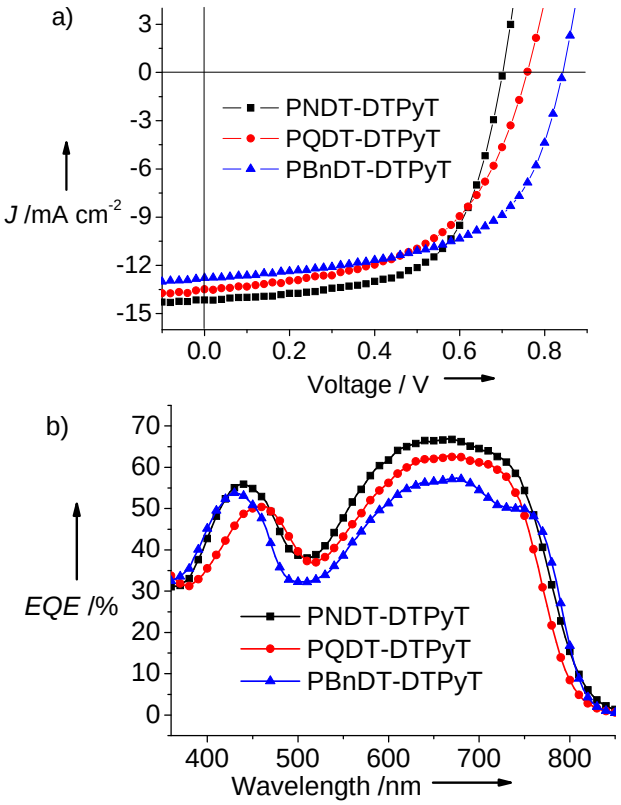

Figure 5-3. (a) Current density-voltage (J-V) curves of polymer/$PC_{61}BM$ based solar cell devices under AM 1.5G illumination (100 mW cm^{-2}). (b) External quantum efficiency (EQE) curves of polymer/$PC_{61}BM$ based solar cell devices.

To further confirm the accuracy of the measurements, the external quantum efficiency (EQE) curves of the devices based on these three polymers were acquired and shown in **Figure 5-3b**. All devices showed very high incident photo-conversion efficiency, with maxima around 670 nm. Further increase on the J_{sc} is still possible when $PC_{71}BM$ is employed to replace $PC_{61}BM$, since $PC_{71}BM$ [2,48,82] has significantly more absorption in the visible region than $PC_{61}BM$.

Table 5-3. Photovoltaic properties of PNDT-DTPyT, PQDT-DTPyT and PBnDT-DTPyT based BHJ solar cells processed with polymer/$PC_{61}BM$ 1:1 (w/w) blend in DCB.

Polymers	Thickness [nm]	J_{sc} [mA/cm^2]	V_{oc} [V]	*FF* [%]	PCE_{max} ($PCE_{average}$) [%]
PNDT-DTPyT	85	14.16	0.71	61.7	6.20 (6.07)
PQDT-DTPyT	90	13.49	0.75	55.1	5.57 (5.32)
PBnDT-DTPyT	90	12.78	0.85	58.2	6.32 (6.11)

5.6. Summary

In summary, a soluble strong acceptor, DTPyT, which is stronger than the commonly used 2,1,3-benzothiadiazole acceptors, has been synthesized and incorporated into our "weak donor-strong acceptor" copolymer strategy. Three new polymers (PNDT-DTPyT, PQDT-DTPyT and PBnDT-DTPyT) showed noticeably reduced LUMO levels, slightly reduced HOMO levels, and thus smaller band gaps than their DTBT counterparts. The smaller band gap significantly improves the observed J_{sc} of the related BHJ devices, while the low HOMO energy level maintains the high V_{oc}. Therefore all three polymers achieved high efficiency numbers in the BHJ devices, demonstrating the great utility of DTPyT acceptor moiety in designing high performance solar cell materials.

5.7. Experimental Section

For the experimental details about electrochemistry, spectroscopy and SCLC mobility measurements please check **Appendix 1**. And please check **Appendix 5** for supporting information.

Reagents and Instrumentation. All reagents and chemicals were purchased from commercial sources (Aldrich, Acros, Matrix Scientific) and used without further

purification unless stated otherwise. Reagent grade solvents were dried when necessary and purified by distillation. Microwave assisted polymerizations were conducted in a CEM Discover Benchmate microwave reactor. Gel permeation chromatography (GPC) measurements were performed on a Polymer Laboratories PL-GPC 220 instrument (at the University of Chicago) using 1,2,4-trichlorobenzene as the eluent (stabilized with 125 ppm BHT) at 135 °C. The obtained molecular weight is relative to the polystyrene standard. ^{1}H and ^{13}C nuclear magnetic resonance (NMR) measurements were recorded either with a Bruker Avance 300MHz AMX or Bruker 400 MHz DRX spectrometer. UV-visible absorption spectra were obtained by a Shimadzu UV-2401PC spectrophotometer. The film thicknesses were recorded by a profilometer (Alpha-Step 200, Tencor Instruments).

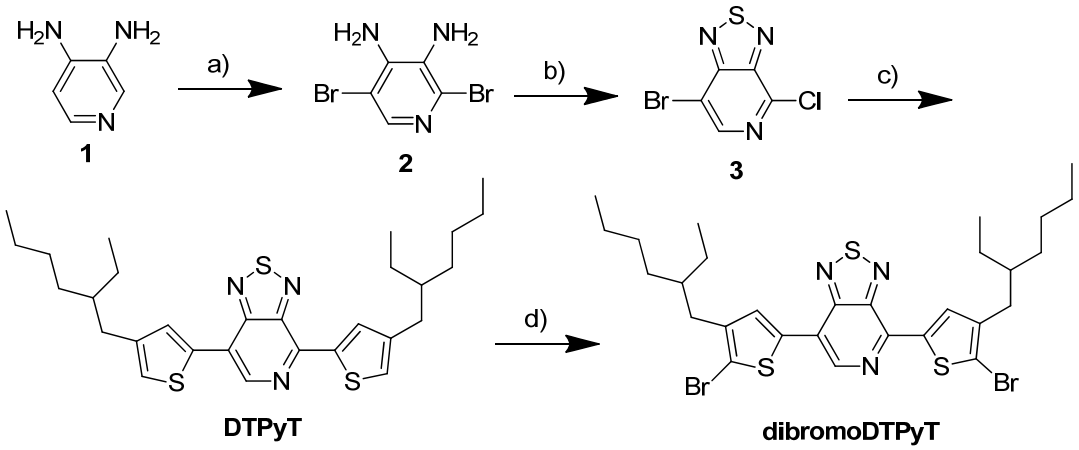

Figure 5-4. Synthetic route of alkylated DTPyT. a). HBr, Br_2, reflux 40% b). $SOCl_2$ reflux 55% c). (4-(2-ethylhexyl)thiophen-2-yl)trimethylstannane, $PdCl_2(PPh_3)_2$, DMF, THF, reflux, 74% d). NBS, THF, rt, 80%.

The 7-bromo-4-chloro[1,2,5]thiadiazoleo[3,4-*c*]pyridine **(3)**[100] and (4-(2-ethylhexyl)thiophen-2-yl) trimethylstannane[141] have been reported in the literature. Other compounds have been synthesized following procedures described below.

Synthesis of DTPyT. In a 250 mL flame-dried 2-neck round-bottom flask with a condenser, (4-(2-ethylhexyl)thiophen-2-yl)trimethylstannane (2.04g, 4.2mmol, 2.2 eq), 7-bromo-4-chloro[1,2,5]thiadiazoleo[3,4-*c*]pyridine (0.475g, 1.90mmol, 1eq) and argon-saturated DMF 10 mL and THF 10 mL were added. The mixture was then purged with argon for 15min. Then, bis(triphenylphosphine)palladium(II) dichloride ($Pd(PPh_3)_2Cl_2$) was added and the reaction mixture was heated to reflux overnight. The reaction mixture was then cooled to room temperature and the solvent was evaporated. The crude red product was re-dissolved in THF and filtered through a short silica gel. The solvent was evaporated and the product was recrystallized from ethanol. Yield: 0.74 g (74%) ^{1}H NMR (400MHz, $CDCl_3$): δ 8.81 (s, 1H), 8.50 (s, 1H), 7.93 (s, 1H), 7.18 (s, 1H), 7.05 (s, 1H), 2.64 (m, 4H), 1.67 (m, 2H), 1.21-1.42 (m, 16H), 0.95 (m, 12H).

Synthesis of dibromoDTPyT. **DTPyT** (0.24g, 0.456mmol) and N-bromosuccinimide (NBS) (178mg, 0.1mmol) were added into THF under stirring. The reaction mixture was stirred at a room temperature for 6 h, then the reaction mixture washed with washed with brine and dried over anhydrous sodium sulfate. The solvent was removed at a reduced pressure to give the product as a red solid. Needle-like crystal was obtained by recrystallizing from ethanol. Yield: 249 mg (80%). ^{1}H NMR (400MHz, $CDCl_3$): δ 8.65 (s, 1H), 8.29 (s, 1H), 7.72 (s, 1H), 2.58 (m, 4H), 1.71 (m, 2H), 1.20-1.40

(m, 16H), 0.91 (m, 12H). ^{13}C NMR (400MHz, CDCl3): δ 154.59, 145.49, 143.41, 142.49, 140.16, 140.82, 135.76, 133.06, 129.06, 119.85, 117.08, 112.55, 40.00, 34.07, 32.55, 28.81, 25.79, 23.05, 14.08, 10.86.

General procedures for Microwave-assisted polymerization. To a 10 mL Microwave pressurized vial equipped with a stirring bar, **NDT** (104 mg, 0.132 mmol), **dibromoDTPyT** (90 mg, 0.132 mmol), $Pd_2(dba)_3$ (6 mg) and $P(o\text{-}tol)_3$,(16.5mg) were added. Then the tube was sealed and evacuated and refilled with argon for three cycles, followed by the addition of o-xylene (0.6 mL) and DMF (0.1 mL) into the tube in a glovebox. Reaction tube was put into microwave reactor and heated to 150 °C under 300 watt microwave for 20 min. After cooling to room temperature, the organic solution was added dropwise to 200 mL of methanol to obtain precipitate, which was collected by filtration and washed with methanol and dried. The crude polymer was then extracted subsequently with methanol, acetone, hexane and $CHCl_3$ in a Soxhlet's extractor. The fraction from chloroform was concentrated under reduced pressure and precipitated into methanol to give the polymer **PNDT-4DTBT** (120 mg, 92%) as a dark green solid.

PNDT-DTPyT. ^{1}H NMR (400MHz, $CDCl_2CDCl_2$): δ 8.98-7.53 (br, 7H), 3.21-2.40 (br, 8H), 2.12-1.22 (br, 42H), 1.22-0.75 (br, 18H).

PQDT-DTPyT. ^{1}H NMR (400MHz, $CDCl_2CDCl_2$): δ 8.95-7.65 (br, 5H), 3.31-2.42 (br, 8H), 2.22-1.83 (br, 6H), 1.83-1.23 (br, 36H), 1.23-0.81 (br, 18H).

PBnDT-DTPyT. ^{1}H NMR (400MHz, $CDCl_2CDCl_2$): δ 8.95 (s, 1H), 8.64 (s, 1H), 8.09 (s, 1H), 7.76 (s, 1H), 7.70 (s, 1H), 3.28 (br, 4H), 3.07 (br, 4H), 1.96 (br, 6H), 1.70-1.27 (br, 50H), 1.08-0.85 (br, 24H).

Polymer solar cell fabrication and testing. Glass substrates coated with patterned indium-doped tin oxide (ITO) were purchased from Thin Film Devices, Inc. The 150 nm sputtered ITO pattern had a resistivity of 15Ω/□. Prior to use, the substrates were ultrasonicated for 20 minutes in acetone followed by deionized water and 2-propanol. The substrates were dried under a stream of nitrogen and subjected to the treatment of UV-Ozone over 30 minutes. A filtered dispersion of PEDOT:PSS in water (Baytron PH500) was then spun cast onto clean ITO substrates and then baked at 140 °C for 15 minutes. A blend of polymer and $PC_{61}BM$ was dissolved in chlorinated solvent with heating at 110 °C for 8 hours. All the solutions were then spun cast onto PEDOT:PSS layer and dried at room temperature in the glovebox under nitrogen atmosphere for 12 hours. Then a 40 nm film of calcium and a 70 nm aluminum film were thermal deposited at a pressure of ~ 1×10^{-6} mbar. here are 8 devices per substrate, with an active area of 0.12 cm^2 per device. Device characterization was carried out under AM 1.5G irradiation with the intensity of 100 mW/cm^2 (Oriel 91160, 300 W) calibrated by a NREL certified standard silicon cell. Current density versus potential (*J*-V) curves were recorded with a Keithley 2400 digital source meter. EQE were detected under monochromatic illumination (Oriel Cornerstone 260 ¼ m monochromator equipped with Oriel 70613NS QTH lamp) and the calibration of the incident light was performed with a monocrystalline silicon diode. All fabrication steps after adding the PEDOT:PSS layer

onto ITO substrate, and characterizations were performed in gloveboxes under nitrogen atmosphere.

CHAPTER 6

DEVELOPMENT OF FLUORINATED BENZOTHIADIAZOLE AS STRUCTURAL UNIT TOWARDS A 7% POLYMER SOLAR CELL

Huaxing Zhou, Liqiang Yang, Andrew C. Stuart, Samuel C. Price, Shubin Liu, and Wei You

Adapted from *Angew. Chem. Int. Ed.* 2011, 50, 2995

6.1. Introduction

Fluorinated organic molecules exhibit a series of unique features such as great thermal and oxidative stability,[153] elevated resistance to degradation,[154] enhanced hydrophobicity , high lipophobicity in perfluorinated substances,[155] and inverted charge density distribution in fluorinated aromatic compounds.[156] These special features are related to the unique properties of the fluorine atom:[157] (a) fluorine is the most electronegative element in the periodic table, with a Pauling electronegativity of 4.0, much larger than that of hydrogen (2.2); (b) fluorine is the smallest electron withdrawing group (van der Waals radius, r = 1.35 Å, only slightly larger than hydrogen, r = 1.2 Å). Furthermore, these fluorine atoms often have a great influence on inter- and intramolecular interactions via C-F···H, F···S and C-F···π_F interactions.[154,158] Therefore the fluorinated conjugated materials have been explored for their applications in organic field effect transistors (OFET)[159-161] and organic light emitting diode (OLED).[156,162] However, there are only a few examples of applying fluorinated compounds in organic

photovoltaics,[143,163,164] especially as p-type semiconductor in bulk heterojunction (BHJ) polymer solar cells.

Since the fluorine atom is a strong electron-withdrawing substituent, the introduction of F to the conjugated backbone would lower both the LUMO and HOMO levels of the conjugated polymers, as demonstrated by Heeger and Brédas in a theoretical study of poly(phenylene vinylene) (PPV) with various substituents.[165] Experimentally, Yu et al. confirmed the electronic effect of the fluorine substituent in their study of a series of low band gap conjugated polymers via the quinoid approach.[143] After one fluorine atom was substituted on the thieno[3,4-*b*]thiophene unit, the corresponding copolymer with the benzodithiophene unit exhibited decreased LUMO and HOMO levels yet a similar low band gap, compared with those of the non-fluorinated analog. A larger open circuit voltage (V_{oc}) was observed from the BHJ device based on the F-substituted polymer, largely due to the lower HOMO energy level. Moreover, the short circuit current (J_{sc}) and the fill factor (*FF*) were noticeably increased by judicious selection of solvent and additives,[80] possibly due to an optimized film morphology facilitated by these F atoms. Similar enhancement on morphology by employing F atoms was observed by Kim et al. in their study of poly(3-hexylthiophene) (P3HT) with various end-groups.[163] The CF_3 end group modified P3HT showed significant improvement in both J_{sc} and *FF* in its BHJ devices, leading to a total 40% increase on the efficiency (η). The much improved morphology of the polymer:$PC_{61}BM$ blend was attributed to the decreased surface energy of the fluorine containing polymer. We can see that fluorine atom plays an important role in controlling energy levels, mobility and active layer morphology. To further study this fluorine impact, we envision to study the photovoltaic properties of F atom containing

low band gap polymers constructed by the donor-acceptor strategy,[166] which is the dominant approach in creating new polymers for BHJ polymer solar cells and , has not been studied previously. [60,61,167]

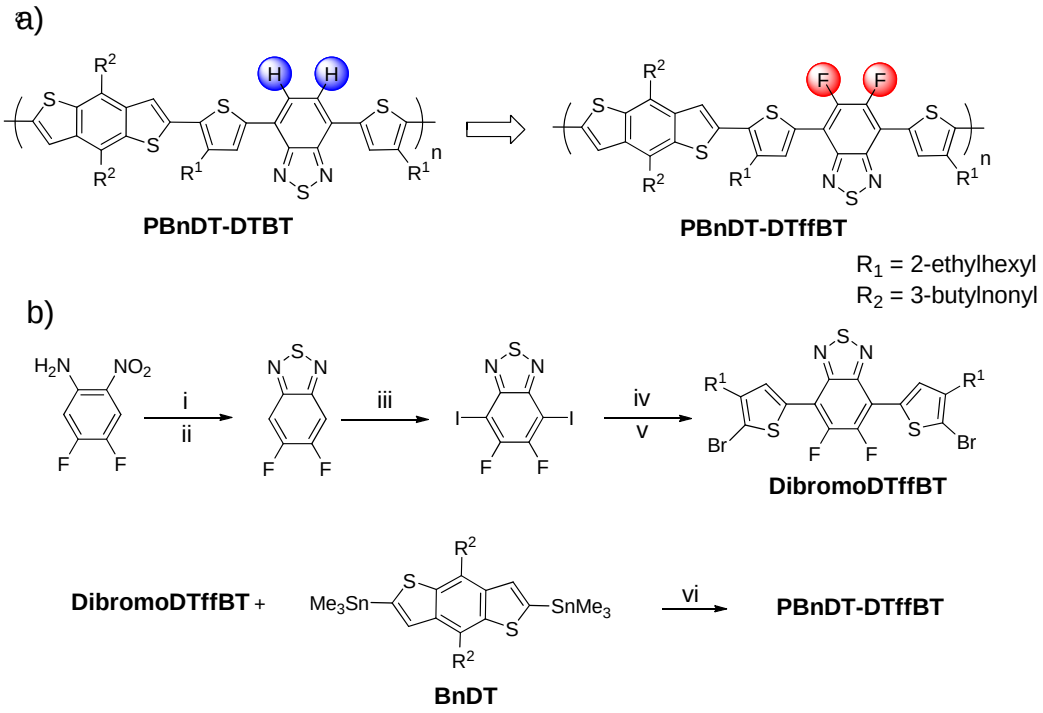

[a] (i) Pd/C, H_2, methanol/HOAc, 3 d; (ii) $SOCl_2$, Et_3N, chloroform, 5 h; (iii) I_2, fuming H_2SO_4, 60°C, 24h; (iv) (2-ethylhexylthiophen-2-yl) trimethylstannane, $Pd(PPh_3)_4$, toluene, reflux, 2d; (v) NBS, THF, 8 h; (vi) $Pd_2(dba)_3$, $P(o\text{-}tolyl)_3$, o-xylene, Microwave, 150 °C, 20 min.

Figure 6-1. a) Structure of PBnDT-DTBT and PBnDT-DTffBT; b) Synthetic Route of PBnDT-DTffBT polymer

6.2. Polymer Design Strategy

Herein we report the first successful application of the fluorine in donor-acceptor (D-A) conjugated polymers with exceptionaly high performance in polymer solar cells (**Figure 6-1a**). In the acceptor front, we chose the ubiquitous 2,1,3-benzothiadiazole (BT).[5-7,150] By replacing the remaining two hydrogen atoms on the BT unit with two

fluorine atoms, we envisioned that the electron density on the benzene ring would be decreased, and both of the LUMO and HOMO levels of the resulting polymer would decrease.[168] Furthermore, substituting hydrogen atoms with fluorine of similar size would not impose additional steric hindrance between adjacent monomers. Finally, the two alkylated thienyl units flanking the fluorinated BT unit can provide the necessary solubility of the resulting polymer with negligible twisting between conjugated units, as shown by us earlier.[94,141,151] These thienyl units could also promote the polymer chain interaction in the solid state, increasing the hole mobility. The structure of the newly conceived 5,6-difluoro-4,7-dithien-2-yl-2,1,3-benzothiadiazole (DTffBT) is sketched in **Figure 6-1**.

As for the donor, benzo[1,2-*b*:4,5-*b'*]dithiophene (BnDT) was chosen for the following reasons: (a) as a "weak donor", it would maintain a low HOMO level of the resulting polymer,[144] as demonstrated in other "weak donor-strong acceptor" polymers;[151,168,169] (b) its structural symmetry and the rigid fused aromatic system could enhance the electron delocalization and inter-chain interaction to improve the charge mobility.[170] PBnDT-DTffBT was therefore envisioned (**Figure 6-1**). Our preliminary investigation of PBnDT-DTffBT based BHJ devices demonstrated a signficant improvement on the efficiency: ~ 45% increase compared with that of the non-fluorinated analog PBnDT-DTBT (**Figure 6-1**). To the best of our knowledge, PBnDT-DTffBT is among the top high-performing polymers with total efficiencies exceding 7%.[77,80] . This indicates great potential of the DTffBT unit and the incorporation of fluorine atoms in creating high performance materials for BHJ solar cells.

6.3. Monomer and Polymer Synthesis

The syntheses of the DTffBT structure unit and the PBnDT-DTffBT are shown in **Figure 6-1b**. Detailed synthetic procedures are described in the **experimental section**. A microwave-assisted Stille coupling reaction[6] was used to prepare both PBnDT-DTBT and PBnDT-DTffBT with high yields. In order to eleminate any complications of the chain effect on photovoltaic properties, identical side chains were employed for both PBnDT-DTBT and PBnDT-DTffBT.[94,151] Therefore these two polymers only differ by two F atoms, enabling us to accurately investigate the impact of F substituents on physical properties of PBnDT-DTffBT and related BHJ solar cells. We tried to achieve good solubility by anchoring 2-ethylhexyl and 3-butylnonyl side chains on the DTffBT and BnDT, respectively.[141] However, both of the polymers exhibit limited solubility in common organic solvents at room temperature. This is because the low molecular weight fractions during Soxhlet extraction were discarded and the chlorobenzene fractions were collected, which leads to exceptionally high molecular weights of both polymers (**Table 6-1**). And the similar molecular weights enable a fair comparison on the properties of both polymers.

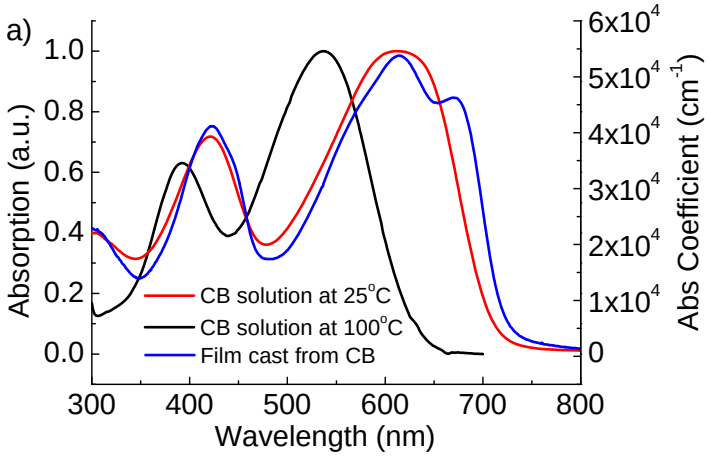

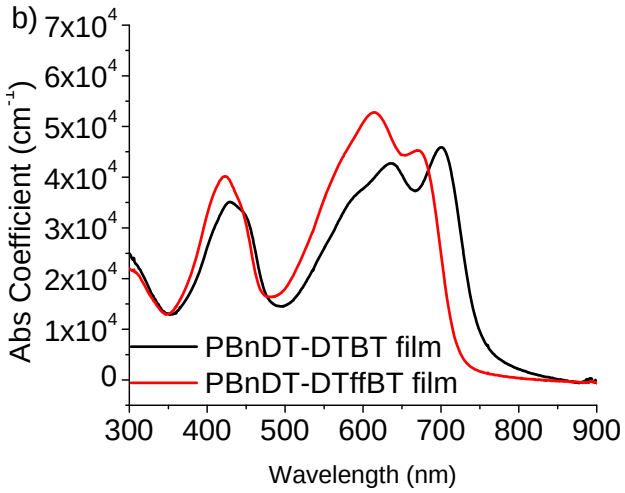

Figure 6-2. a) Absorption spectra of PBnDT-DTffBT in CB at room temperature (red), 100°C (black) and as thin film (blue). **b)**. UV-vis spectrum of PBnDT-DTBT and PBnDT-DTffBT film spincast from chlorobenzene

6.4. Optical and Electrochemical Properties

UV-vis absorption spectra of PBnDT-DTffBT under various conditions are shown in **Figure 6-2**. The absorption maximum of PBnDT-DTffBT in chlorobenzene (CB) solution is red-shifted by ~ 80 nm when the temperature drops from 100°C to room temperature, due to aggregation of polymers. The film absorption of PBnDT-DTffBT exhibits a similar absorption maximum at 615 nm as the solution absorption at room temperature, with an additional absorption shoulder observed in thin films, reflecting further polymer chain stacking in the solid state.[6] A band gap of 1.7 eV for PBnDT-DTffBT was calculated from the onset of the film absorption, similar to that of PBnDT-DTBT. In addition, the HOMO and LUMO energy levels of PBnDT-DTffBT were estimated from its cyclic voltammogram, both of which were lower than those of

PBnDT-DTBT (**Table 6-1 and Figure 6-3**), in addition, the band gaps of both polymers calculated from the difference of HOMO and LUMO levels are very similar .

Table 6-1. Polymerization results and energy levels of PBnDT-DTBT, and PBnDT-DTffBT

Polymer	Yield	Mn [kg/mol][a] /PDI	Measured by CV		Simulated	
			HOMO [eV][b]	LUMO [eV][b]	HOMO [eV][c]	LUMO [eV][c]
PBnDT-DTBT	77%	41.2/1.7	– 5.40	– 3.13	– 5.20	– 2.92
PBnDT-DTffBT	89%	33.8/2.6	– 5.54	– 3.33	– 5.30	– 2.97

[a] Determined by GPC in TCB at 135°C using polystyrene standards; [b] HOMO and LUMO levels were calculated from the cyclic voltammogram;[c] HOMO and LUMO levels simulated by DFT theory.

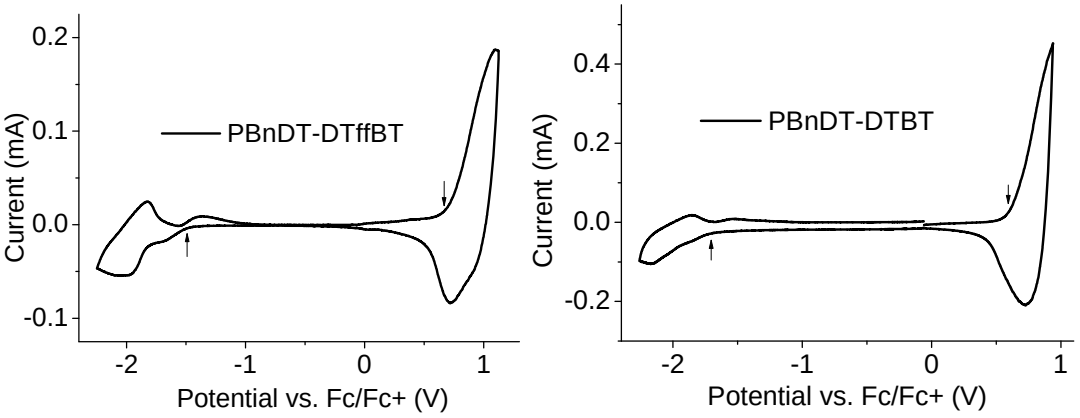

Figure 6-3: Cyclic voltammogram (50 mV s^{-1}) of **PBnDT-DTffBT** (left) and **PBnDT-DTBT** (right) film drop cast on a glassy carbon electrode in Bu_4NBF_4/CH_3CN

6.5. Computational studies

Computational studies using density functional theory (DFT) were further performed to evaluate the influence of these fluorine atoms on the electronic and optical properties of PBnDT-DTffBT, compared with those of PBnDT-DTBT (**Table 6-1**). Both LUMO and HOMO levels were slightly lower in PBnDT-DTffBT than those in PBnDT-DTBT. PBnDT-DTffBT was predicted to have both similar band gap and UV-vis absorption spectrum as PBnDT-DTBT. These simulated data from the DFT calculation are in concordance with the experimental results estimated from their cyclic voltammograms. Our results corroborate the previous discovery of the utility of F atoms in lowering both HOMO and LUMO energy levels of related conjugated polymers.[154,155] With a similar band gap but a deeper HOMO level, PBnDT-DTffBT based BHJ devices would offer a similar J_{sc}, but a larger V_{oc} than the non-fluorinated analog (PBnDT-DTBT).

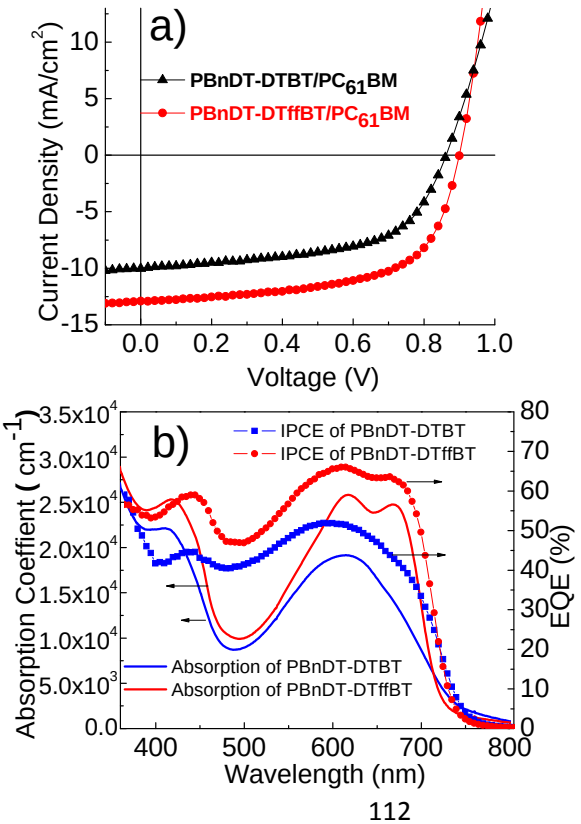

Figure 6-4. (a) Characteristic *J*-V curves of the devices of PBnDT-DTffBT(red circle) and PBnDT-DTBT (black triangle) based BHJ solar cells under 1 Sun condition (100 mW/cm^2). (b) IPCE and absorption spectra of PBnDT-DTffBT and PBnDT-DTBT based BHJ devices

6.6. Photovoltaic Properties

To probe for the photovoltaic properties of PBnDT-DTffBT, typical BHJ solar cells consisting of PBnDT-DTffBT as the electron donor and $PC_{61}BM$ as the electron acceptor were fabricated and then tested under simulated AM1.5G illumination (100 mW/cm^2). The best performing PBnDT-DTffBT/$PC_{61}BM$ BHJ solar cells were fabricated by spin-coating a polymer:$PC_{61}BM$ (1:1 w/w) blend in dichlorobenzene onto a PEDOT:PSS coated ITO substrate, with a thick active layer of 190 nm. The devices were then completed by adding the top electrode of Ca (40 nm)/Al (70 nm). The active area of each cell is 0.12 cm^2. Typical current density-voltage (*J*-V) curve is shown in **Figure 6-4a**. With a deep HOMO level of – 5.54 eV, the PBnDT-DTffBT based device exhibits a V_{oc} of 0.91 V, 0.04 V larger than that of the PBnDT-DTBT based device. Despite similar band gap of these two polymers, we achieved a great improvement on J_{sc} from 10.1 mA/cm^2 for PBnDT-DTBT devices to 12.9 mA/cm^2 for PBnDT-DTffBT devices. Incident photon to current efficiency (IPCE) of PBnDT-DTffBT BHJ devices was then acquired to verify the measured J_{sc} (**Figure 6-4b**). Significant photon-to-current response was obtained in nearly the entire visible range, suggesting a highly efficient photoconversion process in the PBnDT-DTffBT device. The maximum IPCE of 66% at 610 nm is among the highest IPCE values in low band gap polymer solar cells.[80,169] In

contrast, the IPCE of PBnDT-DTBT device is noticeably smaller. Integrating the spectral response of both cells against the standard AM 1.5 spectrum yields the calculated J_{sc}, in agreement with the photocurrent obtained by the *J-V* measurements (within 2% error). This high IPCE response of PBnDT-DTffBT device, together with a high fill factor of 61.2 %, suggests balanced charge transport and improved active layer morphology of the PBnDT-DTffBT device, likely due to the introduction of the F atoms. It is worth mentioning that the active layer thickness of semi-optimized PBnDT-DTffBT device almost doubles the typically observed 100 nm in most low band gap polymers based BHJ devices[80,151,169,171] and is close to that of P3HT based devices after annealing,[147,172] indicating the formation of near optimal morphology of PBnDT-DTffBT devices *without* annealing or additives. PBnDT-DTffBT blend with PC61BM has a higher absorption coefficient than that of PBnDT-DTBT. Therefore at the similar thickness, PBnDT-DTffBT films can absorb more photons, which likely accounts for the higher J_{sc} observed in PBnDT-DTffBT devices than that in PBnDT-DTBT devices. We are further investigating how these F atoms affect the morphology of PBnDT-DTffBT BHJ devices, and whether the newly emerged DTffBT can also be used in conjunction with other "weak donors" to offer highly efficient polymers for BHJ solar cells.

Table 6-2. Photovoltaic properties of PBnDT-DTBT and PBnDT-DTffBT based BHJ solar cells processed with polymer/$PC_{61}BM$ 1:1 (w/w) blend in DCB.

Polymers	Thickness [nm]	J_{sc} [mA/cm^2]	V_{oc} [V]	*FF* [%]	PCE_{max} ($PCE_{average}$) [%]
PBnDT-DTBT	175	10.03	0.87	57.3	5.00 (4.74)
PBnDT-DTffBT	190	12.91	0.91	61.2	7.19(6.86)

6.7. Conclusion

In summary, a new structural unit – DTffBT – was successfully synthesized and applied in constructing a new low band gap polymer – PBnDT-DTffBT – with both decreased HOMO and LUMO levels. With a noticeably high V_{oc} of 0.91 V, a fairly high J_{sc} of 12.9 mA/cm^2 and an enhanced *FF* of 0.61, the overall efficiency of the PBnDT-DTffBT BHJ device reaches 7.19 % in initial trials. This is among the highest efficiency obtained by polymer/$PC_{61}BM$ BHJ solar cells cells.[80,169] which indicates great potential of the DTffBT unit and the incorporation of fluorine atoms in creating high performance materials for BHJ solar cells.

6.8. Experimental Section

For the experimental details about electrochemistry, spectroscopy and SCLC mobility measurements please check **Appendix 1**. And please check **Appendix 6** for supporting information.

Reagents and Instrumentation. All reagents and chemicals were purchased from commercial sources (Aldrich, Acros, Matrix Scientific) and used without further purification unless stated otherwise. Reagent grade solvents were dried when necessary and purified by distillation. Microwave assisted polymerizations were conducted in a CEM Discover Benchmate microwave reactor. Gel permeation chromatography (GPC) measurements were performed on a Polymer Laboratories PL-GPC 220 instrument (at the University of Chicago) using 1,2,4-trichlorobenzene as the eluent (stabilized with 125 ppm BHT) at 135 °C. The obtained molecular weight is relative to the polystyrene

standard. ^{1}H and ^{13}C nuclear magnetic resonance (NMR) measurements were recorded either with a Bruker Avance 300MHz AMX or Bruker 400 MHz DRX spectrometer. UV-visible absorption spectra were obtained by a Shimadzu UV-2401PC spectrophotometer. The film thicknesses were recorded by a profilometer (Alpha-Step 200, Tencor Instruments).

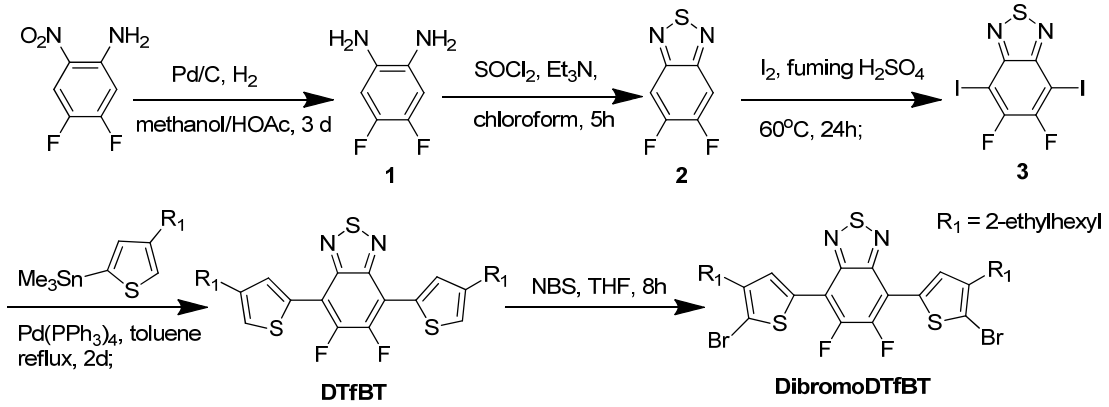

Figure 6-5. Synthetic Route for **DibromoDTffBT**

Monomer and Polymer Synthesis.

4,5-difluorobenzene-1,2-diamine (1): A solution of 4,5-difluoro-2-nitroaniline (10 g, 57.4 mmol) in methanol (200 mL) was saturated with argon and then catalytic amount of 10% Pd on carbon (1 g) suspended in degassed methanol was transferred into the solution. Acetic acid (30 mL) was added and the black mixture was purged with hydrogen gas for 5 min and a H_2 balloon was attached to the reaction flask. The reaction mixture was stirred at room temperature for 3 days and filtered to remove Pd and carbon. Excess solvent was evaporated under reduced vacuum. The residue was then dissolved in chloroform and washed with saturated Na_2CO_3 solution. The organic layer was then dried

over $MgSO_4$ and the solvent was removed by vacuum. The brown product (6.8 g) was obtained by recrystallizing from hexane/ethyl acetate 1:1. Yield: 82%. ^{1}H NMR (400MHz, $CDCl_3$): δ 6.52 (t, 2H, J= 9.6 Hz), 3.31 (br, 4H).

5,6-difluorobenzo[c][1,2,5]thiadiazole (2). To a round bottom flask were added **1** (0.2 g, 1.38 mmol), $CHCl_3$ (20 mL) and triethylamine (0.57 mL, 5.6 mmol). The solution was stirred until compound **1** was completely dissolved. Thionyl chloride (0.36 g, 2.8 mmol) was added dropwise and the mixture was heated to reflux for 5 h. The mixture was then cooled to room temperature before it was extracted with CH_2Cl_2 (10 mL×3). The organic layer was combined and dried over $MgSO_4$. Solvent was evaporated and the product as white needle-like crystal (0.2 g) was obtained by column chromatography using hexane/ethyl acetate (1:4) as the eluent. Yield: 84%. ^{1}H NMR (400MHz, $CDCl_3$): δ 7.76 (t, 2H, J= 8.8 Hz). ^{13}C NMR (400MHz, CDCl3): δ 155.17, 154.97, 152.58, 152.38, 150.81, 150.76, 106.22, 106.16, 106.07, 106.01.

5,6-difluoro-4,7-diiodobenzo[c][1,2,5]thiadiazole (3). A mixture of **2** (0.89 g, 5 mmol) I_2 (5 g, 20 mmol) and fuming sulfuric acid (25 mL) in a RB flask was stirred at 60°C for 24 h. After cooling to room temperature, the reaction mixture was poured into a 500 mL beaker with crushed ice. Chloroform was added and the mixture was transferred into a separatory funnel and washed with distilled water, followed by 1M NaOH solution several times to remove excess iodine and finally washed with saturated $NaHCO_3$. The organic layer was then dried over $MgSO_4$. After the solvent removal, the yellow needle-like crystalline product was used without further purification.

5,6-Difluoro-4,7-bis(4-(2-ethylhexyl)-2-thienyl)-2,1,3-benzothiadiazole (DTffBT). In a 250 mL flame-dried 2-neck round-bottom flask with a condenser, the white crystal from last step (5 mmol), excess of (4-(2-ethylhexyl)thiophen-2-yl)trimethylstannane (5.2 g, 11 mmol) and dry toluene 20 mL were added. The mixture was then purged with argon for 15min. Then, $Pd(PPh_3)_4$ (80 mg)was added and the reaction mixture was heated to reflux for 2d. The reaction mixture was then cooled to room temperature and the solvent was evaporated. The crude orange product was purified by column chromatography with hexane/ethyl acetate (100:1) as eluent. The solvent was evaporated and the product was recrystallized from ethanol as orange solid. Yield: 1.204g (43% from compound **2**). ^{1}H NMR (400MHz, $CDCl_3$): δ 8.08 (s, 2H), 7.18 (s, 2H), 2.65 (d, 4H, J=6.8 Hz), 1.65 (m, 2H), 1.21-1.44 (m, 16H), 0.80-0.94 (m, 12H). ^{13}C NMR (400MHz, CDCl3): δ 151.05, 150.85, 148.81, 148.77, 148.47, 148.27, 142.23, 132.70, 131.03, 124.81, 111.57, 111.48, 40.45, 34.53, 32.56, 29.16, 25.72, 23.06, 14.11, 10.88. Element analysis: Theory: C: 64.25, H: 6.83. Found: C: 64.15, H: 6.81.

Synthesis of 5,6-Difluoro-4,7-bis(5-bromo-4-(2-ethylhexyl)-2-thienyl)-2,1,3-benzothiadiazole (dibromoDTffBT). **DTffBT** (0.24 g, 0.46 mmol) and N-bromosuccinimide (NBS) (178 mg, 0.1 mmol) were added into THF under stirring. The reaction mixture was stirred at a room temperature for 8 h, then the reaction mixture washed with brine and dried over anhydrous sodium sulfate. The solvent was removed under a reduced pressure to give the product as an orange solid. Needle-like crystal was obtained by recrystallization from ethanol. Yield: 249 mg (80%). ^{1}H NMR (400MHz,

$CDCl_3$): δ 7.94 (s, 2H), 2.60 (d, 4H), 1.71 (m, 2H), 1.18-1.45 (m, 16H), 0.79-0.91 (m, 12H). ^{13}C NMR (400MHz, CDCl3): δ 150.73, 150.53, 148.14, 147.96, 147.93, 141.53, 132.10, 132.05, 130.97, 115.22, 110.58, 110.49, 39.97, 33.71, 32.48, 28.77, 25.70, 23.11, 14.18, 10.87.

Synthesis of PBnDT-DTffBT via Microwave-assisted Stille Coupling Polymerization. To a 10 mL Microwave pressurized vial equipped with a stir bar, distannylated BnDT (127 mg, 0.145 mmol), dibromoDTffBT (104 mg, 0.145 mmol), $Pd_2(dba)_3$ (2.5%) and P(o-tol)$_3$ (20%) were added. Then the tube was sealed and evacuated and refilled with argon for three cycles and then o-xylene was added inside a glovebox. Reaction tube was put into microwave reactor and heated to 150 °C under 300 watt microwave for 20 min. After cooling to room temperature, the organic solution was added dropwise to 200 mL of methanol to obtain precipitate, which was collected by filtration and washed with methanol and dried. The crude polymer was then extracted subsequently with methanol, acetone, hexane and $CHCl_3$ in a Soxhlet's extractor. The residue after extracting with $CHCl_3$ was collected and dried under reduced pressure and to give the polymer **PBnDT-DTffBT** (147 mg, 89%) as a dark green solid. ^{1}HNMR (400 MHz, $CDCl_2CDCl_2$, 400K): δ 0.84-1.02 (24H, br), 1.27-1.62 (48H, br), 1.82-2.00 (6H, br), 3.02 (4H,br), 3.23 (4H, br), 7.66 (2H, br), 8.23 (2H, br)

Polymer solar cell fabrication and testing. Glass substrates coated with patterned indium-doped tin oxide (ITO) were purchased from Thin Film Devices, Inc. The 150 nm sputtered ITO pattern had a resistivity of 15Ω/□. Prior to use, the substrates were

ultrasonicated for 20 minutes in acetone followed by deionized water and 2-propanol. The substrates were dried under a stream of nitrogen and subjected to the treatment of UV-Ozone over 30 minutes. A filtered dispersion of PEDOT:PSS in water (Baytron PH500) was then spun cast onto clean ITO substrates and then baked at 140 °C for 15 minutes. A blend of polymer and $PC_{61}BM$ was dissolved in chlorinated solvent with heating at 110 °C for 8 hours. All the solutions were then spun cast onto PEDOT:PSS layer and dried at room temperature in the glovebox under nitrogen atmosphere for 12 hours. Then a 40 nm film of calcium and a 70 nm aluminum film were thermal deposited at a pressure of ~ 1×10^{-6} mbar. There are 8 devices per substrate, with an active area of 0.12 cm^2 per device. Device characterization was carried out under AM 1.5G irradiation with the intensity of 100 mW/cm^2 (Oriel 91160, 300 W) calibrated by a NREL certified standard silicon cell. Current density versus potential (*J*-V) curves were recorded with a Keithley 2400 digital source meter. EQE were detected under monochromatic illumination (Oriel Cornerstone 260 ¼ m monochromator equipped with Oriel 70613NS QTH lamp) and the calibration of the incident light was performed with a monocrystalline silicon diode. All fabrication steps after adding the PEDOT:PSS layer onto ITO substrate, and characterizations were performed in gloveboxes under nitrogen atmosphere.

CHAPTER 7

CONCLUSION AND FUTURE DIRECTIONS

Part of this chapter is adapted from Macromolecule Prospective

7.1. Conclusion

In previous chapters, some rational design methods to construct "ideal" conjugated polymers for organic solar cells have been presented. With those methods, several real examples of conjugated polymers were successfully designed and synthesized. Among them, several conjugated polymers have demonstrated excellent photovoltaic properties with PCE >7%.

Of all the seven desired properties for conjugated polymers, four of them were investigated in this dissertation (molecular weight, HOMO and LUMO energy levels and solubility) and successfully combined in conjugated polymers by rational design. Although great progress has been made, there is still a long way to go towards the "ideal" polymers. The rest of properties (mobility, morphology and stability) are hard to investigate and even harder to be incorporated in a single material. And now we are collaborating with other groups trying to find the relationship between those properties and the chemical structures of conjugated polymers.

In the rest of this chapter, I will try to expand the horizon beyond conjugated polymer design and synthesis and discuss some future development directions for the whole field of polymer solar cell.

7.2. Maximum Efficiency Reachable with Polymer:Fullerene BHJ Solar Cell

The record high efficiency has been constantly updated in the past three years by the synergistic efforts between the academic researchers (e.g., design and synthesis of new polymers) and companies (e.g., device optimizations). Furthermore, the design and synthesis of these novel polymers would not have been possible without a deeper understanding of the governing physical principles ,[152,173,174] device physics,[55,175,176] and morphology investigation and control.[127,139,177-180] So far the J_{sc} can reach as high as 17.3 mA/cm^2,[6] with absorption up to 900 nm (~ 1.3 eV); the highest V_{oc} obtained has been over 1 V; [46-48] and the highest obtained *FF* has breached 70%.[49,50] If we could achieve all these impressive values with one system, this champion BHJ solar cell would offer an unprecedented value of 12%! This is the bright future of the exciting field of polymer solar cells, and also the goal that numerous researchers strive for. Unfortunately, all these high values are obtained from different polymer based BHJ systems, partly due to the inter-relation between some of the properties such as the balance between J_{sc} and V_{oc}, as elaborated on in Chapter 1[144]. A more rigorous model calculation on the ultimate performance of polymer:fullerene BHJ cells was recently accomplished by Blom and co-workers.[181] They predict a maximum power efficiency of 11.7% for single cells and 14.1% for tandem structures.

7.3. How to obtain a higher PCE?

However, if polymer solar cells (and organic solar cells in general) intend to compete with other thin film PV technologies (such as CIGS or CdTe) as a viable economic solution for renewable energy future, higher efficiencies (15 – 20%) will be strongly

desirable if not required. For example, flexible thin film CIGS solar cells can reach an energy conversion efficiency as high as 18.7%,[182] and the efficiency of mass-produced CIGS thin film modules has breached 13%.[183] Can polymer (organic) solar cells achieve similar performances? To answer this challenge, one has to analyze the J_{sc}, V_{oc} and *FF* individually, since these three parameters ultimately decide the efficiency of any solar cells. To facilitate the discussion and related recommendations, we collected roughly 200 data sets from different polymer/fullerene BHJ systems in the literature reports, and plotted the J_{sc} versus the band gap of the polymer (**Figure 7-1**), and V_{oc} versus the HOMO energy level of the polymer (**Figure 7-2**). To make the analysis meaningful, we averaged all the experimental values in related intervals in both figures.

7.3.1. Further Improve Short Circuit Current (Jsc)

Figure 7.1 clearly shows that a smaller band gap favors a higher short circuit current. However, this trend reaches its maximum around 1.3 eV. Polymers with even smaller band gap than 1.3 eV fail to offer more current as expected from their absorption extending into near IR. Two possible reasons account for this observation. The first is related with the energy levels of these polymers having extremely small band gaps. Often a very strong acceptor (such as benzobisthiadiazole) was paired with a strong donor to achieve the small band gap via the donor-acceptor low band gap approach; however, these strong acceptors would lower the LUMO level below -3.9 eV, leading to an inefficient exciton dissociation when $PC_{61}BM$ was used as the electron acceptor in the BHJ solar cells. The second is the usually small full width at half maximum (FWHM) of these conjugated polymers, normally on the order of 200 nm. Thus continuously shifting

the absorption of the polymer towards IR end of the solar spectrum would inevitably diminish its ability to absorb the light in the visible region. In addition, these near IR/IR absorbing polymers usually have low absorption coefficients, which exacerbate the light harvesting.

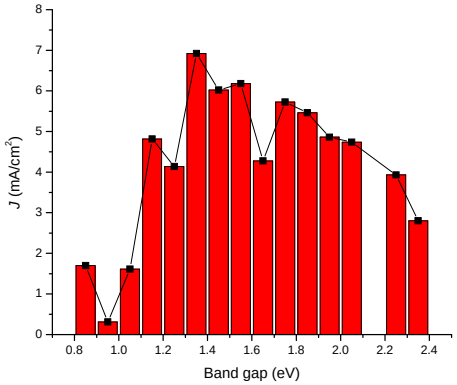

Figure 7-1. E_g vs. J_{sc} plot. A total of ~200 data points were taken and summarized with 0.1eV interval, e.g. 0.80-0.89, 0.90-0.99eV

Based on these analyses, we identify a few potential directions worth of further research:

a. ***Increasing full width at half maximum (FWHM)***: As we discussed, in addition to small band gap, the width of absorption spectrum is equally important. Two possible solutions have emerged to increase the FWHW, both of which used random copolymerization to bring more than two monomers into the conjugated backbone, though in a slightly different manner. Liang et al. incorporated the pro-quinoid unit of thieno[3,4-b]thiophene (TT) into the polythiophene backbone, basically introducing the low band gap character of the TT into the backbone.[75] Depending upon the feed ration of the TT vs. thiophene, the band gap and the energy level of the random copolymer can be tuned. In an earlier report, Li and co-workers added another conjugated oligomer

(bithienylenevinylene) to the 3 position of the thiophene, and polymerized this modified thiophene unit with 3-hexylthiophene and unsubstituted thiophene monomers in a random manner into the biTV-PT.[184] These conjugated side chains add strong absorption from 350 to 480 nm, thereby leading to a broad absorption spectrum from 350 nm to 650 nm of these copolymers. Both reports did obtain better performance from these random copolymers than that of the benchmark P3HT in their studies, though still noticeably lower than the optimized P3HT based cell of 5% efficiency. Nevertheless, considering the effective broadening of the absorption by these approaches, further investigation is still warranted.

b. ***Making n-type material absorb***: Alternatively, one can employ electron accepting materials that absorb complementary part of the solar spectrum in regard to the absorption of the electron donating polymers, thereby broadening the light harvesting of the active layer. The most successful example is the $PC_{71}BM$, whose less symmetry (compared with $PC_{61}BM$) renders a much enhanced absorption from 300 to 600 nm.[37] This strong absorption in the UV-Vis region by the $PC_{71}BM$ effectively complements the absorption usually ranging from 600 nm to 800 nm offered by these narrow band gap polymers, thereby leading to an appreciable increase (20% or more) in the J_{sc} of related solar cells when compared with that of $PC_{61}BM$ based ones. Almost all reported polymer/$PC_{61}BM$ based solar cells with over 7% efficiency have used $PC_{71}BM$,[63,65,77,80] with only few exceptions.[50,64] A more elegant solution comes from the design and synthesis of electron accepting polymers with tunable absorption. Though these polymer:polymer solar cells have not reached high efficiency (highest around 2.5%[185]) as polymer:fullerene solar cells, the full tunability (e.g., energy level and band gap) of these

electron accepting polymers offer a viable approach towards not only a higher J_{sc}, also a high V_{oc} in these all polymer solar cells.

c. ***Improving EQE***: In contrast to the internal quantum efficiency (IQE) which already reached 100% in some recent reports,[5] the external quantum efficiency (EQE) remains relatively low (50% – 80%), even in these highly efficient polymers/fullerene BHJ solar cells. For example, the highest reported J_{sc} of 17.3 mA/cm^2 could have been 30 mA/cm^2 based on its band gap of 1.3 eV, if the EQE were 100% instead of the observed ~ 55%.[6] This is mainly due to the low mobility of charge carriers in these polymer:fullerene blends and the intrinsically disordered morphology of the BHJ cells, which limits the optimal film thickness of the active layer to less than 200 nm. A thicker film would be able to harvest all the light within the film absorption; however, the generated charges after dissociating these excitons would not be able to transverse the thick film and reach the individual electrode before various recombination mechanisms kick in to annihilate these energy carrying charges. Thus further improving the carrier mobilities (both holes and electronics), controlling the morphology, and finding methods to slow down or diminish charge recombination, should be among the research priorities.

7.3.2. Further Improvement on Open Circuit Voltage (Voc)

A similar trend has been observed for V_{oc} vs. HOMO level (**Figure 7-2**). The open circuit voltage increases as the HOMO energy level lowers, reaching the maximum of 1.02 V around a HOMO level of – 5.56 eV and then drops.[186] After years of investigation, it is generally accepted that the V_{oc} is proportional to the difference between the HOMO of the donor and the LUMO of the acceptor, though recent advances

in understanding the origin of the V_{oc} have provided further insights.[51,53,54,187] Achieving a V_{oc} of 1.1 V is indeed applaudable; however, if we take – 4.2 eV as the LUMO of the $PC_{61}BM$, we still lose 0.4 eV from the energy gap ($E_{LUMO(acceptor)} - E_{HOMO(donor)}$) to the V_{oc}, which is typically observed in polymer solar cells. If we consider another source of the voltage loss, the empirical 0.3 eV between the LUMOs of the donor polymer and the fullerene, we have lost ~ 0.7 eV altogether, which could have doubled the V_{oc} if all converted into part of V_{oc}! Therefore, much work needs to be done on two possible fronts:

a. ***Further understanding the origin of V_{oc} & searching for new acceptors***: First, is the empirical 0.3 eV required for effective exciton splitting at the interface really necessary? With a recently developed new π electron acceptor (D99'BF)[188] Heeger and Wudl showed that a V_{oc} of 1.2 V could be obtained from the P3HT/D99'BF BHJ solar cell,[189] as opposed to the usually obtained 0.6 V in the case of P3HT/$PC_{61}BM$ solar cells. More importantly, these authors demonstrated that electron transfer could still occur even with only 0.12 eV in the LUMOs offset. Apparently, the exciton binding energy could be as small as 0.1 eV (at least in the case of P3HT). This exciting discovery points to a potential further increase on the V_{oc} via designing non-fullerene based acceptors. However, even in this successful demonstration, a loss of over 0.5 eV was still observed since the difference between the LUMO of D99'BF and the HOMO of P3HT was 1.78 eV. This leads the second question: can we minimize the commonly observed loss of 0.4 – 0.6 eV from the energy level difference between $E_{LUMO(acceptor)}$ and $E_{HOMO(donor)}$? There have been some suggestions that reducing the electron-phonon coupling of these excitons thereby smaller Stokes shift would help diminish this loss mechanism.[190] This would call

for well-ordered polymers with delocalized excitons. Further, recent advances in further understanding of the V_{oc} suggest that reducing the electronic coupling between the polymer and the fullerene would increase the V_{oc}.[36-38,196] Nevertheless, there is still a lot to be done to determine a clearer structure-property relationship regarding the V_{oc}, so the chemists will know how to design better materials (both electron donating and electron accepting materials).

b. ***Engineering the fullerene***: Alternatively, before we find new acceptors that can replace the fullerene on all fronts, we can still modify the structure of this fascinating group of molecules to raise up their LUMO energy levels, in order to gain a higher V_{oc}. There have been successful examples such as trimetallic nitride endohedral fullerenes (TNEFs, in particular $Lu_3N@C80$),[35] indene-C_{60} bisadduct (ICBA),[34] among others.[191] The V_{oc} of related P3HT:modified fullerene BHJ cells can be increased as much as 0.26 V when compared with P3HT/$PC_{61}BM$ cells,[34] because of the raised LUMO energy level of the modified fullerene.

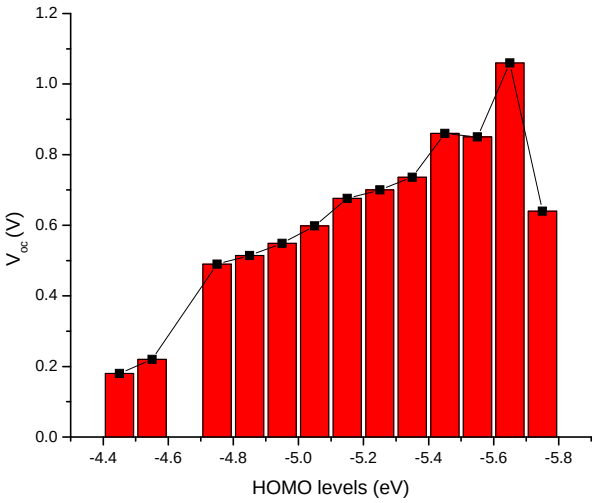

Figure 7-2. HOMO vs. V_{oc} plot. A total of ~200 data points were taken and summarized with 0.1eV interval, e.g. 4.40-4.49, 4.50-5.59eV

7.3.3. Improvement on Fill Factor (FF)

Unlike silicon solar cell or even dye sensitized solar cells, both of which give high fill factors (75 – 80% or higher), the polymer solar cells usually only offer a fill factor around 60%. Fill factor is ultimately determined by the series resistance (R_s) and the shunt resistance (R_{sh}) of the devices. Due to the low charge carrier mobilities (esp. holes) and the disorded nature of the BHJ film, BHJ solar cells usually have a relatively high R_s and relatively low R_{sh}. In order to get a high *FF*, one would require achieving both a low R_s and a high R_{sh}. Research efforts are needed to reach a balanced and rapid charge transport (holes vs. electrons), to optimize and control the film morphology into more ordered structure, and to improve all electric contacts.

All these challenges (also opportunities) compose the major part of the rather long wish list for the research community of polymer (organic) solar cells. This is tall order; however, if we could achieve these goals via collaborative efforts, the payoff would be huge – single junction polymer solar cells with 15% efficiency would be within reach (for example, a band gap of 1.3 eV with an EQE of 80%, a V_{oc} 0.8, and an *FF* of 0.75)!

Appendix 1:

Common Experimental Details

Electrochemistry:

Cyclic voltammetry measurements were carried out using a Bioanalytical Systems (BAS) Epsilon potentiostat equipped with a standard three-electrode configuration. Typically, a three electrodes cell equipped with a glass carbon working electrode, a $Ag/AgNO_3$ (0.01M in anhydrous acetonitrile) reference electrode, and a Pt wire counter electrode was employed. The measurements were done in anhydrous acetonitrile with tetrabutyl ammonium hexafluorophosphate (0.1 M) as the supporting electrolyte under an argon atmosphere at a scan rate of 100 mV/s. Polymer films were drop cast onto the glassy carbon working electrode from a 2.5 mg/mL chloroform solution and dried under house nitrogen stream prior to measurements. The electrochemical onsets were determined at the position where the current starts to differ from the baseline. The potential of $Ag/AgNO_3$ reference electrode was internally calibrated by using the ferrocene/ferrocenium redox couple (Fc/Fc^+), which has a known reduction potential of –4.8e V[192,193] The highest occupied molecular orbital (HOMO) and lowest unoccupied molecular orbital (LUMO) energy levels of copolymers were calculated from the onset oxidation potentials (E_{onest}^{ox}) and onset reductive potentials (E_{onest}^{red}), respectively, according to equation (1) and (2). The electrochemically determined band gaps were deduced from the difference between onset potentials from oxidation and reduction of copolymers as depicted in equation (3).

$$\text{HOMO} = -(E_{onest}^{ox} + 4.8)\ (\text{eV}) \qquad (1)$$

$$\text{LUMO} = -(E_{onest}^{ox} + 4.8)\ (\text{eV}) \qquad (2)$$

$$E_{gap}^{EC} = E_{onest}^{ox} - E_{onest}^{red} \qquad (3)$$

Spectroscopy:

UV-Visible absorption spectra were obtained by a Shimadzu UV-2401PC spectrophotometer. Fluorescence spectra were recorded on a Shimadzu RF-5301PC spectrofluorophotometer. For the measurements of thin films, polymers were spun coated onto pre-cleaned glass slides from 10 mg/mL polymer solutions in chloroform. The thicknesses of films were recorded by a profilometer (Alpha-Step 200, Tencor Instruments).

SCLC mobility

For mobility measurements, the hole-only devices in a configuration of ITO/PEDOT:PSS (40 nm)/copolymer-PCBM/Pd (50 nm) were fabricated. The experimental dark current densities J of polymer: PCBM blends were measured when applied with voltage from 0 to 6 V. The applied voltage V was corrected from the built-in voltage V_{bi} which was taken as a compensation voltage $V_{bi}=V_{oc}$ + 0.05 V and the voltage drop V_{rs} across the indium tin oxide/poly(3,4-ethylene-dioxythiophene):poly(styrene sulfonic acid) (ITO/PEDOT:PSS) series resistance and contact resistance, which is found to be around 35 Ω from a reference device without the polymer layer. From the plots of $J^{0.5}$ vs. V (supporting information), hole mobilities of copolymers can be deduced from

$$J = \frac{9}{8}\varepsilon_r \varepsilon_0 \mu_h \frac{V^2}{L^3}$$

where ε_0 is the permittivity of free space, ε_r is the dielectric constant of the polymer which is assumed to be around 3 for the conjugated polymers, μ_h is the hole mobility, V is the voltage drop across the device, and L is the film thickness of active layer.

Appendix 2:

Supporting Information for Chapter 2

NMR spectra

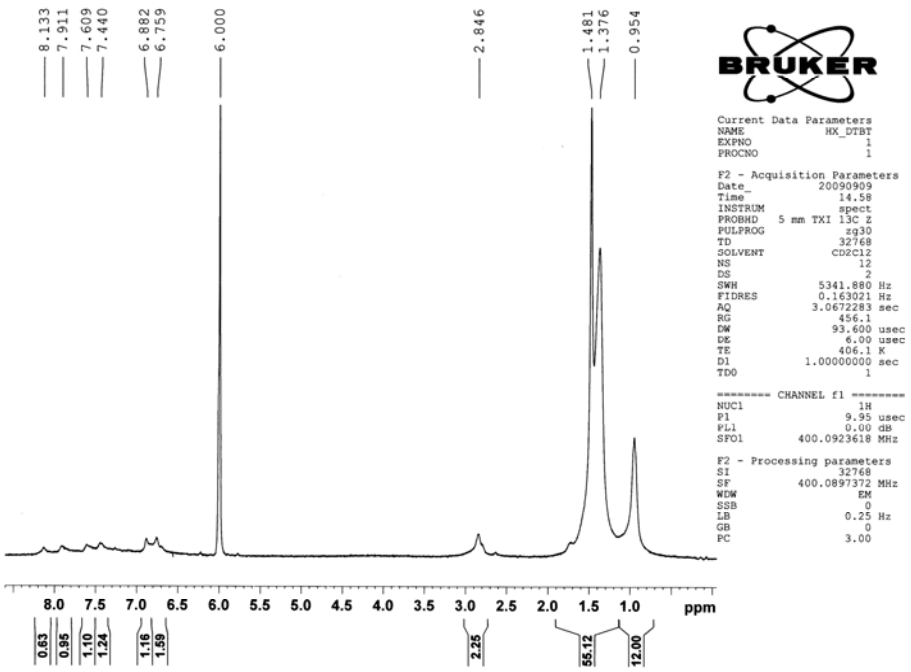

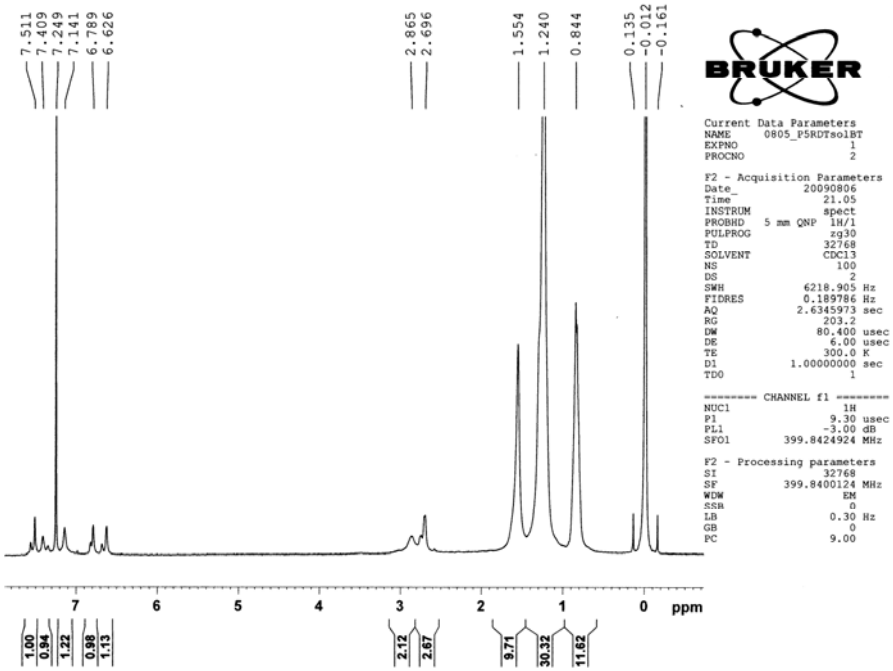

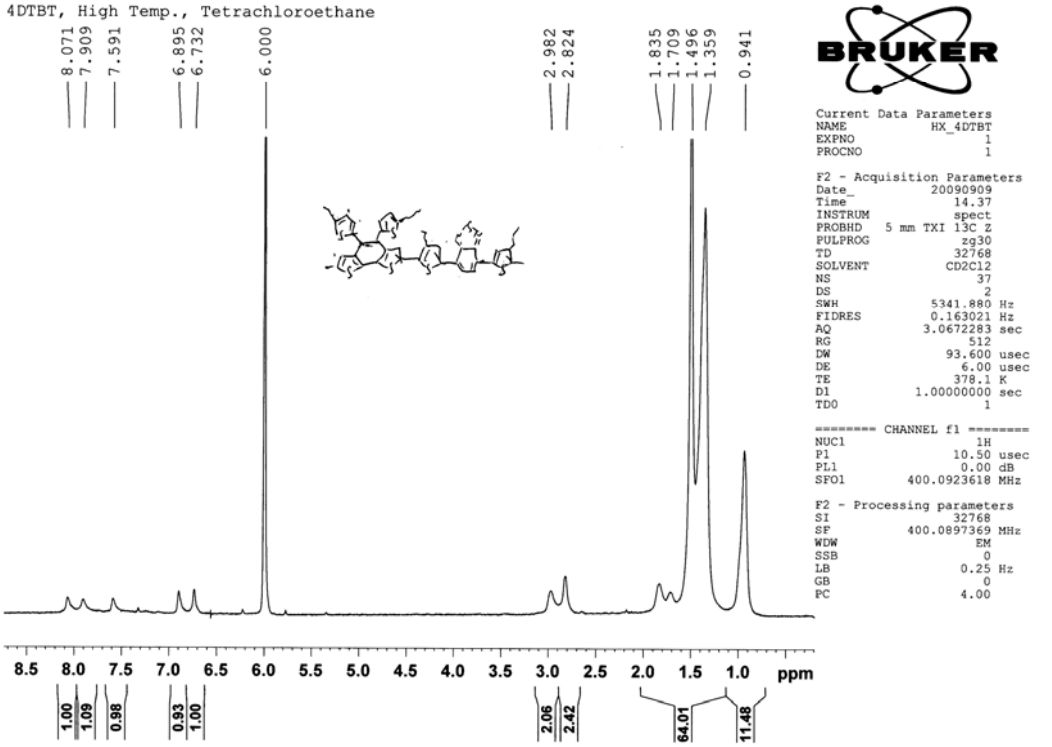
4DTBT, High Temp., Tetrachloroethane
8.071
7.909
7.591
6.895
6.732
6.000
2.982
2.824
1.835
1.709
1.496
1.359
0.941
8.5 8.0 7.5 7.0 6.5 6.0 5.5 5.0 4.5 4.0 3.5 3.0 2.5 2.0 1.5 1.0 ppm
1.00
1.09
0.98
0.93
1.00
2.06
2.42
64.01
11.48
BRUKER
Current Data Parameters
NAME HX_4DTBT
EXPNO 1
PROCNO 1
F2 - Acquisition Parameters
Date_ 20090909
Time 14.37
INSTRUM spect
PROBHD 5 mm TXI 13C Z
PULPROG zg30
TD 32768
SOLVENT CD2C12
NS 37
DS 2
SWH 5341.880 Hz
FIDRES 0.163021 Hz
AQ 3.0672283 sec
RG 512
DW 93.600 usec
DE 6.00 usec
TE 378.1 K
D1 1.00000000 sec
TD0 1
======== CHANNEL f1 ========
NUC1 1H
P1 10.50 usec
PL1 0.00 dB
SFO1 400.0923618 MHz
F2 - Processing parameters
SI 32768
SF 400.0897369 MHz
WDW EM
SSB 0
LB 0.25 Hz
GB 0
PC 4.00

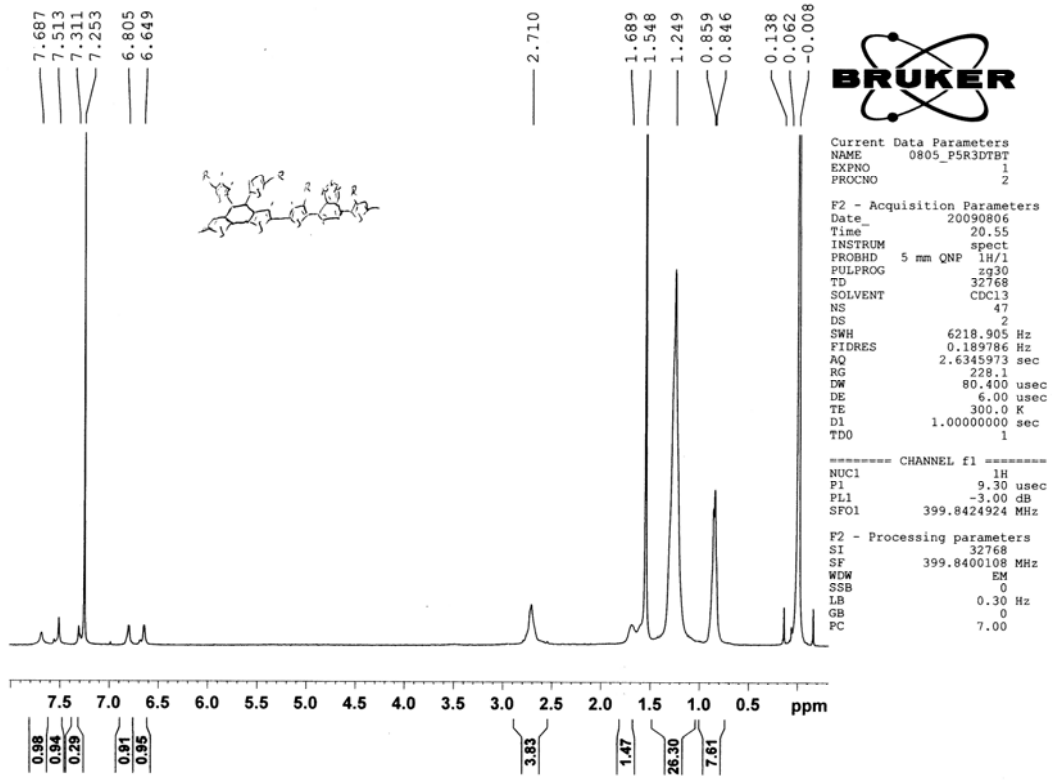
7.687
7.513
7.311
7.253
6.805
6.649
2.710
1.689
1.548
1.249
0.859
0.846
0.138
0.062
-0.008
7.5 7.0 6.5 6.0 5.5 5.0 4.5 4.0 3.5 3.0 2.5 2.0 1.5 1.0 0.5 ppm
0.98
0.94
0.29
0.91
0.95
3.83
1.47
26.30
7.61
BRUKER
Current Data Parameters
NAME 0805_P5R3DTBT
EXPNO 1
PROCNO 2
F2 - Acquisition Parameters
Date_ 20090806
Time 20.55
INSTRUM spect
PROBHD 5 mm QNP 1H/1
PULPROG zg30
TD 32768
SOLVENT CDCl3
NS 47
DS 2
SWH 6218.905 Hz
FIDRES 0.189786 Hz
AQ 2.6345973 sec
RG 228.1
DW 80.400 usec
DE 6.00 usec
TE 300.0 K
D1 1.00000000 sec
TD0 1
======== CHANNEL f1 ========
NUC1 1H
P1 9.30 usec
PL1 -3.00 dB
SFO1 399.8424924 MHz
F2 - Processing parameters
SI 32768
SF 399.8400108 MHz
WDW EM
SSB 0
LB 0.30 Hz
GB 0
PC 7.00

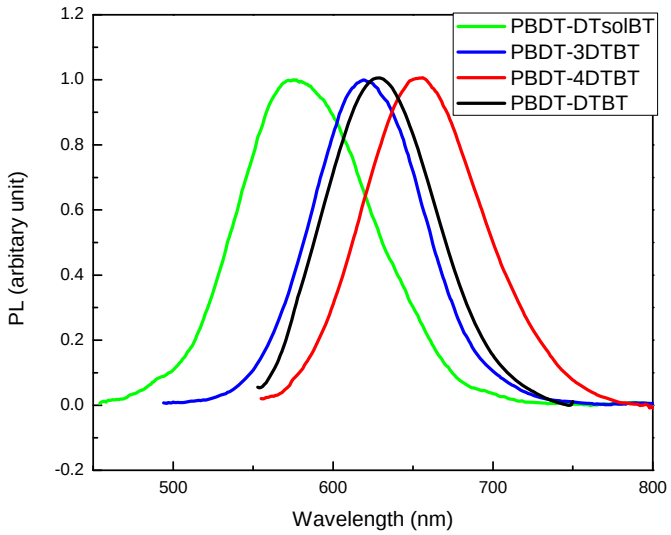

Figure A2-1. Fluorescence of four copolymers in chloroform at room temperature.

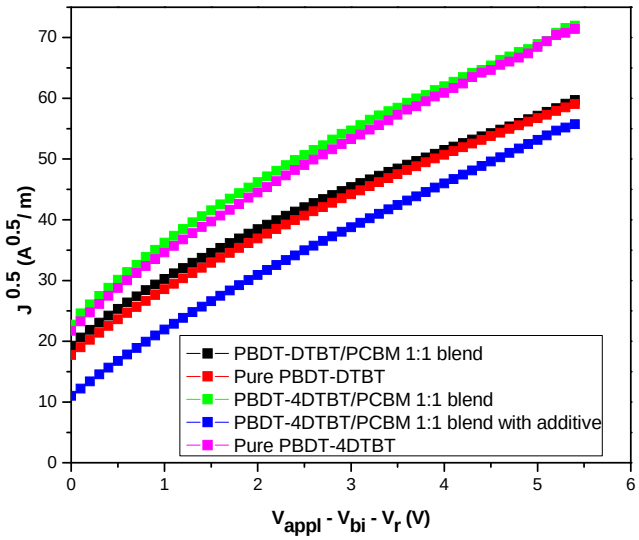

Figure A2-2. $J^{0.5}$ vs V plots for the polymer films at room temperature from a hole-only device of ITO/PEDOT:PSS (40 nm)/pure polymer or blend with PCBM/Pd (50 nm).

Appendix 3:

Supporting Information for Chapter 3

Table A3-1. Element analysis of polymers

Polymers	Element Analysis			Calculated Value			
	C	H	N	C	H	N	S
HMPNDT	80.14	10.42		80.28	10.40		9.32
PNDT-T	77.87	9.41		78.06	9.43		12.50
PNDT-BT	76.00	8.97	3.40	76.04	8.84	3.41	11.71

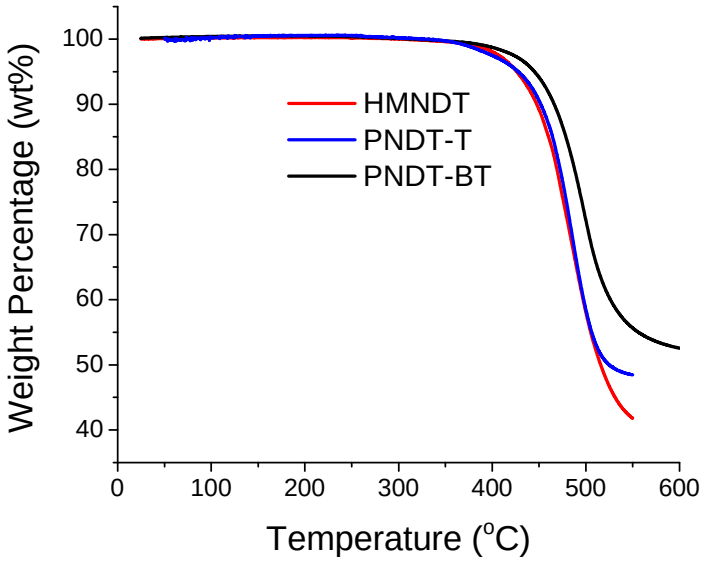

Figure A3-1. Thermogravimetric analysis (TGA) curves of polymers at a heating rate of 10˚C/min

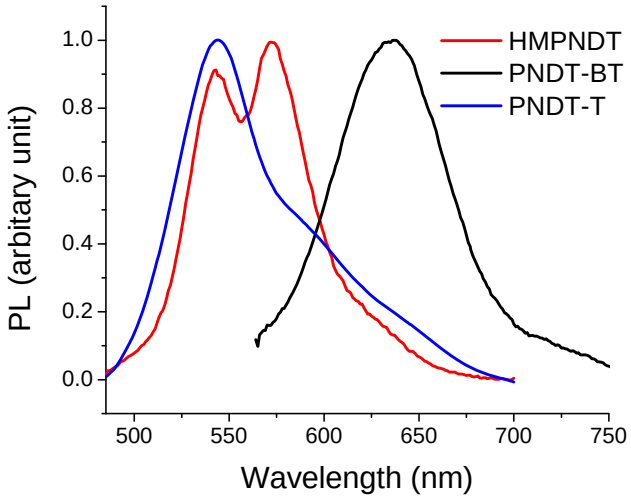

Figure A3-2. Fluorescence spectra of polymers in chloroform at room temperature.

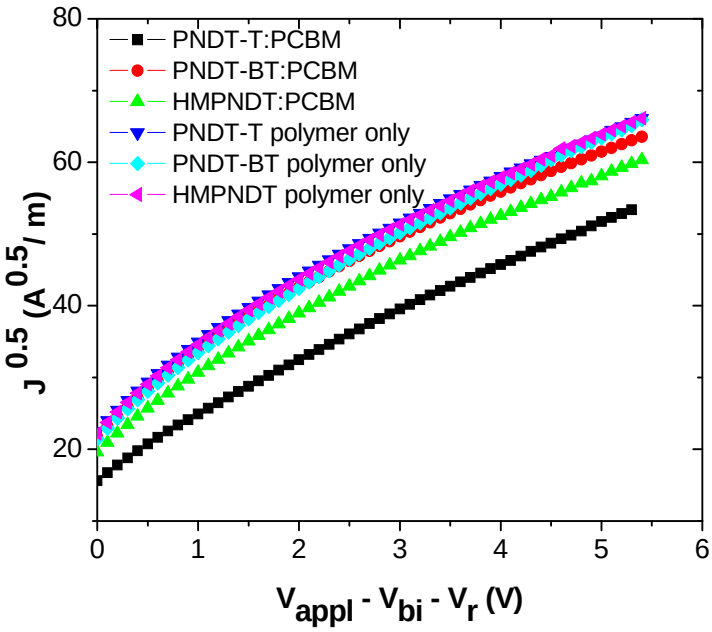

Figure A3-3. $J^{0.5}$ vs. V plots for the polymer films at room temperature from a hole-only device of ITO/PEDOT:PSS (40 nm)/pure polymer or blend with PCBM/Pd (50 nm).

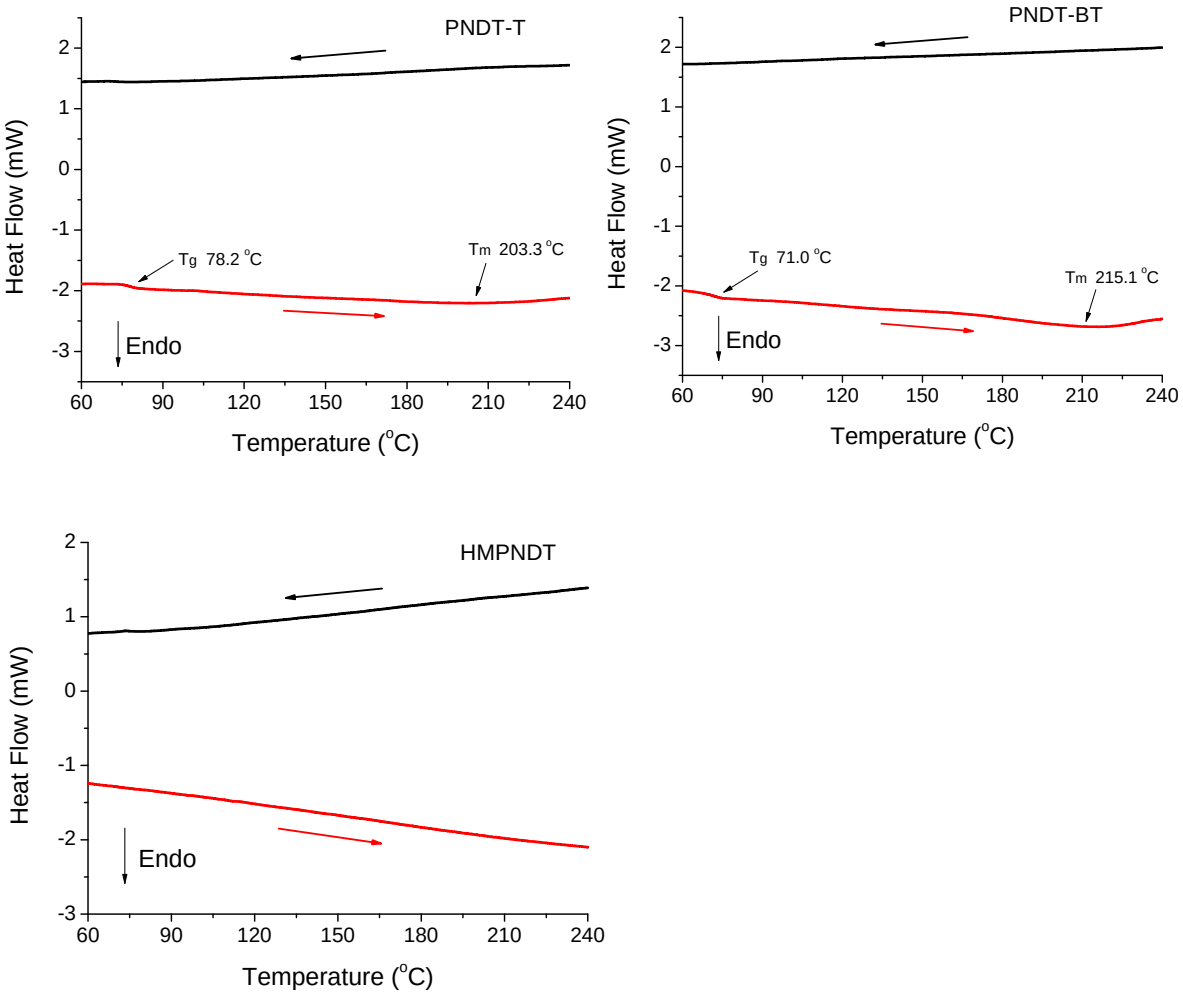

Figure A3-4. Differential scanning calorimetry heating and cooling curves of three polymers at 10°C/min.

Table A3-2. Photovoltaic data of **HMPNDT**, **PNDT-T** and **PNDT-BT**:

Polymer	Polymer /PCBM ratio (w/w)	Processing Solvent [a]	Active Layer Thickness (nm)	J_{sc} (mA/ cm^2) [b]	V_{oc} (V) [b]	FF [b]	PCE (%)[b]
HMPNDT	1:1	$CHCl_3$	110	1.41	0.86	0.35	0.43
	1:1	$CHCl_3$	90	1.20	0.85	0.35	0.36
	1:1	$CHCl_3$	65	1.42	0.83	0.47	0.56
	1:2	$CHCl_3$	120	1.53	0.81	0.46	0.56
	1:2	$CHCl_3$	105	1.26	0.79	0.43	0.43
	1:1	CB	85	1.12	0.65	0.36	0.26
	1:1	CB	60	1.13	0.63	0.38	0.26
	1:2	CB	60	0.84	0.69	0.40	0.23
	1:2	CB	80	0.74	0.73	0.42	0.22
	1:3	CB	95	0.74	0.63	0.40	0.19
	1:3	CB	80	0.78	0.63	0.46	0.23
PNDT-T	1:2	$CHCl_3$	100	1.95	0.75	0.48	0.70
	1:2	$CHCl_3$	90	2.17	0.75	0.47	0.76
	1:2	$CHCl_3$	80	2.40	0.75	0.48	0.86
	1:1	CB	80	3.00	0.67	0.36	0.73
	1:1	CB	65	2.56	0.66	0.37	0.63
	1:2	CB	120	1.97	0.62	0.45	0.56
	1:2	CB	90	1.92	0.69	0.39	0.52
	1:2	CB	85	2.32	0.71	0.42	0.71
	1:2	CB	80	2.97	0.70	0.42	0.88
	1:2	CB	60	2.94	0.71	0.47	0.97
	1:2	CB	55	3.25	0.73	0.50	1.18
	1:3	CB	100	2.30	0.73	0.49	0.82
	1:3	CB	70	2.77	0.70	0.49	0.94
	1:3	CB	50	2.74	0.67	0.48	0.88
PNDT-BT	1:2	$CHCl_3$	105	1.06	0.79	0.43	0.36
	1:1	CB	75	1.52	0.73	0.39	0.43
	1:1	CB	45	1.23	0.65	0.34	0.27
	1:2	CB	120	1.06	0.75	0.42	0.34
	1:2	CB	70	1.74	0.77	0.52	0.69
	1:2	CB	55	1.71	0.73	0.44	0.55

1:3	CB	100	2.25	0.83	0.43	0.79
1:3	CB	95	1.81	0.77	0.39	0.55
1:3	CB	75	2.48	0.76	0.48	0.82
1:3	CB	60	2.81	0.74	0.45	0.93
1:4	CB	90	2.54	0.82	0.37	0.77
1:4	CB	70	2.73	0.86	0.52	1.21
1:4	CB	55	2.65	0.87	0.48	1.11

[a] Chlorobenzene (CB), *o*-dichlorobenzene (DCB); [b] Result was the average of 8 cells of 12mm^2 on one device.

Appendix 4:

Supporting Information for Chapter 4

NMR spectra

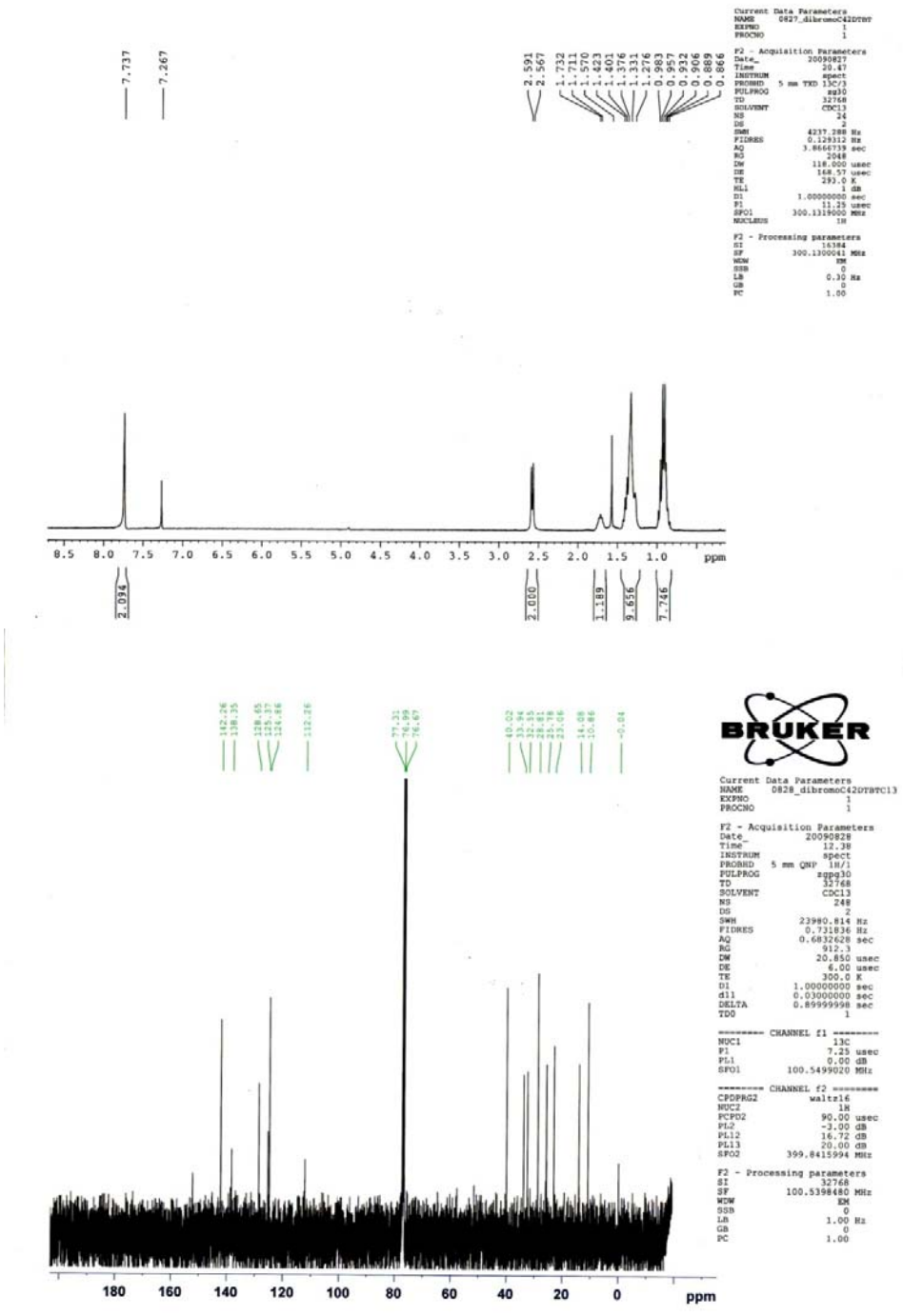

Figure A4-1. ^{1}H NMR and ^{13}C NMR spectra of **4DTBT** at 295K.

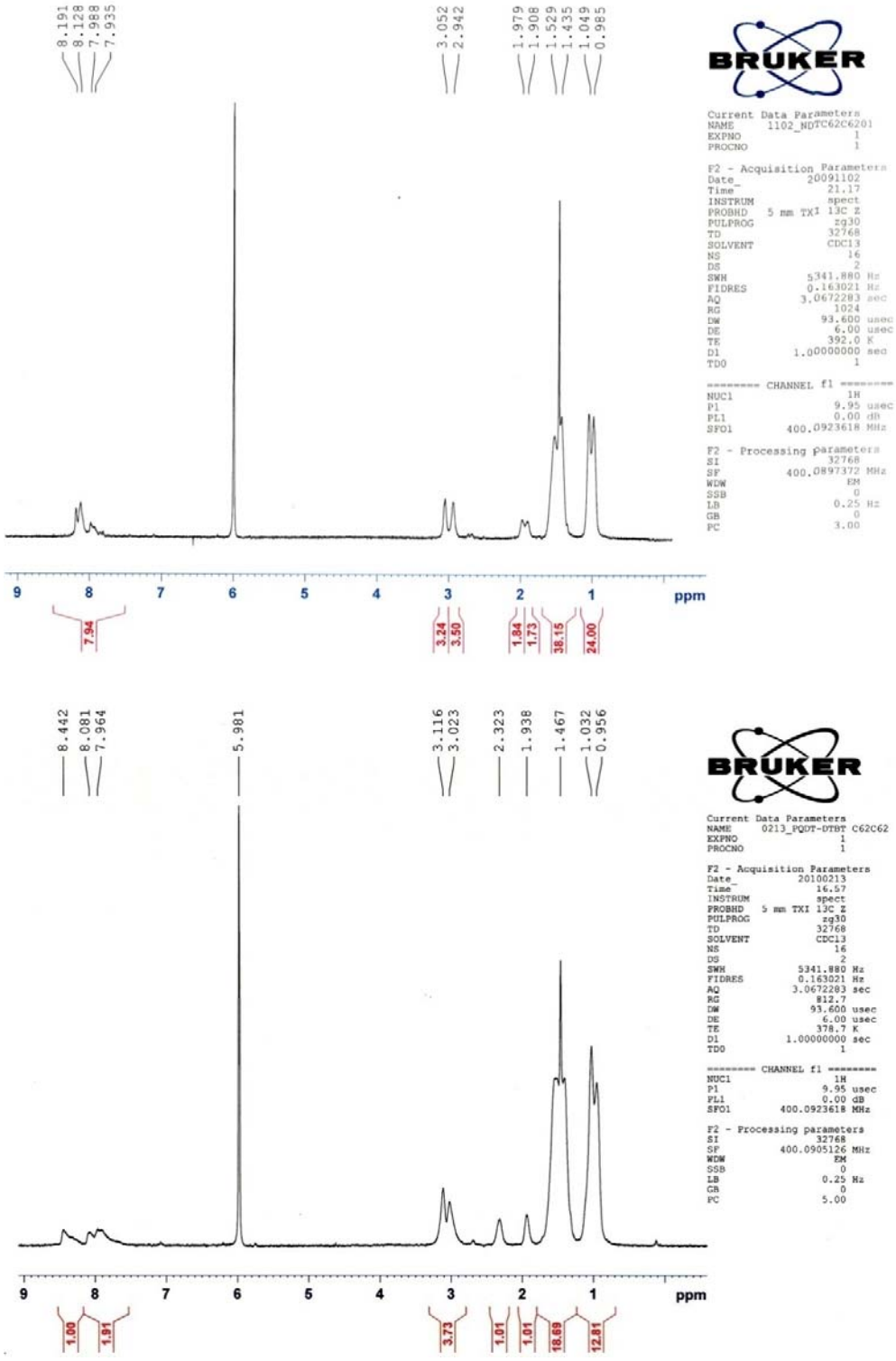

Figure A4-2. ^{1}H NMR spectra of **PNDT-4DTBT** and **PQDT-4DTBT** at ~400K (400 MHz).

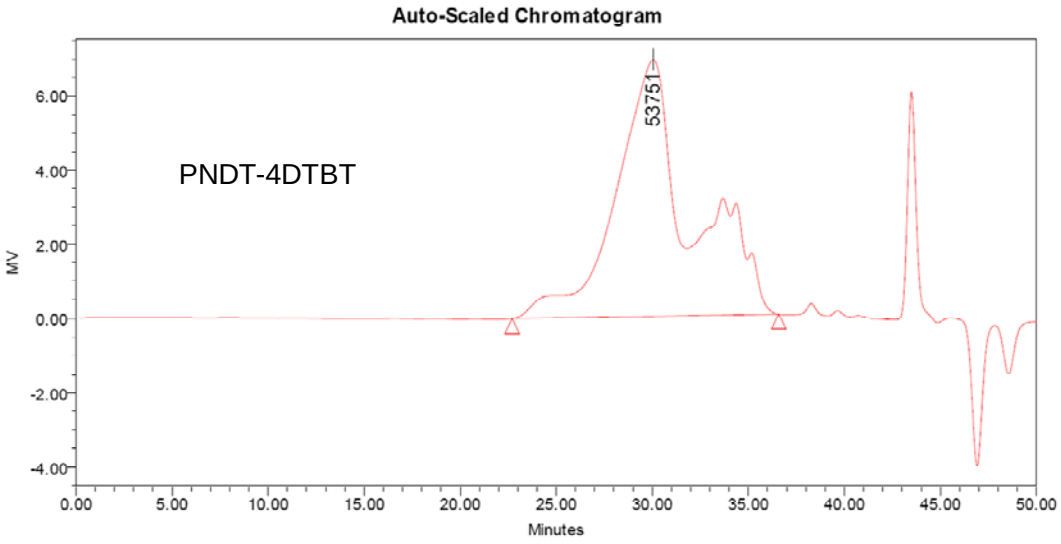

GPC Results

	Dist Name	Mn	Mw	Mv	MP	Mz	Mz+1	Poly dispersity	K	alpha
1		25722	101258		53751	457850	1016487	3.936589		

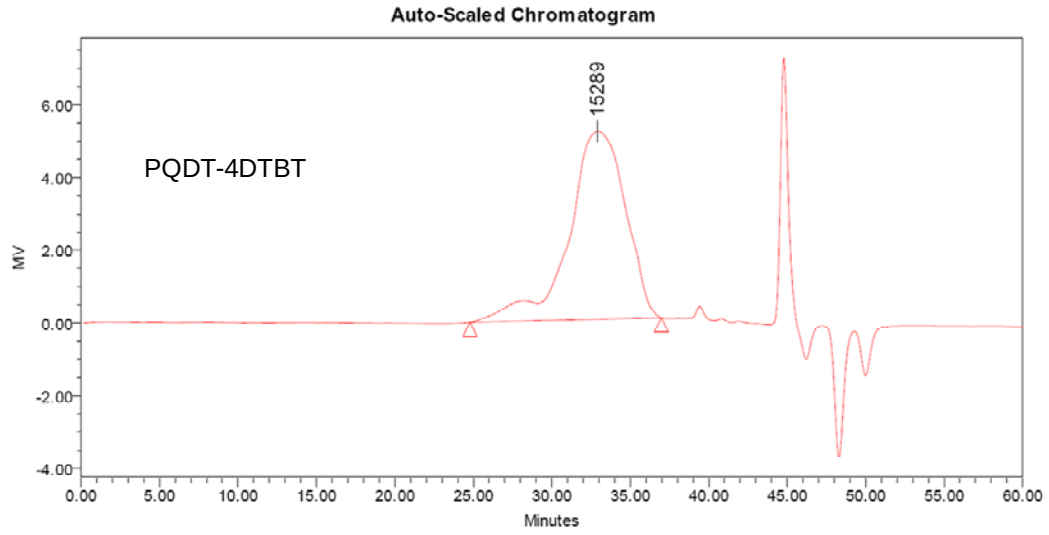

GPC Results

	Dist Name	Mn	Mw	Mv	MP	Mz	Mz+1	Poly dispersity	K	alpha
1		12973	29289		15289	115984	272936	2.257687		

Figure A4-3. GPC results of PNDT-4DTBT and PQDT-4DTBT in tetrahydrofuran (THF) at room temperature using polystyrene standards

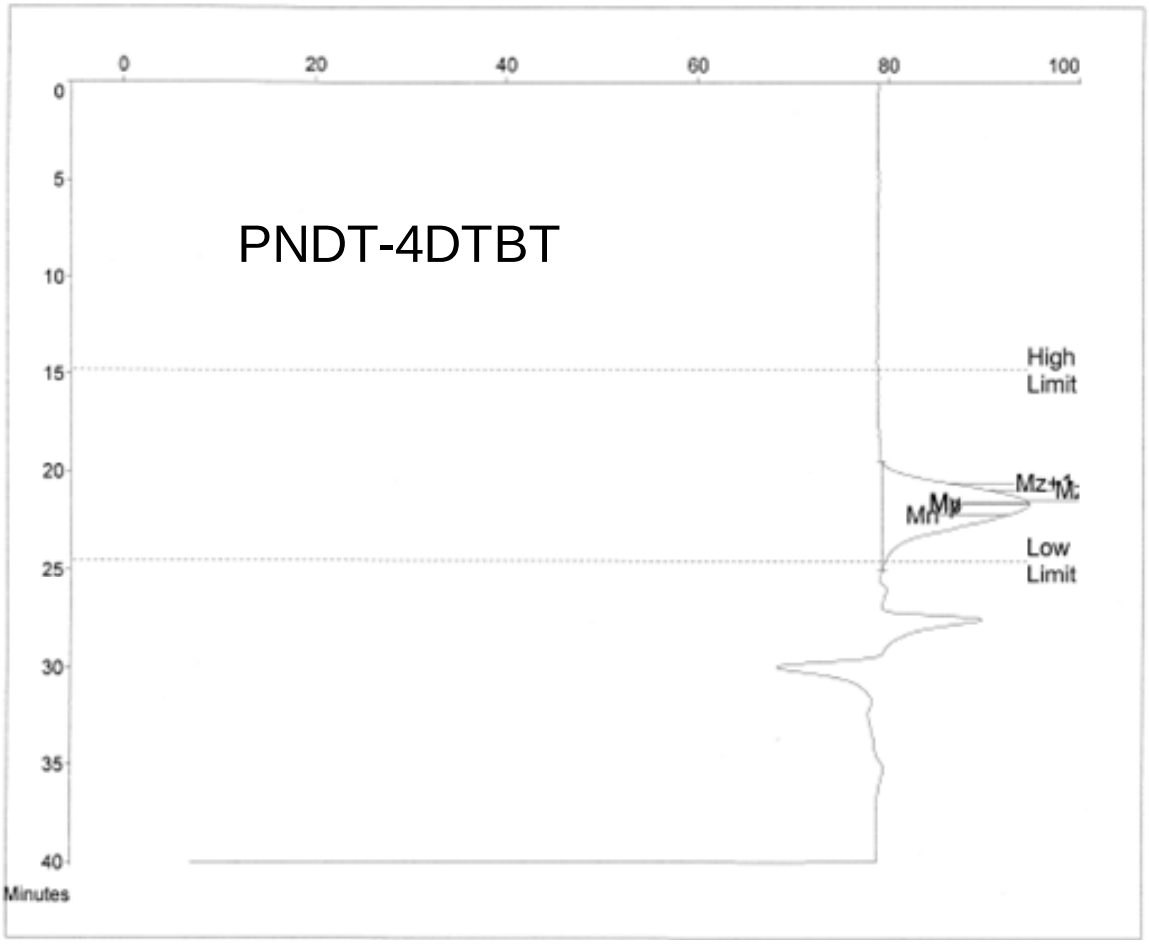

Molecular Weight Averages

Mp =	11585	Mz =	23217
Mn =	6761	Mz+1 =	32455
Mw =	14038	Mv =	12724
Polydispersity =	2.076	Peak Area =	429688

Molecular Weight Averages

Mp =	8366	Mz =	16354
Mn =	5242	Mz+1 =	23416
Mw =	10000	Mv =	9122
Polydispersity =	1.908	Peak Area =	557366

Figure S4. GPC results of PNDT-4DTBT and PQDT-4DTBT in 1,2,4-trichlorobenzene at 135 °C using polystyrene standards.

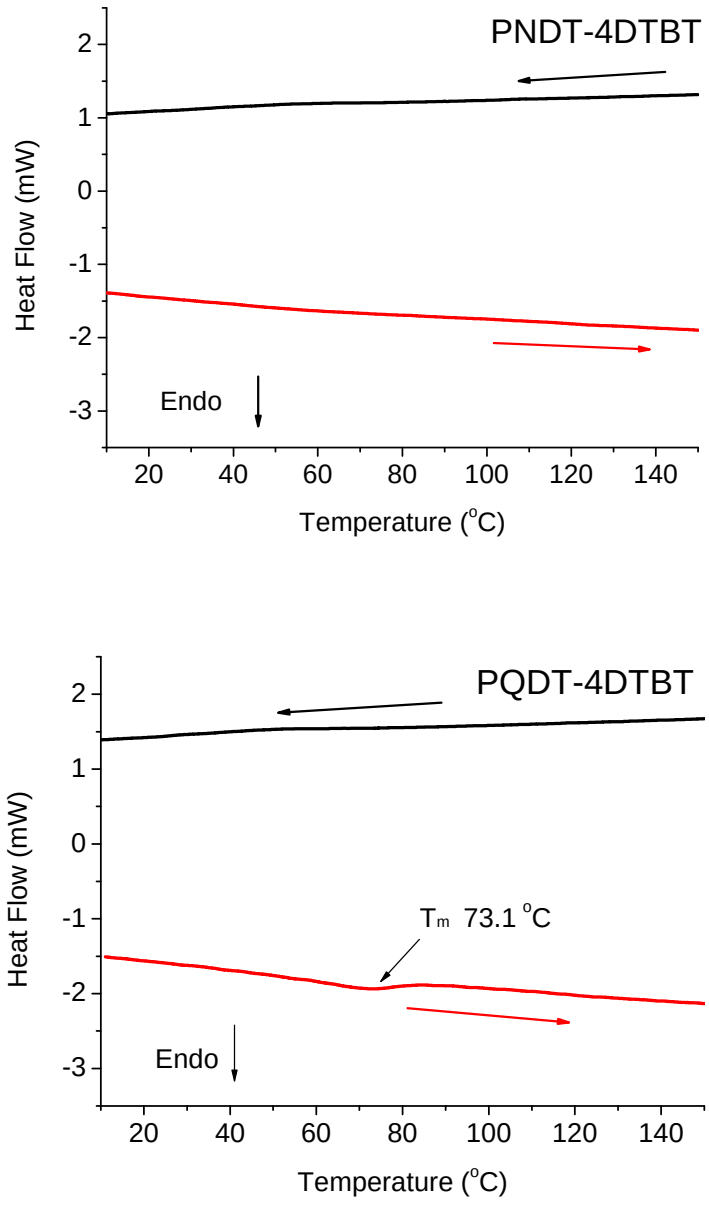

Figure A4-4. Differential scanning calorimetry heating and cooling curves of two polymers at 10°C/min.

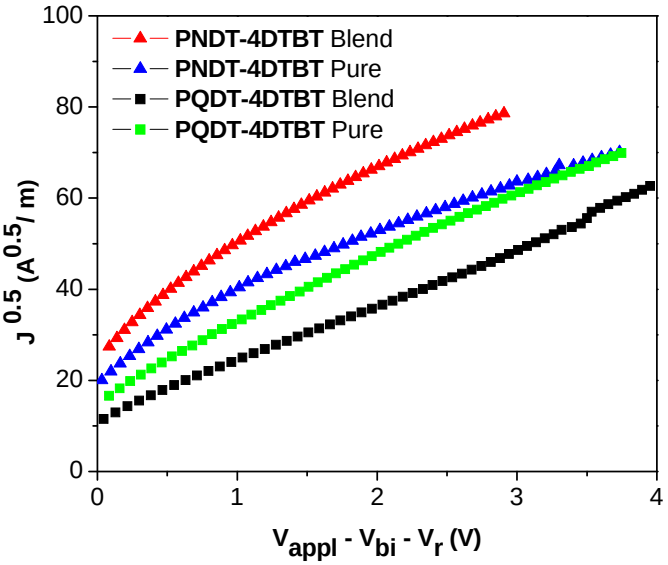

Figure A4-5. $J^{0.5}$ vs V plots for the polymer films at room temperature from a hole-only device of ITO/PEDOT:PSS (40 nm)/pure polymer or blend with $PC_{61}BM$/Pd (50 nm).

Appendix 5:

Supporting Information for Chapter 5

NMR spectra

-

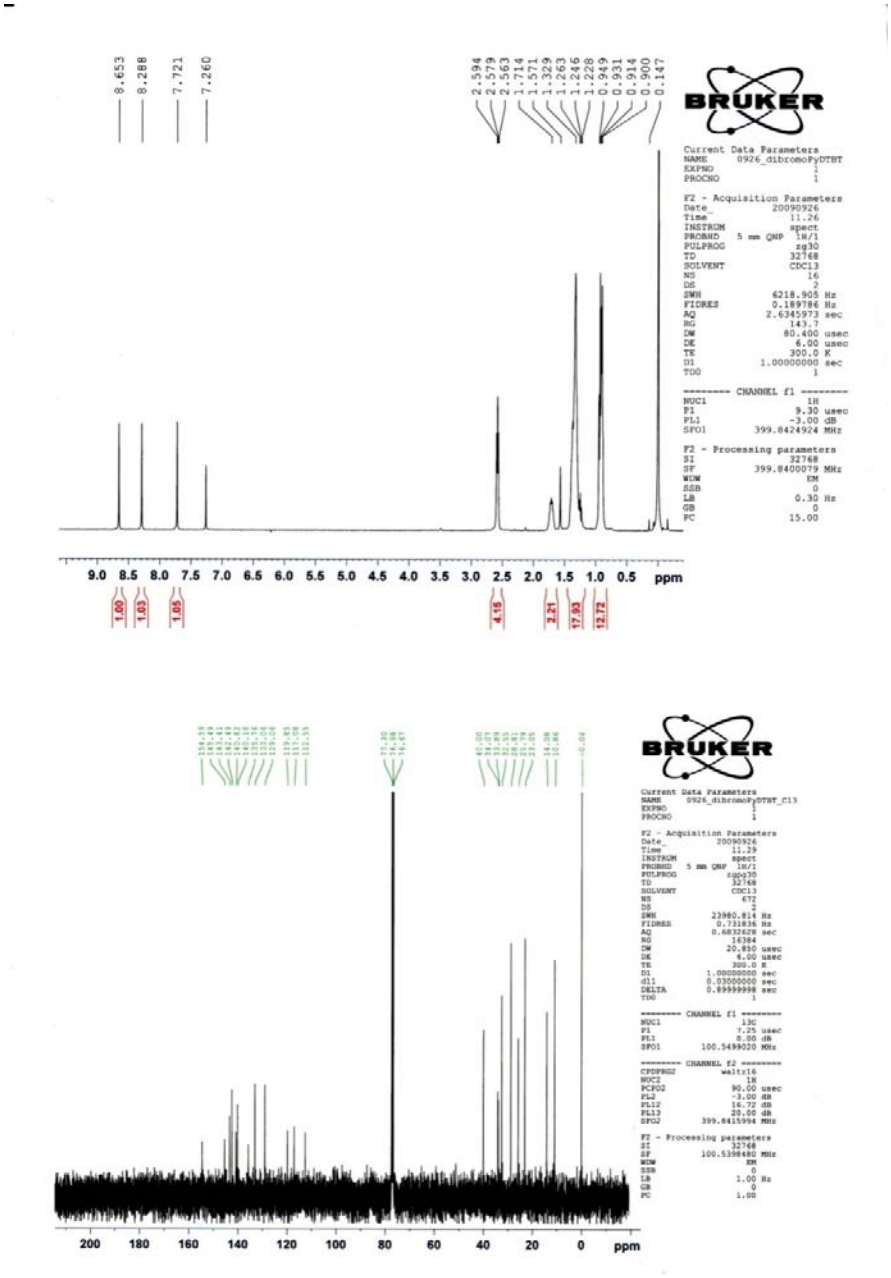

Figure A5-1. ^{1}H-NMR and ^{13}C-NMR spectra of **dibromoDTPyT** in $CDCl_3$.

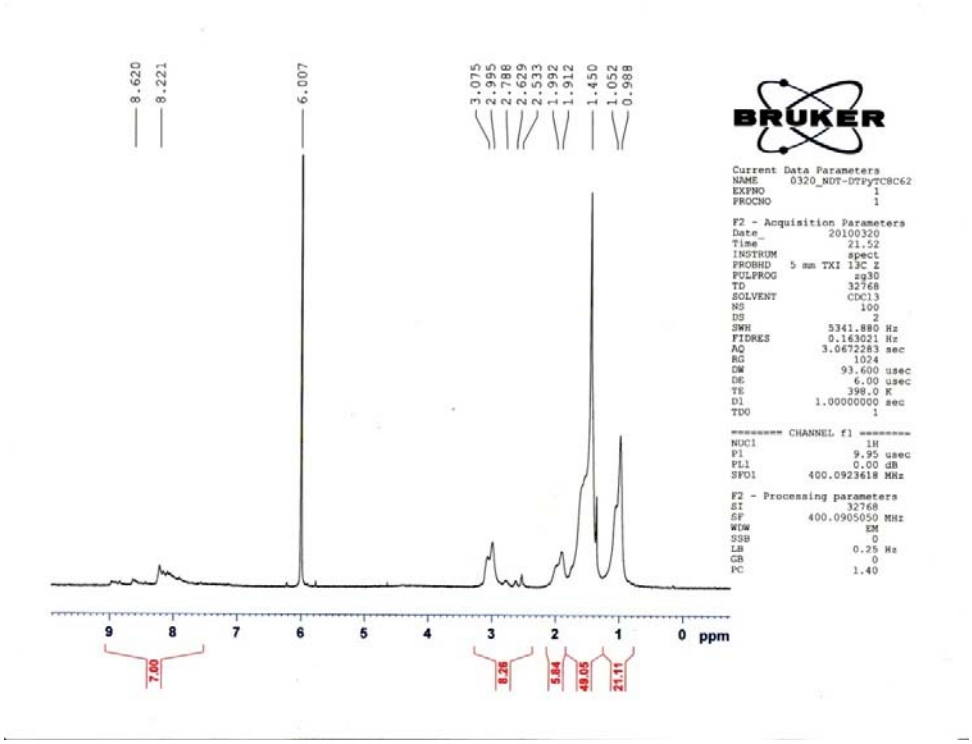

Current Data Parameters
NAME 0320_NDT-DTPyTC8C62
EXPNO 1
PROCNO 1

F2 - Acquisition Parameters
Date_ 20100320
Time 21.52
INSTRUM spect
PROBHD 5 mm TXI 13C Z
PULPROG zg30
TD 32768
SOLVENT CDCl3
NS 100
DS 2
SWH 5341.880 Hz
FIDRES 0.163021 Hz
AQ 3.0672283 sec
RG 1024
DW 93.600 usec
DE 6.00 usec
TE 398.0 K
D1 1.00000000 sec
TD0 1

======== CHANNEL f1 ========
NUC1 1H
P1 9.95 usec
PL1 0.00 dB
SFO1 400.0923618 MHz

F2 - Processing parameters
SI 32768
SF 400.0905050 MHz
WDW EM
SSB 0
LB 0.25 Hz
GB 0
PC 1.40

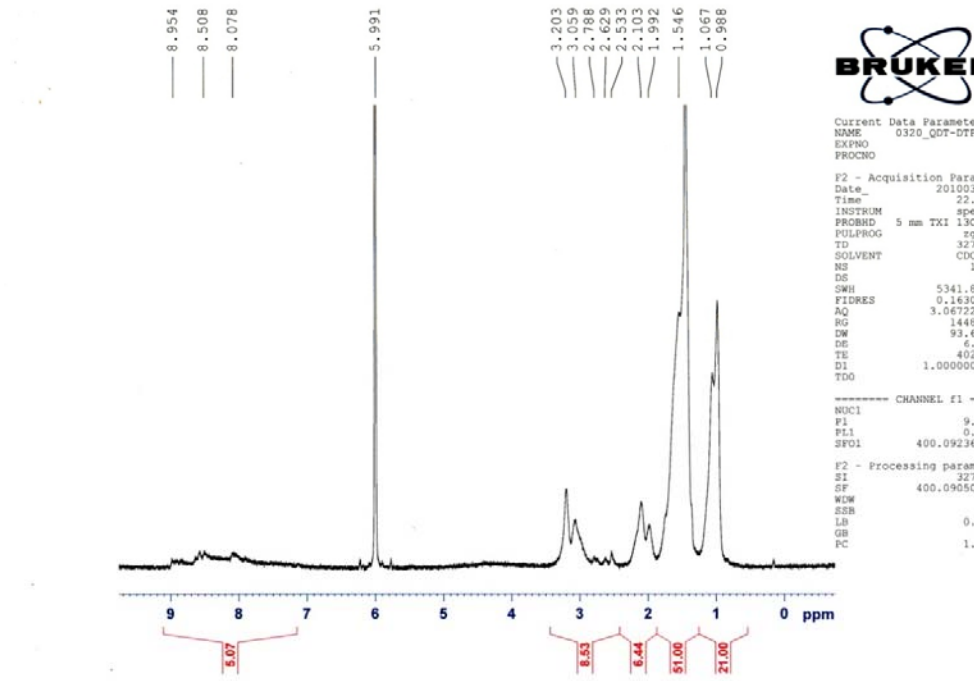

Current Data Parameters
NAME 0320_QDT-DTPyTC8C62
EXPNO 1
PROCNO 1

F2 - Acquisition Parameters
Date_ 20100320
Time 22.13
INSTRUM spect
PROBHD 5 mm TXI 13C Z
PULPROG zg30
TD 32768
SOLVENT CDCl3
NS 100
DS 2
SWH 5341.880 Hz
FIDRES 0.163021 Hz
AQ 3.0672283 sec
RG 1448.2
DW 93.600 usec
DE 6.00 usec
TE 402.4 K
D1 1.00000000 sec
TD0 1

======== CHANNEL f1 ========
NUC1 1H
P1 9.95 usec
PL1 0.00 dB
SFO1 400.0923618 MHz

F2 - Processing parameters
SI 32768
SF 400.0905048 MHz
WDW EM
SSB 0
LB 0.25 Hz
GB 0
PC 1.40

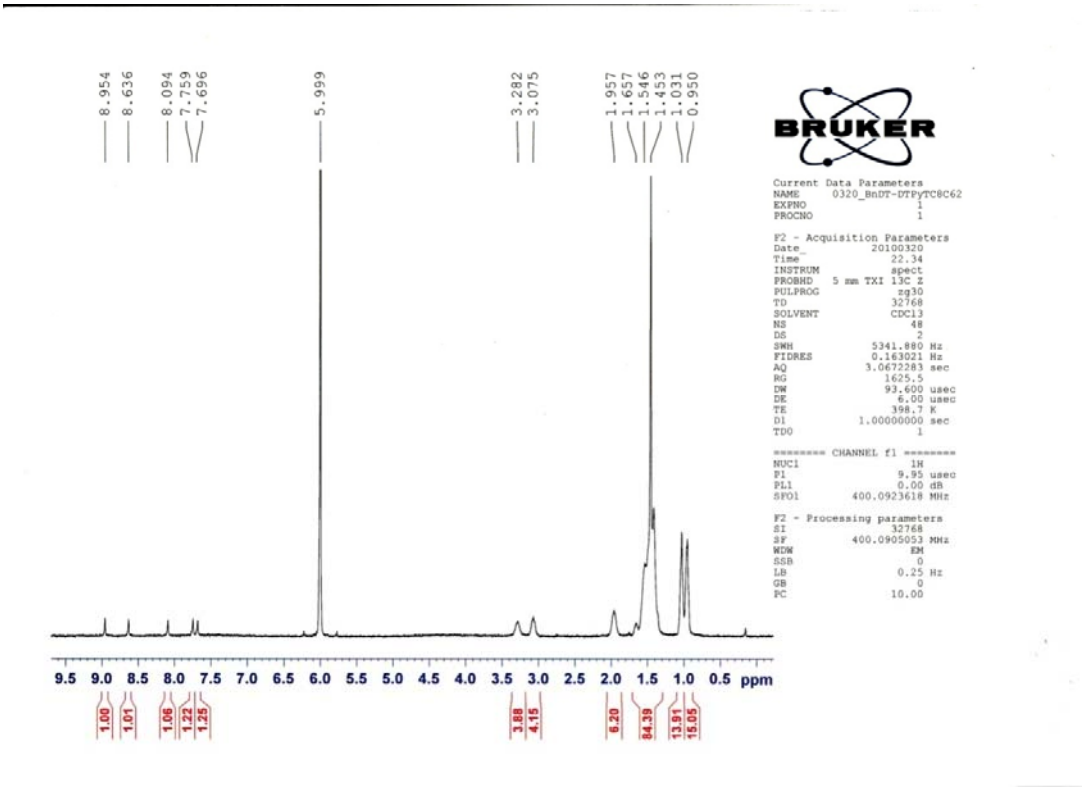

Figure A5-2. ^{1}H-NMR spectra of **PNDT-DTPyT**, **PQDT-DTPyT** and **PBnDT-DTPyT** in $CDCl_2CDCl_2$ at 400K.

Figure A5-3. Electrochemical cyclic voltammetry curves of PNDT-DTPyT, PQDT-DTPyT and PBnDT-DTPyT

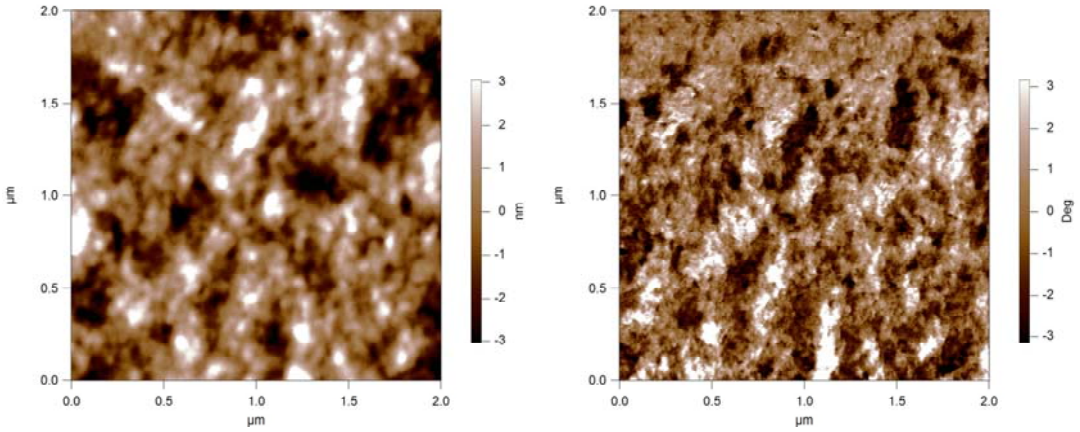

Figure A5-4. AFM images of **PNDT-DTPyT**:$PC_{61}BM$ film in a 1:1 ratio blend. (left: height image; right: phase image).

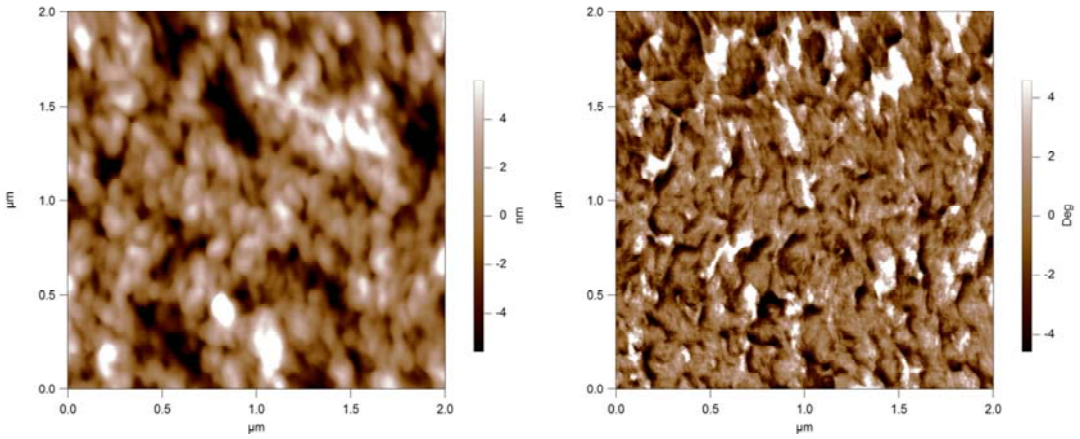

Figure A5-5. AFM images of **PQDT-DTPyT**:$PC_{61}BM$ film in a 1:1 ratio blend. (left: height image; right: phase image).

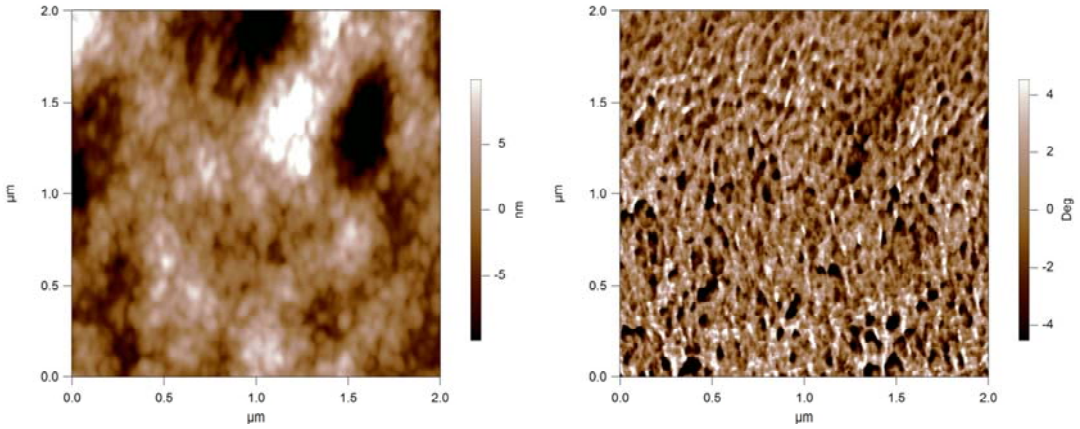

Figure A5-6. AFM images of **PBnDT-DTPyT**:$PC_{61}BM$ film in a 1:1 ratio blend. (left: height image; right: phase image).

Table A5-1. Mobility of polymers under SCLC condition.

	Polymer Only		Polymer:PCBM (1:1)	
	Thickness (nm)	Mobility (cm2/V·s)	Thickness (nm)	Mobility (cm2/V·s)
PNDT-DTPyT	50	1.94×10^{-6}	70	4.97×10^{-6}
PQDT-DTPyT	60	1.58×10^{-6}	90	1.79×10^{-5}
PBnDT-DTPyT	60	2.76×10^{-6}	75	5.91×10^{-6}

Appendix 6:

Supporting Information for Chapter 6

NMR spectra

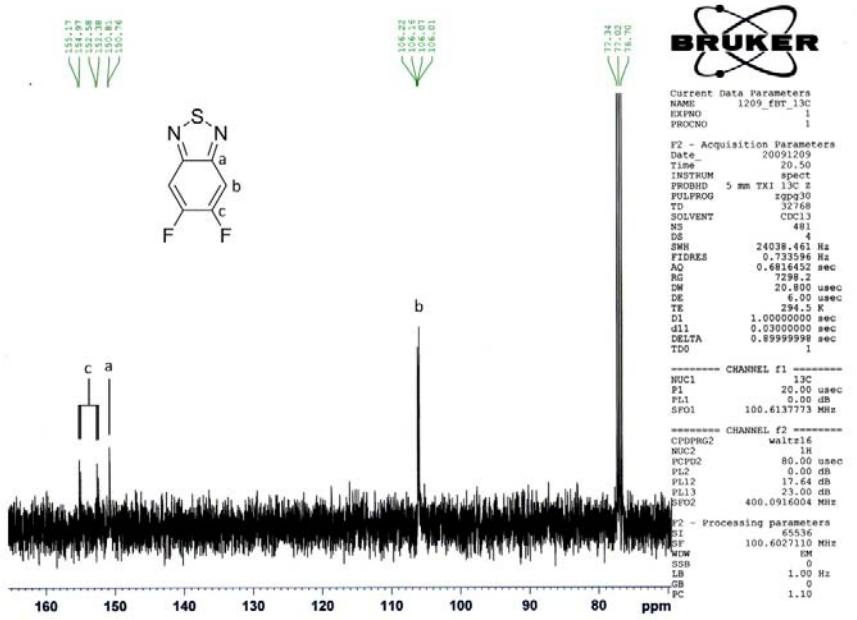

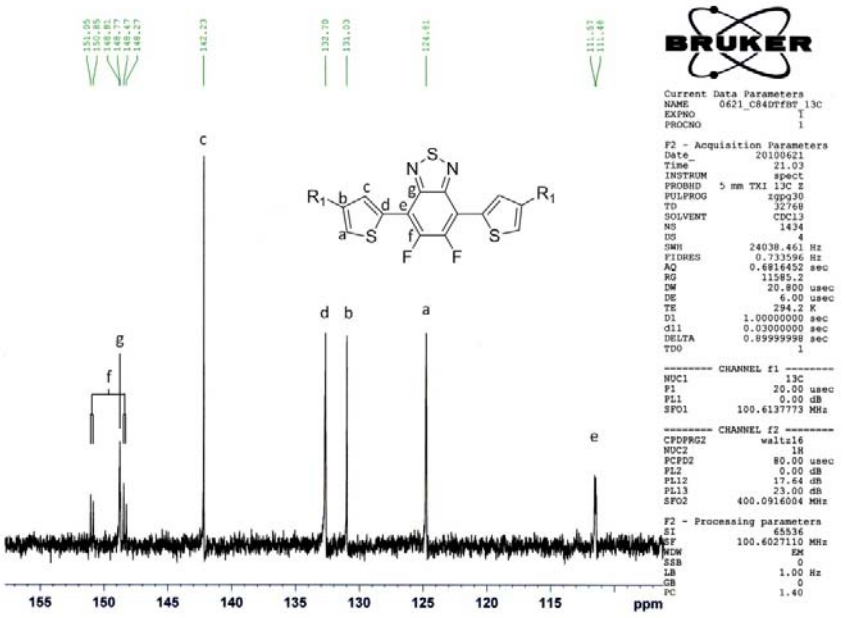

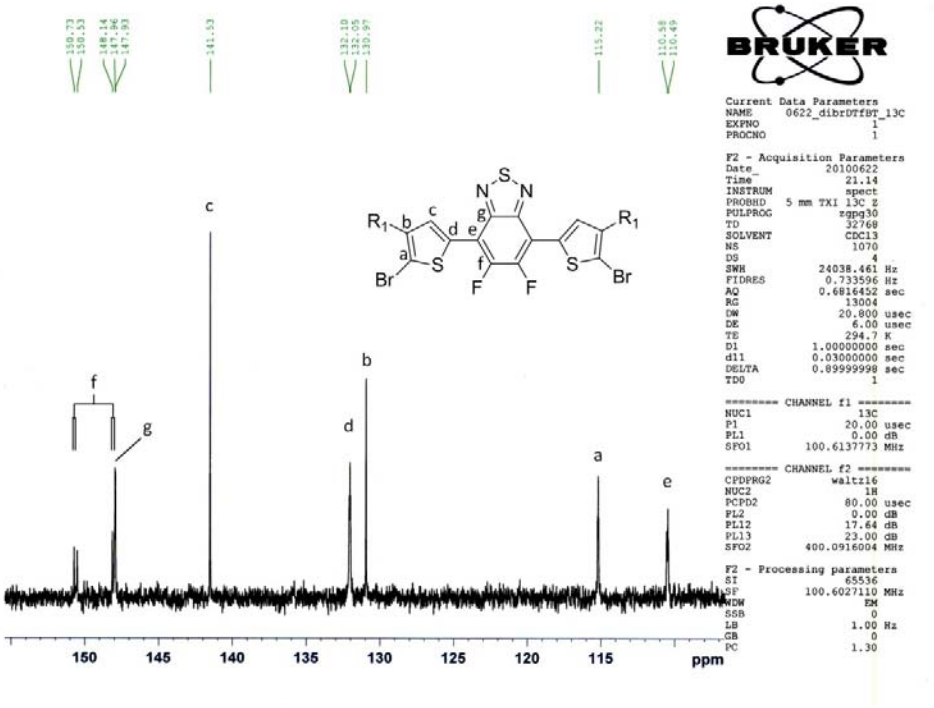

Figure A6-1. ^{13}C NMR spectra of compound **2**, **DTffBT** and **dibromoDTffBT** at 295K (only the peaks above 70 ppm are shown for clarity).

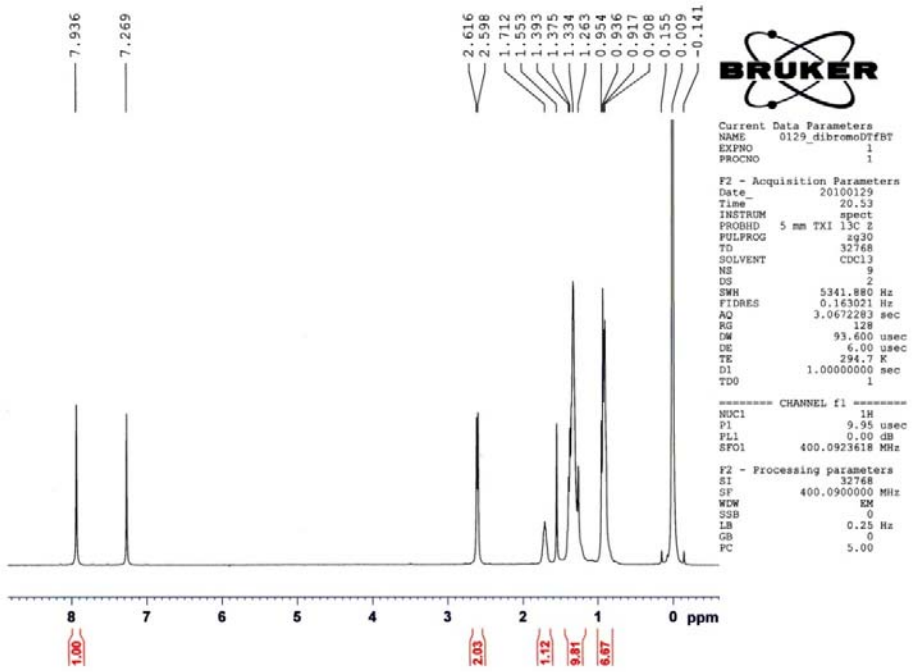

Figure A6-2. ^{1}H NMR spectrum of **dibromoDTffBT** at 295K.

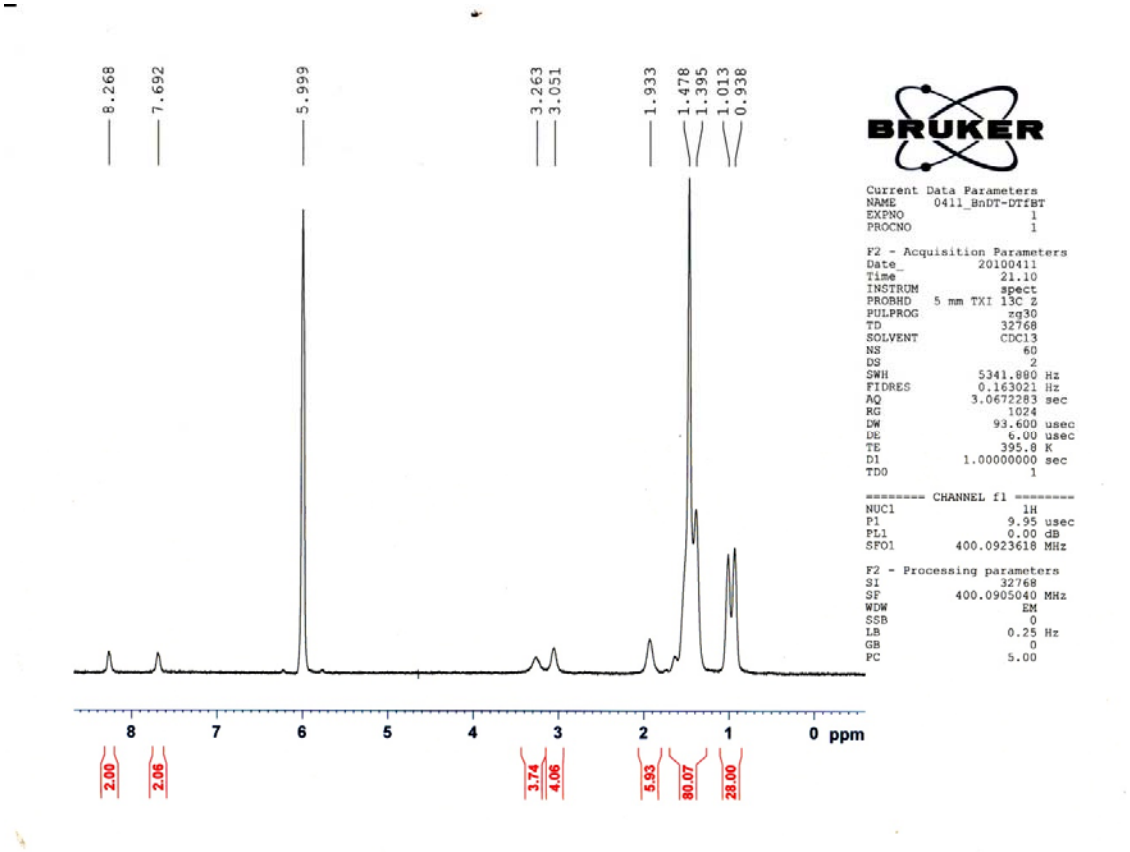

Figure A6-3. ^{1}H NMR spectra of **PBnDT-DTffBT** at 400K (400 MHz).

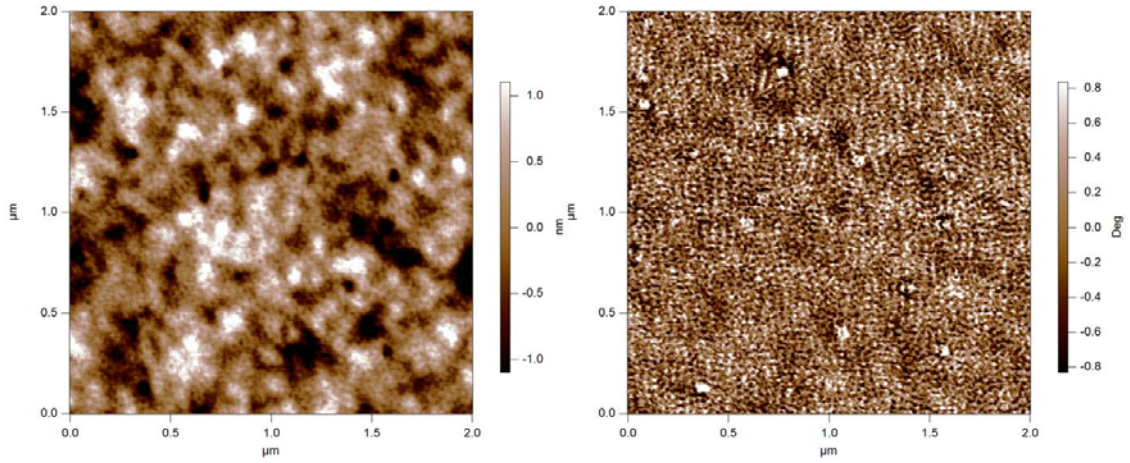

Figure A6-4. AFM images of **PBnDT-DTBT**:**PCBM** film in a 1:1 ratio blend. (left: height image; right: phase image).

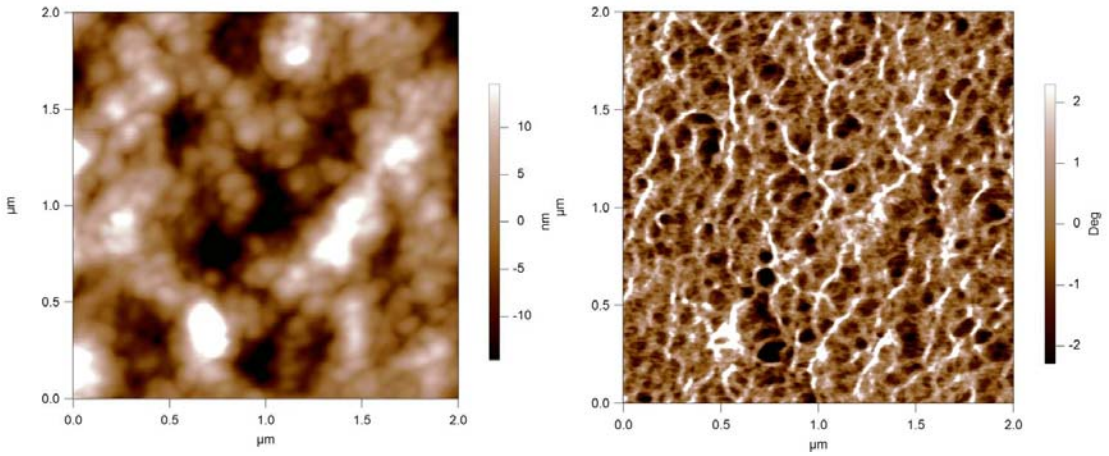

Figure A6-5. AFM images of **PBnDT-DTffBT**:**PCBM** film in a 1:1 ratio blend. (left: height image; right: phase image).

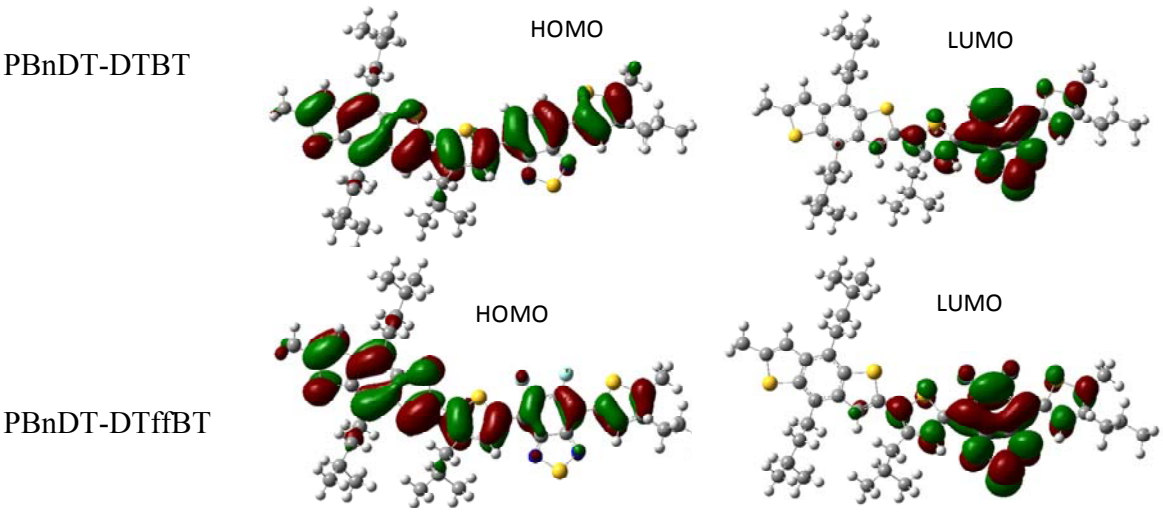

Figure A6-6: Calculation of HOMO (left) and LUMO (right) orbitals of **PBnDT-DTBT** and **PBnDT-DTffBT**.

Table A6-1. Mobility under SCLC condition.

Polymer Only	Thickness (nm)	Mobility(cm^2/V·s)	Polymer: PCBM	Thickness (nm)	Mobility(cm^2/V·s)
PBnDT-DTffBT	75	8.21E-05	1:1	80	8.38E-05

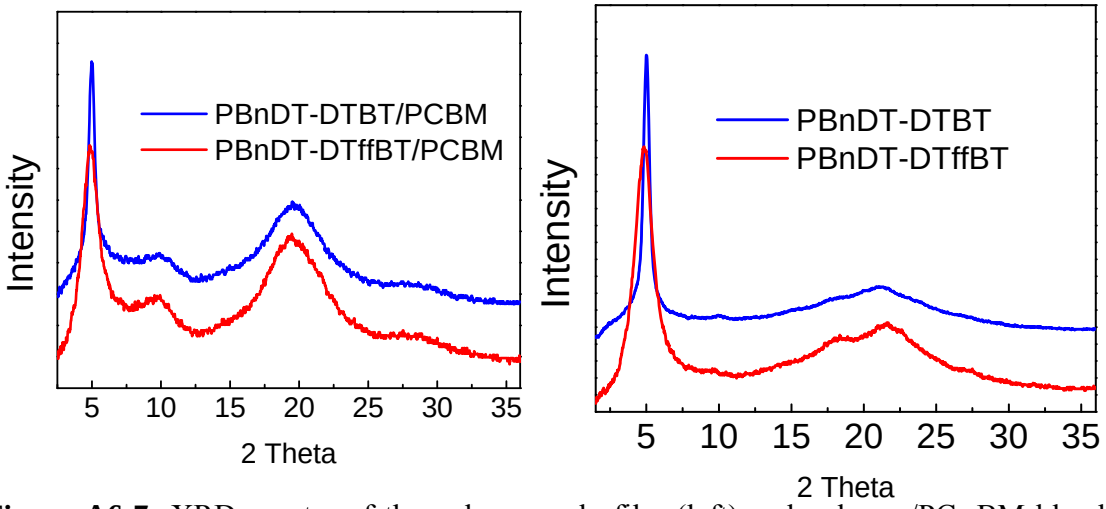

Figure A6-7: XRD spectra of the polymer-only film (left) and polymer/$PC_{61}BM$ blend film (right)

Table A6-2. XRD data of polymer-only film and polymer/$PC_{61}BM$ blend film

Polymer	*Polymer Only*		*Polymer:PCBM (1:1)*	
	2θ (°)	*d-spacing (Å)*	*2θ(°)*	*d-spacing (Å)*
PBnDT-DTBT	5	17.67333	4.98	17.74427
PBnDT-DTffBT	4.84	18.25721	4.88	18.10765

REFERENCES

(1) Green, M. A.; Emery, K.; Hishikawa, Y.; Warta, W.; Dunlop, E. D. *Progress in Photovoltaics: Research and Applications* **2011**, *19*, 565.

(2) Bijleveld, J. C.; Zoombelt, A. P.; Mathijssen, S. G. J.; Wienk, M. M.; Turbiez, M.; de Leeuw, D. M.; Janssen, R. A. J. *Journal of the American Chemical Society* **2009**, *131*, 16616.

(3) Lewis, N. S. *Science* **2007**, *315*, 798.

(4) Yu, G.; Gao, J.; Hummelen, J. C.; Wudl, F.; Heeger, A. J. *Science* **1995**, *270*, 1789.

(5) Park, S. H.; Roy, A.; Beaupre, S.; Cho, S.; Coates, N.; Moon, J. S.; Moses, D.; Leclerc, M.; Lee, K.; Heeger, A. J. *Nature Photonics* **2009**, *3*, 297.

(6) Coffin, R. C.; Peet, J.; Rogers, J.; Bazan, G. C. *Nature Chemistry* **2009**, *1*, 657.

(7) Huo, L.; Hou, J.; Zhang, S.; Chen, H.-Y.; Yang, Y. *Angewandte Chemie International Edition* **2010**, *49*, 1500.

(8) Xiao, S.; Price, S. C.; Zhou, H.; You, W. *ACS Symposium Series* **2010**, *1034* 71.

(9) Kirchmeyer, S.; Reuter, K. *Journal of Materials Chemistry* **2005**, *15*, 2077.

(10) Sun, Y.; Takacs, C. J.; Cowan, S. R.; Seo, J. H.; Gong, X.; Roy, A.; Heeger, A. J. *Advanced Materials* **2011**, *23*, 2226.

(11)Subbiah, J.; Kim, D. Y.; Hartel, M.; So, F. *Applied Physics Letters* **2010**, *96*, 063303.

(12) Kröger, M.; Hamwi, S.; Meyer, J.; Riedl, T.; Kowalsky, W.; Kahn, A. *Applied Physics Letters* **2009**, *95*, 123301.

(13) Tao, C.; Ruan, S. P.; Xie, G. H.; Kong, X. Z.; Shen, L.; Meng, F. X.; Liu, C. X.; Zhang, X. D.; Dong, W.; Chen, W. Y. *Applied Physics Letters* **2009**, *94*.

(14) Meyer, J.; Kroger, M.; Hamwi, S.; Gnam, F.; Riedl, T.; Kowalsky, W.; Kahn, A. *Applied Physics Letters* **2010**, *96*, 193302.

(15) Hayakawa, A.; Yoshikawa, O.; Fujieda, T.; Uehara, K.; Yoshikawaa, S. *Applied Physics Letters* **2007**, *90*.

(16) Kim, J. Y.; Kim, S. H.; Lee, H. H.; Lee, K.; Ma, W. L.; Gong, X.; Heeger, A. J. *Advanced Materials* **2006**, *18*, 572.

(17) Sun, Y.; Seo, J. H.; Takacs, C. J.; Seifter, J.; Heeger, A. J. *Advanced Materials* **2011**, *23*, 1679.

(18) Yip, H.-L.; Hau, S. K.; Baek, N. S.; Ma, H.; Jen, A. K. Y. *Advanced Materials* **2008**, *20*, 2376.

(19) Bulliard, X.; Ihn, S.-G.; Yun, S.; Kim, Y.; Choi, D.; Choi, J.-Y.; Kim, M.; Sim, M.; Park, J.-H.; Choi, W.; Cho, K. *Advanced Functional Materials* **2010**, *20*, 4381.

(20) Peumans, P.; Uchida, S.; Forrest, S. R. *Nature* **2003**, *425*, 158.

(21) Kallmann, H.; Pope, M. *Journal of Chemical Physics* **1959**, *30*, 585.

(22) Tang, C. W. *Applied Physics Letters* **1986**, *48*, 183.

(23) Sariciftci, N. S.; Smilowitz, L.; Heeger, A. J.; Wudl, F. *Science* **1992**, *258*, 1474.

(24) Hummelen, J. C.; Knight, B. W.; Lepeq, F.; Wudl, F.; Yao, J.; Wilkins, C. L. *Journal of Organic Chemistry* **1995**, *60*, 532.

(25) Dennler, G.; Scharber, M. C.; Brabec, C. J. *Advanced Materials* **2009**, *21*, 1323.

(26) Kim, Y.; Cook, S.; Tuladhar, S. M.; Choulis, S. A.; Nelson, J.; Durrant, J. R.; Bradley, D. D. C.; Giles, M.; McCulloch, I.; Ha, C.-S.; Ree, M. *Nature Materials* **2006**, *5*, 197.

(27) Service, R. F. *Science* **2011**, *332*, 293.

(28) Thompson, B. C.; Fréchet, J. M. J. *Angewandte Chemie International Edition* **2008**, *47*, 58.

(29) Kroon, R.; Lenes, M.; Hummelen, J. C.; Blom, P. W. M.; de Boer, B. *Polymer Reviews* **2008**, *48*, 531

(30) Kippelen, B.; Bredas, J.-L. *Energy & Environmental Science* **2009**, *2*, 251.

(31) Helgesen, M.; Sondergaard, R.; Krebs, F. C. *Journal of Materials Chemistry* **2010**, *20*, 36.

(32) Cheng, Y.-J.; Yang, S.-H.; Hsu, C.-S. *Chemical Reviews* **2009**, *109*, 5868.

(33) Chen, J.; Cao, Y. *Accounts of Chemical Research* **2009**, *42*, 1709.

(34) Facchetti, A. *Chemistry of Materials* **2010**, *23*, 733.

(35) Ross, R. B.; Cardona, C. M.; Guldi, D. M.; Sankaranarayanan, S. G.; Reese, M. O.; Kopidakis, N.; Peet, J.; Walker, B.; Bazan, G. C.; Van Keuren, E.; Holloway, B. C.; Drees, M. *Nature Materials* **2009**, *8*, 208.

(36) Lenes, M.; Wetzelaer, G.-J. A. H.; Kooistra, F. B.; Veenstra, S. C.; Hummelen, J. C.; Blom, P. W. M. *Advanced Materials* **2008**, *20*, 2116.

(37) Wienk, M. M.; Kroon, J. M.; Verhees, W. J. H.; Knol, J.; Hummelen, J. C.; van Hal, P. A.; Janssen, R. A. J. *Angewandte Chemie International Edition* **2003**, *42*, 3371.

(38) Zhao, G.; He, Y.; Li, Y. *Advanced Materials* **2010**, *22*, 4355.

(39) Murata, M.; Morinaka, Y.; Murata, Y.; Yoshikawa, O.; Sagawa, T.; Yoshikawa, S. *Chemical Communications* **2011**, *47*, 7335.

(40) Matsuo, Y.; Sato, Y.; Niinomi, T.; Soga, I.; Tanaka, H.; Nakamura, E. *Journal of the American Chemical Society* **2009**, *131*, 16048.

(41) Shaheen, S. E.; Brabec, C. J.; Sariciftci, N. S.; Padinger, F.; Fromherz, T.; Hummelen, J. C. *Applied Physics Letters* **2001**, *78*, 841.

(42) Brabec, C. J.; Shaheen, S. E.; Winder, C.; Sariciftci, N. S.; Denk, P. *Applied Physics Letters* **2002**, *80*, 1288.

(43) Reyes-Reyes, M.; Kim, K.; Carroll, D. L. *Applied Physics Letters* **2005**, *87*, 3.

(44) Ma, W. L.; Yang, C. Y.; Gong, X.; Lee, K.; Heeger, A. J. *Advanced Functional Materials* **2005**, *15*, 1617.

(45) Li, G.; Shrotriya, V.; Huang, J. S.; Yao, Y.; Moriarty, T.; Emery, K.; Yang, Y. *Nature Materials* **2005**, *4*, 864.

(46) Gadisa, A.; Mammo, W.; Andersson, L. M.; Admassie, S.; Zhang, F.; Andersson, M. R.; Inganäs, O. *Advanced Functional Materials* **2007**, *17*, 3836.

(47) Zhang, F.; Jespersen, K. G.; Björström, C.; Svensson, M.; Andersson, M. R.; Sundström, V.; Magnusson, K.; Moons, E.; Yartsev, A.; Inganäs, O. *Advanced Functional Materials* **2006**, *16*, 667.

(48) Zheng, Q.; Jung, B. J.; Sun, J.; Katz, H. E. *Journal of the American Chemical Society* **2010**, *132*, 5394.

(49) Zoombelt, A. P.; Mathijssen, S. G. J.; Turbiez, M. G. R.; Wienk, M. M.; Janssen, R. A. J. *Journal of Materials Chemistry* **2010**, *20*, 2240.

(50) Price, S. C.; Stuart, A. C.; Yang, L.; Zhou, H.; You, W. *Journal of the American Chemical Society* **2011**, *133*, 4625.

(51) Zhou, H.; Yang, L.; Liu, S.; You, W. *Macromolecules* **2010**, *43*, 10390.

(52) Scharber, M. C.; Mühlbacher, D.; Koppe, M.; Denk, P.; Waldauf, C.; Heeger, A. J.; Brabec, C. J. *Advanced Materials* **2006**, *18*, 789.

(53) Perez, M. D.; Borek, C.; Forrest, S. R.; Thompson, M. E. *Journal of the American Chemical Society* **2009**, *131*, 9281.

(54) Vandewal, K.; Tvingstedt, K.; Gadisa, A.; Inganas, O.; Manca, J. V. *Nature Materials* **2009**, *8*, 904.

(55) Moliton, A.; Nunzi, J.-M. *Polymer International* **2006**, *55*, 583.

(56) Bowden, S.; Honsberg, C.

(57) Mauer, R.; Kastler, M.; Laquai, F. *Advanced Functional Materials* **2010**, *20*, 2085.

(58) Kim, Y.; Nelson, J.; Durrant, J. R.; Bradley, D. D. C.; Heo, K.; Park, J.; Kim, H.; McCulloch, I.; Heeney, M.; Ree, M.; Ha, C.-S. *Soft Matter* **2007**, *3*, 117.

(59) Roncali, J. *Chemical Reviews* **1997**, *97*, 173.

(60) Havinga, E. E.; ten Hoeve, W.; Wynberg, H. *Synthetic Metals* **1993**, *55*, 299.

(61) Ajayaghosh, A. *Chemical Society Reviews* **2003**, *32*, 181.

(62)Zhang, Q. T.; Tour, J. M. *Journal of the American Chemical Society* **1998**, *120*, 5355.

(63) Chu, T.-Y.; Lu, J.; Beaupré, S.; Zhang, Y.; Pouliot, J.-R. m.; Wakim, S.; Zhou, J.; Leclerc, M.; Li, Z.; Ding, J.; Tao, Y. *Journal of the American Chemical Society* **2011**, *133*, 4250.

(64) Zhou, H.; Yang, L.; Stuart, A. C.; Price, S. C.; Liu, S.; You, W. *Angewandte Chemie International Edition* **2011**, *50*, 2995.

(65) Amb, C. M.; Chen, S.; Graham, K. R.; Subbiah, J.; Small, C. E.; So, F.; Reynolds, J. R. *Journal of the American Chemical Society* **2011**, *133*, 10062.

(66) Su, M.-S.; Kuo, C.-Y.; Yuan, M.-C.; Jeng, U. S.; Su, C.-J.; Wei, K.-H. *Advanced Materials* **2011**, DOI: 10.1002/adma.201101274.

(67) Wudl, F.; Kobayashi, M.; Heeger, A. J. *Journal of Organic Chemistry* **1984**, *49*, 3382.

(68) Pomerantz, M.; Chalonergill, B.; Harding, L. O.; Tseng, J. J.; Pomerantz, W. J. *Journal of the Chemical Society-Chemical Communications* **1992**, 1672.

(69) Hong, S. Y.; Marynick, D. S. *Macromolecules* **1992**, *25*, 4652.

(70) Sotzing, G. A.; Lee, K. H. *Macromolecules* **2002**, *35*, 7281.

(71) Qin, Y.; Kim, J. Y.; Frisbie, C. D.; Hillmyer, M. A. *Macromolecules* **2008**, *41*, 5563.

(72) Hou, J. H.; Park, M. H.; Zhang, S. Q.; Yao, Y.; Chen, L. M.; Li, J. H.; Yang, Y. *Macromolecules* **2008**, *41*, 6012.

(73) Wienk, M. M.; Turbiez, M. G. R.; Struijk, M. P.; Fonrodona, M.; Janssen, R. A. J. *Applied Physics Letters* **2006**, *88*.

(74)Zhang, F.; Mammo, W.; Andersson, L. M.; Admassie, S.; Andersson, M. R.; Inganäs, O. *Advanced Materials* **2006**, *18*, 2169.

(75) Liang, Y. Y.; Xiao, S. Q.; Feng, D. Q.; Yu, L. P. *Journal of Physical Chemistry C* **2008**, *112*, 7866.

(76) Kleinhenz, N.; Yang, L.; Zhou, H.; Price, S. C.; You, W. *Macromolecules* **2011**, *44*, 872.

(77) Chen, H.-Y.; Hou, J.; Zhang, S.; Liang, Y.; Yang, G.; Yang, Y.; Yu, L.; Wu, Y.; Li, G. *Nature Photonics* **2009**, *3*, 649.

(78) Wen, S.; Pei, J.; Zhou, Y.; Li, P.; Xue, L.; Li, Y.; Xu, B.; Tian, W. *Macromolecules* **2009**, *42*, 4977.

(79) Son, H. J.; Wang, W.; Xu, T.; Liang, Y.; Wu, Y.; Li, G.; Yu, L. *Journal of the American Chemical Society* **2011**, *133*, 1885.

(80) Liang, Y.; Xu, Z.; Xia, J.; Tsai, S.-T.; Wu, Y.; Li, G.; Ray, C.; Yu, L. *Advanced Materials* **2010**, *22*, E135.

(81) Li, Y.; Zou, Y. *Advanced Materials* **2008**, *20*, 2952.

(82)Huang, F.; Chen, K.-S.; Yip, H.-L.; Hau, S. K.; Acton, O.; Zhang, Y.; Luo, J.; Jen, A. K. Y. *Journal of the American Chemical Society* **2009**, *131*, 13886.

(83) Duan, C.; Chen, K.-S.; Huang, F.; Yip, H.-L.; Liu, S.; Zhang, J.; Jen, A. K. Y.; Cao, Y. *Chemistry of Materials* **2010**, *22*, 6444.

(84) Cravino, A.; Sariciftci, N. S. *Journal of Materials Chemistry* **2002**, *12*, 1931.

(85) Giacalone, F.; Martín, N. *Chemical Reviews* **2006**, *106*, 5136.

(86) Ramos, A. M.; Rispens, M. T.; van Duren, J. K. J.; Hummelen, J. C.; Janssen, R. A. J. *Journal of the American Chemical Society* **2001**, *123*, 6714.

(87) Yang, C.; Li, H.; Sun, Q.; Qiao, J.; Li, Y.; Li, Y.; Zhu, D. *Solar Energy Materials and Solar Cells* **2005**, *85*, 241.

(88) Tan, Z. a.; Hou, J.; He, Y.; Zhou, E.; Yang, C.; Li, Y. *Macromolecules* **2007**, *40*, 1868.

(89) Martín, N.; Sánchez, L.; Herranz, M. a. Á.; Illescas, B.; Guldi, D. M. *Accounts of Chemical Research* **2007**, *40*, 1015.

(90) Hirayama, D.; Takimiya, K.; Aso, Y.; Otsubo, T.; Hasobe, T.; Yamada, H.; Imahori, H.; Fukuzumi, S.; Sakata, Y. *Journal of the American Chemical Society* **2002**, *124*, 532.

(91) Miyanishi, S.; Zhang, Y.; Tajima, K.; Hashimoto, K. *Chemical Communications* **2010**, *46*, 6723.

(92) Cravino, A.; Sariciftci, N. S. *Nat Mater* **2003**, *2*, 360.

(93) Roncali, J. *Advanced Energy Materials* **2011**, *1*, 147.

(94)Yang, L.; Zhou, H.; You, W. *The Journal of Physical Chemistry C* **2010**, *114*, 16793.

(95) van Mullekom, H. A. M.; Vekemans, J. A. J. M.; Havinga, E. E.; Meijer, E. W. *Materials Science & Engineering R-Reports* **2001**, *32*, 1.

(96) Mühlbacher, D.; Scharber, M.; Morana, M.; Zhu, Z.; Waller, D.; Gaudiana, R.; Brabec, C. *Advanced Materials* **2006**, *18*, 2884.

(97) Peet, J.; Kim, J. Y.; Coates, N. E.; Ma, W. L.; Moses, D.; Heeger, A. J.; Bazan, G. C. *Nature Materials* **2007**, *6*, 497.

(98) Hou, J.; Chen, H.-Y.; Zhang, S.; Li, G.; Yang, Y. *Journal of the American Chemical Society* **2008**, *130*, 16144.

(99) Blouin, N.; Michaud, A.; Leclerc, M. *Advanced Materials* **2007**, *19*, 2295.

(100) Blouin, N.; Michaud, A.; Gendron, D.; Wakim, S.; Blair, E.; Neagu-Plesu, R.; Belletete, M.; Durocher, G.; Tao, Y.; Leclerc, M. *Journal of the American Chemical Society* **2008**, *130*, 732.

(101) Wang, E.; Wang, L.; Lan, L.; Luo, C.; Zhuang, W.; Peng, J.; Cao, Y. *Applied Physics Letters* **2008**, *92*, 033307.

(102) Andersson, L. M.; Zhang, F.; Inganas, O. *Applied Physics Letters* **2007**, *91*, 071108.

(103) Slooff, L. H.; Veenstra, S. C.; Kroon, J. M.; Moet, D. J. D.; Sweelssen, J.; Koetse, M. M. *Applied Physics Letters* **2007**, *90*, 143506.

(104) Kline, R. J.; McGehee, M. D.; Kadnikova, E. N.; Liu, J.; Fréchet, J. M. J.; Toney, M. F. *Macromolecules* **2005**, *38*, 3312.

(105) Svensson, M.; Zhang, F. L.; Veenstra, S. C.; Verhees, W. J. H.; Hummelen, J. C.; Kroon, J. M.; Inganas, O.; Andersson, M. R. *Advanced Materials* **2003**, *15*, 988.

(106) Moule, A. J.; Tsami, A.; Buennagel, T. W.; Forster, M.; Kronenberg, N. M.; Scharber, M.; Koppe, M.; Morana, M.; Brabec, C. J.; Meerholz, K.; Scherf, U. *Chemistry of Materials* **2008**, *20*, 4045.

(107) Wu, P.-T.; Bull, T.; Kim, F. S.; Luscombe, C. K.; Jenekhe, S. A. *Macromolecules* **2009**, *42*, 671.

(108) Schilinsky, P.; Asawapirom, U.; Scherf, U.; Biele, M.; Brabec, C. J. *Chemistry of Materials* **2005**, *17*, 2175.

(109) Ma, W.; Kim, J. Y.; Lee, K.; Heeger, A. J. *Macromolecular Rapid Communications* **2007**, *28*, 1776.

(110) Ballantyne, A. M.; Chen, L.; Dane, J.; Hammant, T.; Braun, F. M.; Heeney, M.; Duffy, W.; McCulloch, I.; Bradley, D. D. C.; Nelson, J. *Advanced Functional Materials* **2008**, *18*, 2373.

(111) Moon, J. S.; Lee, J. K.; Cho, S.; Byun, J.; Heeger, A. J. *Nano Letters* **2009**, *9*, 230.

(112) Shi, C. J.; Yao, Y.; Yang, Y.; Pei, Q. B. *Journal of the American Chemical Society* **2006**, *128*, 8980.

(113) Wang, E.; Wang, M.; Wang, L.; Duan, C.; Zhang, J.; Cai, W.; He, C.; Wu, H.; Cao, Y. *Macromolecules* **2009**, *42*, 4410.

(114) Inganäs, O.; Svensson, M.; Zhang, F.; Gadisa, A.; Persson, N. K.; Wang, X.; Andersson, M. R. *Applied Physics A: Materials Science & Processing* **2004**, *79*, 31.

(115) Cho, S.; Seo, J. H.; Kim, S. H.; Song, S.; Jin, Y.; Lee, K.; Suh, H.; Heeger, A. J. *Applied Physics Letters* **2008**, *93*.

(116) Jayakannan, M.; Van Hal, P. A.; Janssen, R. A. J. *Journal of Polymer Science Part a-Polymer Chemistry* **2002**, *40*, 2360.

(117) Karikomi, M.; Kitamura, C.; Tanaka, S.; Yamashita, Y. *Journal of the American Chemical Society* **2002**, *117*, 6791.

(118) Xiao, S.; Stuart, A. C.; Liu, S.; You, W. *ACS Applied Materials & Interfaces* **2009**, *1*, 1613.

(119) Hou, Q.; Zhou, Q. M.; Zhang, Y.; Yang, W.; Yang, R. Q.; Cao, Y. *Macromolecules* **2004**, *37*, 6299.

(120) Zhang, C.; C07D417/14 ed. U.S, 2004; Vol. US 2004/0229925 A1.

(121) Nehls, B. S.; Asawapirom, U.; Fuldner, S.; Preis, E.; Farrell, T.; Scherf, U. *Advanced Functional Materials* **2004**, *14*, 352.

(122) Galbrecht, F.; Bunnagel, T. W.; Scherf, U.; Farrell, T. *Macromolecular Rapid Communications* **2007**, *28*, 387.

(123) Becke, A. D. *Journal of Chemical Physics* **1993**, *98*, 5648.

(124) Lee, C. T.; Yang, W. T.; Parr, R. G. *Phys. Rev. B* **1988**, *37*, 785.

(125) Frisch, M. J. T., G. W.; Schlegel, H. B.; Scuseria, G. E.; Robb, M. A.; Cheeseman, J. R.; Montgomery Jr., J. A.; Vreven, T.; Kudin, K. N.; Burant, J. C.; Millam, J. M.; Iyengar, S. S.; Tomasi, J.; Barone, V.; Mennucci, B.; Cossi, M.; Scalmani, G.; Rega, N.; Petersson, G. A.; Nakatsuji, H.; Hada, M.; Ehara, M.; Toyota, K.; Fukuda, R.; Hasegawa, J.; Ishida, M.; Nakajima, T.; Honda, Y.; Kitao, O.; Nakai, H.; Klene, M.; Li, X.; Knox, J. E.; Hratchian, H. P.; Cross, J. B.; Adamo, C.; Jaramillo, J.; Gomperts, R.; Stratmann, R. E.; Yazyev, O.; Austin, A. J.; Cammi, R.; Pomelli, C.; Ochterski, J. W.; Ayala, P. Y.; Morokuma, K.; Voth, G. A.; Salvador, P.; Dannenberg, J. J.; Zakrzewski, V. G.; Dapprich, S.; Daniels, A. D.; Strain, M. C.; Farkas, O.; Malick, D. K.; Rabuck, A. D.; Raghavachari, K.; Foresman, J. B.; Ortiz, J. V.; Cui, Q.; Baboul, A. G.; Clifford, S.; Cioslowski, J.; Stefanov, B. B.; Liu, G.; Liashenko, A.; Piskorz, P.; Komaromi, I.; Martin, R. L.; Fox, D. J.; Keith, T.; Al-Laham, M. A.; Peng, C. Y.; Nanayakkara, A.; Challacombe, M.; Gill, P. M. W.; Johnson, B.; Chen, W.; Wong, M. W.; Gonzalez, C.; Pople, J. A. .

(126) Wienk, M. M.; Turbiez, M.; Gilot, J.; Janssen, R. A. J. *Advanced Materials* **2008**, *20*, 2556.

(127) Peet, J.; Senatore, M. L.; Heeger, A. J.; Bazan, G. C. *Advanced Materials* **2009**, *21*, 1521.

(128) Peet, J.; Cho, N. S.; Lee, S. K.; Bazan, G. C. *Macromolecules* **2008**, *41*, 8655.

(129) Melzer, C.; Koop, E. J.; Mihailetchi, V. D.; Blom, P. W. M. *Advanced Functional Materials* **2004**, *14*, 865.

(130) Mihailetchi, V. D.; Koster, L. J. A.; Blom, P. W. M.; Melzer, C.; de Boer, B.; van Duren, J. K. J.; Janssen, R. A. J. *Advanced Functional Materials* **2005**, *15*, 795.

(131) Kline, R. J.; McGehee, M. D.; Kadnikova, E. N.; Liu, J. S.; Frechet, J. M. J. *Advanced Materials* **2003**, *15*, 1519.

(132) Soci, C.; Hwang, I. W.; Moses, D.; Zhu, Z.; Waller, D.; Gaudiana, R.; Brabec, C. J.; Heeger, A. J. *Advanced Functional Materials* **2007**, *17*, 632.

(133) Xiao, S.; Stuart, A. C.; Liu, S.; Zhou, H.; You, W. *Advanced Functional Materials* **2010**, *ASAP*.

(134) Xiao, S. Q.; Zhou, H. X.; You, W. *Macromolecules* **2008**, *41*, 5688.

(135) Zhang, M.; Tsao, H. N.; Pisula, W.; Yang, C.; Mishra, A. K.; Müllen, K. *Journal of the American Chemical Society* **2007**, *129*, 3472.

(136) Price, S. C.; Stuart, A. C.; You, W. *Macromolecules* **2009**, DOI: 10.1021/ma902164q.

(137) Mandoc, M. M.; Koster, L. J. A.; Blom, P. W. M. *Applied Physics Letters* **2007**, *90*, 133504.

(138) Kirchartz, T.; Pieters, B. E.; Taretto, K.; Rau, U. *Journal of Applied Physics* **2008**, *104*, 094513.

(139) Moulé, A. J.; Meerholz, K. *Advanced Functional Materials* **2009**, *19*, 3028.

(140) Morana, M.; Wegscheider, M.; Bonanni, A.; Kopidakis, N.; Shaheen, S.; Scharber, M.; Zhu, Z.; Waller, D.; Gaudiana, R.; Brabec, C. *Advanced Functional Materials* **2008**, *18*, 1757.

(141) Zhou, H. X.; Yang, L. Q.; Xiao, S. Q.; Liu, S. B.; You, W. *Macromolecules* **2010**, *43*, 811.

(142) Mancilha, F. S.; DaSilveira Neto, B. A.; Lopes, A. S.; Moreira, P. F.; Quina, F. H.; Gonçalves, R. S.; Dupont, J. *European Journal of Organic Chemistry* **2006**, *2006*, 4924.

(143) Liang, Y.; Feng, D.; Wu, Y.; Tsai, S.-T.; Li, G.; Ray, C.; Yu, L. *Journal of the American Chemical Society* **2009**, *131*, 7792.

(144) Zhou, H.; Yang, L.; Stoneking, S.; You, W. *ACS Applied Materials & Interfaces* **2010**, *2*, 1377.

(145) Osaka, I.; McCullough, R. D. *Accounts of Chemical Research* **2008**, *41*, 1202.

(146) Li, G.; Shrotriya, V.; Yao, Y.; Huang, J.; Yang, Y. *Journal of Materials Chemistry* **2007**, *17*, 3126.

(147) Shin, M.; Kim, H.; Park, J.; Nam, S.; Heo, K.; Ree, M.; Ha, C.-S.; Kim, Y. *Advanced Functional Materials* **2010**, *20*, 748.

(148) Chan, S.-H.; Hsiao, Y.-S.; Hung, L.-I.; Hwang, G.-W.; Chen, H.-L.; Ting, C.; Chen, C.-P. *Macromolecules* **2010**, *43*, 3399.

(149) Hsieh, C.-H.; Cheng, Y.-J.; Li, P.-J.; Chen, C.-H.; Dubosc, M.; Liang, R.-M.; Hsu, C.-S. *Journal of the American Chemical Society* **2010**, *132*, 4887.

(150) Hoven, C. V.; Dang, X.-D.; Coffin, R. C.; Peet, J.; Nguyen, T.-Q.; Bazan, G. C. *Advanced Materials* **2010**, *22*, E63.

(151) Price, S. C.; Stuart, A. C.; You, W. *Macromolecules* **2010**, *43*, 4609.

(152) Brédas, J.-L.; Norton, J. E.; Cornil, J.; Coropceanu, V. *Accounts of Chemical Research* **2009**, *42*, 1691.

(153) Wong, S.; Ma, H.; Jen, A. K. Y.; Barto, R.; Frank, C. W. *Macromolecules* **2003**, *36*, 8001.

(154) Reichenbacher, K.; Suss, H. I.; Hulliger, J. *Chemical Society Reviews* **2005**, *34*, 22.

(155) Pagliaro, M.; Ciriminna, R. *Journal of Materials Chemistry* **2005**, *15*, 4981.

(156) Babudri, F.; Farinola, G. M.; Naso, F.; Ragni, R. *Chemical Communications* **2007**, 1003.

(157) Peer, K. *Modern fluoroorganic chemistry : synthesis, reactivity, applications*; WILEY-VCH Verlag GmbH & Co. KGaA, Weinheim, 2004.

(158) Wang, Y.; Parkin, S. R.; Gierschner, J.; Watson, M. D. *Organic Letters* **2008**, *10*, 3307.

(159) Yoon, M.-H.; DiBenedetto, S. A.; Facchetti, A.; Marks, T. J. *Journal of the American Chemical Society* **2005**, *127*, 1348.

(160) Facchetti, A.; Yoon, M. H.; Stern, C. L.; Katz, H. E.; Marks, T. J. *Angewandte Chemie International Edition* **2003**, *42*, 3900.

(161) Oh, J. H.; Suraru, S.; Lee, W. Y.; Könemann, M.; Höffken, H. W.; Röger, C.; Schmidt, R.; Chung, Y.; Chen, W. C.; Würthner, F.; Bao, Z. *Advanced Functional Materials* **2010**, *20*, 2148.

(162) Heidenhain, S. B.; Sakamoto, Y.; Suzuki, T.; Miura, A.; Fujikawa, H.; Mori, T.; Tokito, S.; Taga, Y. *Journal of the American Chemical Society* **2000**, *122*, 10240.

(163) Kim, J. S.; Lee, Y.; Lee, J. H.; Park, J. H.; Kim, J. K.; Cho, K. *Advanced Materials* **2010**, *22*, 1355.

(164) Wei, Q.; Nishizawa, T.; Tajima, K.; Hashimoto, K. *Advanced Materials* **2008**, *20*, 2211.

(165) Brédas, J. L.; Heeger, A. J. *Chemical Physics Letters* **1994**, *217*, 507.

(166) Wang, Y.; Watson, M. D. *Macromolecules* **2008**, *41*, 8643.

(167) Ferraris, J. P.; Bravo, A.; Kim, W.; Hrncir, D. C. *Journal of the Chemical Society-Chemical Communications* **1994**, 991.

(168) Zhou, H.; Yang, L.; Price, S. C.; Knight, K. J.; You, W. *Angewandte Chemie International Edition*, *DOI: 10.1002/anie.201003357*.

(169) Piliego, C.; Holcombe, T. W.; Douglas, J. D.; Woo, C. H.; Beaujuge, P. M.; Fréchet, J. M. J. *Journal of the American Chemical Society* **2010**, *132*, 7595.

(170) Liang, Y.; Wu, Y.; Feng, D.; Tsai, S.-T.; Son, H.-J.; Li, G.; Yu, L. *Journal of the American Chemical Society* **2009**, *131*, 56.

(171) Zou, Y.; Najari, A.; Berrouard, P.; Beaupré, S.; Réda Aïch, B.; Tao, Y.; Leclerc, M. *Journal of the American Chemical Society* **2010**, *132*, 5330.

(172) Wu, P.-T.; Xin, H.; Kim, F. S.; Ren, G.; Jenekhe, S. A. *Macromolecules* **2009**, *42*, 8817.

(173) Clarke, T. M.; Durrant, J. R. *Chemical Reviews* **2010**, *110*, 6736.

(174) Zhu, X. Y.; Yang, Q.; Muntwiler, M. *Accounts of Chemical Research* **2009**, *42*, 1779.

(175) Blom, P. W. M.; Mihailetchi, V. D.; Koster, L. J. A.; Markov, D. E. *Advanced Materials* **2007**, *19*, 1551.

(176) Carsten, D.; Vladimir, D. *Reports on Progress in Physics* **2010**, *73*, 096401.

(177) Peet, J.; Heeger, A. J.; Bazan, G. C. *Accounts of Chemical Research* **2009**, *42*, 1700.

(178) van Bavel, S.; Veenstra, S.; Loos, J. *Macromolecular Rapid Communications* **2010**, *31*, 1835.

(179) Groves, C.; Reid, O. G.; Ginger, D. S. *Accounts of Chemical Research* **2010**, *43*, 612.

(180) Chen, L.-M.; Hong, Z.; Li, G.; Yang, Y. *Advanced Materials* **2009**, *21*, 1434.

(181) Kotlarski, J. D.; Blom, P. W. M. *Applied Physics Letters* **2011**, *98*.

(182) AG., F. **2011**.

(183) SE, Q.-C. **2011**.

(184) Hou, J.; Tan, Z. a.; Yan, Y.; He, Y.; Yang, C.; Li, Y. *Journal of the American Chemical Society* **2006**, *128*, 4911.

(185) Zhou, E.; Cong, J.; Wei, Q.; Tajima, K.; Yang, C.; Hashimoto, K. *Angewandte Chemie International Edition* **2011**, *50*, 2799.

(186) Li, W.; Qin, R.; Zhou, Y.; Andersson, M.; Li, F.; Zhang, C.; Li, B.; Liu, Z.; Bo, Z.; Zhang, F. *Polymer* **2010**, *51*, 3031.

(187) Schlenker, C. W.; Thompson, M. E. *Chemical Communications* **2011**, *47*, 3702.

(188) Brunetti, F. G.; Gong, X.; Tong, M.; Heeger, A. J.; Wudl, F. *Angewandte Chemie International Edition* **2010**, *49*, 532.

(189) Gong, X.; Tong, M.; Brunetti, F. G.; Seo, J.; Sun, Y.; Moses, D.; Wudl, F.; Heeger, A. J. *Advanced Materials* **2011**, *23*, 2272.

(190) Street, R. A. *Applied Physics Letters* **2008**, *93*.

(191) Varotto, A.; Treat, N. D.; Jo, J.; Shuttle, C. G.; Batara, N. A.; Brunetti, F. G.; Seo, J. H.; Chabinyc, M. L.; Hawker, C. J.; Heeger, A. J.; Wudl, F. *Angewandte Chemie International Edition* **2011**, *50*, 5166.

(192) Pommerehne, J.; Vestweber, H.; Guss, W.; Mahrt, R. F.; Bassler, H.; Porsch, M.; Daub, J. *Advanced Materials* **1995**, *7*, 551.

(193) Zhan, X. W.; Liu, Y. Q.; Wu, X.; Wang, S. A.; Zhu, D. B. *Macromolecules* **2002**, *35*, 2529.